

SO&P

Simulations, Observations & Palaeoclimatic data: climate variability over the last 500 years



EVK2-CT-2002-00160 SOAP

Section 6: Detailed final report

This report should be cited as:

Osborn TJ and Briffa KR (editors) (2006) *Simulations, observations and palaeoclimatic data: climate variability over the last 500 years*. Final report to the EU of the SO&P project (EVK2-CT-2002-00160), Climatic Research Unit, University of East Anglia, Norwich, UK.

Contributing authors were:

Brohan P, Burger G, Cubasch U, Gregory J, Guiot J, Jones J, Lowe J, Luterbacher J, Nicault A, Pauling A, Tett S, Tudhope A, van de Plassche O, von Storch H, Wanner H, Wilson R, Wright A, Xoplaki E, Zorita E

Co-ordinators:

Dr. Tim Osborn (t.osborn@uea.ac.uk)

Professor Keith Briffa (k.briffa@uea.ac.uk)

Climatic Research Unit, University of East Anglia, Norwich, NR4 7TJ, UK

SO&P website: <http://www.cru.uea.ac.uk/cru/projects/soap/>

6. Detailed final report for the SO&P project

The SO&P (Simulations, Observations & Palaeoclimatic data: climate variability over the last 500 years) project is a 36-month (extended to 42 months) scientific research project funded by the European Commission. It is a collaborative project between eight institutions in five European countries, listed in Table 1. The SO&P project is coordinated by Tim Osborn and Keith Briffa at UEA. Many more details of the project, including data and publications, are available from the SO&P website: <http://www.cru.uea.ac.uk/cru/projects/soap/>.

Table 1. The SO&P partners

1	UEA	University of East Anglia	UK
2	UEDIN	University of Edinburgh	UK
3	METO	Hadley Centre, Met Office	UK
4	FUB	Freie Universitat Berlin	Germany
5	GKSS	GKSS Research Center	Germany
6	CNRS/UDESAM	CNRS / University of Marseille	France
7	UBERN	University of Bern	Switzerland
8	VUA	Vrije Universiteit Amsterdam	Netherlands

6.1. Scientific background

The SO&P project was designed with the rationale that a combination of modelling and observation based research represents the most productive route towards understanding climate variability and, more specifically for placing the twentieth and twenty-first century climates in the context of previous centuries. To achieve this aim, significantly improved, regionally-resolved palaeoclimate reconstructions needed to be developed and externally-forced climate simulations for the last five centuries had to be undertaken. These new sources of information could then be combined to quantitatively analyse the capability of the latest General Circulation Models (GCMs) to simulate climate changes over past centuries, to explore the nature of simulated and observed responses to historical natural forcing, and to quantify the uncertainty associated with the detection and attribution of climate change signals on hemispheric and regional spatial scales due to anthropogenic forcing.

The majority of climate change signal detection and attribution studies to date assume a model-based estimate of natural climate variability. This is a major and virtually untested assumption, and is potentially a major source of criticism that could be used to detract from all such work. The SO&P project was devised to make an effective contribution towards improving our knowledge and understanding of interannual to multi-century time scale variability of the climate system, and the degree to which this is realistically simulated by the best GCMs. Climate models are clearly unrivalled in their ability to simulate a broad suite of variables across the entire world, but their reliability on decadal and longer time scales requires additional evaluation.

6.2. Scientific/technological and socio-economic objectives

The overall aim of the SO&P project was to provide a state-of-the-art quantitative description of the variability and causes of variability of Northern Hemisphere climate, over the last five centuries. The project investigated the behaviour of important regional systems as well as hemispherically-integrated changes, and quantified the changing influences of natural and anthropogenic climate forcings, using an integrated study of palaeoclimate proxies and carefully prescribed general circulation model (GCM) experiments. Another major objective was to establish the reliability of GCM simulations of natural climate variability, and hence gain additional insights into the uncertainty of model-based anthropogenic climate change detection studies. This should provide a more secure basis from which to assess the likelihood of future abrupt and unusual climate changes.

In reaching these overarching aims, the project achieved many individual measurable objectives. The most important of these are:

- The simulation of climate variations for the period AD 1500-2000 using two state-of-the-art GCM climate models, forced with very similar natural forcing histories (including volcanic aerosol loading, total solar irradiance changes and orbital changes) and separate simulations for the period AD 1750-2000 forced by combined natural and anthropogenic forcings (greenhouse gases, ozone and sulphate aerosols).
- Detailed statistical intercomparison of the simulations with one another, and with already available millennial-length control simulations (with constant external forcings), to enable:
 - the identification of robust climate responses to external forcing on global and regional scales; and
 - the quantification of the relative importance of forced and internally-generated climate variability.
- The production of an enhanced and integrated database of annually-resolved climate proxy records, by assembling many existing records (tree rings, ice cores, corals, etc.) and lower resolution records such as those from lake sediment, peat records and borehole temperature estimates.
- The construction of homogeneous sets of climate data, representing seasonal temperature, precipitation and atmospheric circulation variability over the last 500 years, involving the amalgamation (via appropriate calibration) of instrumental observations, documentary climate archival data and existing and the newly amalgamated palaeoclimate proxy evidence, to allow:
 - a detailed analysis (multiple variables for all seasons, or even at a monthly resolution) for the European region, possible because of the dense network of natural and documentary proxies available;
 - the improved definition of the characteristics and magnitude of natural climate variability during the last five centuries across the full Northern Hemisphere; and
 - the improved reconstruction of past variations in important atmospheric and ocean-atmosphere modes of climate variability, including the North Atlantic Oscillation (NAO, and the related Arctic Oscillation) and the El Niño–Southern Oscillation (ENSO).

- Evaluation of the simulated climate variability, and the simulated climate response to external forcing, by quantitative comparison with the extended observed/reconstructed climate data.
- The use of the model simulations to aid in the interpretation of the real-world climate variability, specifically the use of signal detection techniques to test the extent to which the model response to external forcings is detectable in the observed/reconstructed climate data.
- The generation of improved estimates of natural climate variability, through synthesis of the simulated and observed/reconstructed data.
- The re-assessment of climate change prediction uncertainties and climate change signal detection uncertainty, in the light of these new estimates of natural variability.
- Comparison of estimates of sea level variation generated from the climate model simulations with a synthesised history of North Atlantic sea level changes, based on a combination of long tide gauge records and evidence from a number of ongoing tidal marsh sampling studies.

6.3. Applied methodology, scientific achievements and main deliverables

The SO&P project is structured into five interlinking workpackages, listed below, and this section of the report follows this breakdown.

- WP1: Coordination and dissemination
- WP2: Model simulations of the climate of the last 500 years
- WP3: Amalgamation and calibration of 500-years of high-resolution climate data
- WP4: Synthesis and interpretation of observed/reconstructed and simulated climates
- WP5: Sea level changes over the last 500 years

The linkages between these workpackages are indicated schematically in Figure 1. Model A is the HadCM3 model and Model B is the ECHO-G model.

6.3.1. Workpackage 1: Coordination and dissemination

This workpackage focussed on the coordination of collaborative work carried out within the project and on ensuring widespread dissemination of project data and research outputs (within the project consortium during the project, and outside of the project after completion). The project coordination aspects of the workpackage have been described in detail in the annual management and progress reports, and because they do not relate directly to scientific achievements, it is not necessary to provide details of the meetings and internal reports here.

The project website (<http://www.cru.uea.ac.uk/cru/projects/soap/>) has been developed under this workpackage to facilitate the dissemination of climate proxy data, palaeoclimatic reconstructions and output from the climate model simulations. After the project is complete, much of this data will be available for use by the scientific community, either with open access or for agreed collaborative projects. The website includes extensive description of the data available and their original sources, together with many graphical visualisations of the data to provide an easy overview of their characteristics.

6.3.1.1. Deliverables from WP1 (section 6.3.6 lists all deliverables)

D1 – Dedicated project website (with private and public sections)

D19 – Final project report, draft TIP plan and dissemination of project results and data sets

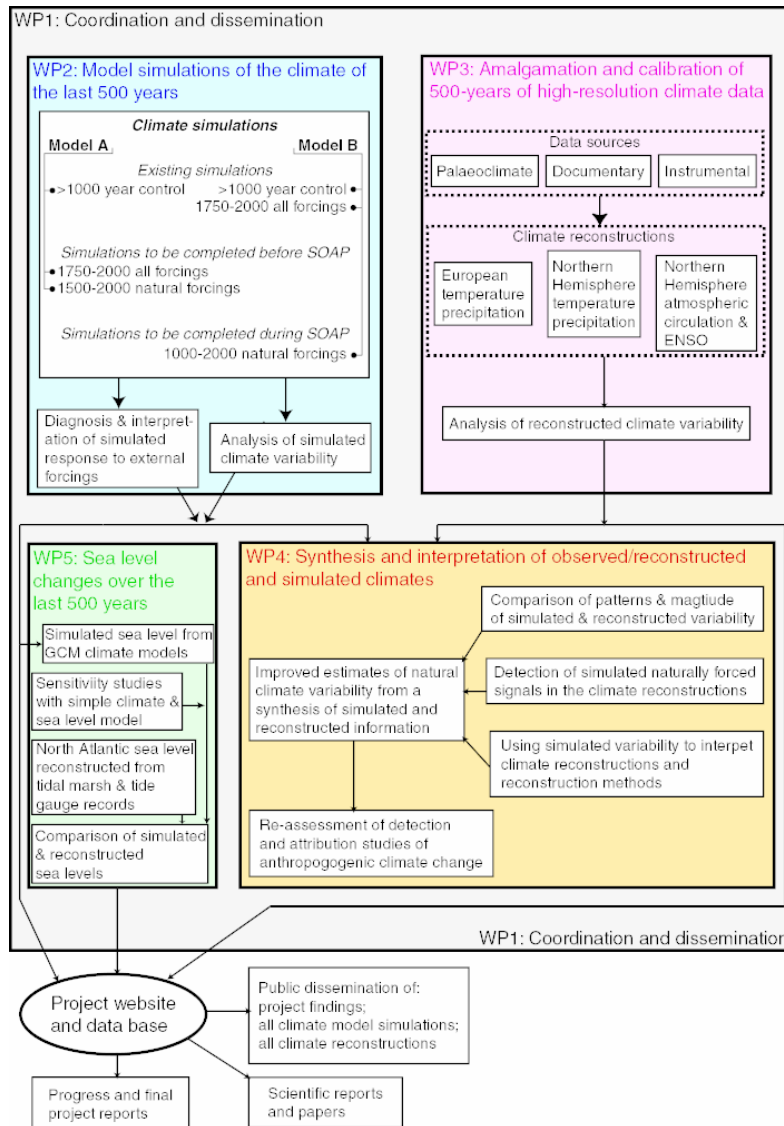


Figure 1. Schematic of project structure and linkages.

6.3.2. Workpackage 2: Model simulations of the climate of the last 500 years

The purpose of the work carried out within workpackage 2 was to produce and analyse simulations of climate variations for the period AD 1500–2000 using two state-of-the-art GCM-based climate models (HadCM3 and ECHO-G). The model experiments were designed to (i) provide simulations that are suitable for comparison with real-world data, by using realistic and comprehensive sets of past natural and anthropogenic forcings; (ii) isolate the influences of natural and anthropogenic forcings, by undertaking additional simulations with only natural forcings included; and (iii) allow comparison between the two climate models by

prescribing very similar forcing histories to both models. The latter goal was only partly achieved, due partly to unavoidable differences in the implementation of forcings within each model (for example, in HadCM3 it was possible to implement volcanic forcing as an explicit stratospheric aerosol loading that interacts with the short- and long-wave radiation, with a cooling effect on the surface but warming in the stratosphere, while in ECHO-G, volcanic forcing was incorporated indirectly by reducing the solar constant, having a cooling effect on the surface but no direct stratospheric warming). A further reason for forcing differences between the models is that the ECHO-G and HadCM3 simulations had to be started before the project commenced to ensure that model output would be available at an early enough stage to allow it to be analysed extensively within the project. As a result, the forcings used by each modelling centre could not be coordinated under the auspices of the SO&P project and different selections were made. Perhaps the two of most impact are (i) that HadCM3 included the direct and indirect effects of anthropogenic tropospheric sulphate aerosols, which act to cool the climate during the last 150 years (especially in the Northern Hemisphere [NH] and during the 1940–1980 period) while ECHO-G did not (resulting in much greater NH warming in the 20th century); and (ii) though both models were prescribed volcanic forcing histories provided by Tom Crowley, ECHO-G used the version described in Crowley, 2000, while HadCM3 used the later version published by Crowley *et al.*, 2003).

6.3.2.1. Model simulations

The HadCM3 coupled climate model used to carry out the simulations has been described in Pope *et al.* (2000) and Gordon *et al.* (2000). We use results from three simulations carried out by the Hadley Centre (partner METO):

- (1) CONTROL – the control simulation of HadCM3 (Collins *et al.*, 2001) was already available for a period of about 2800 years.
- (2) NAT500 – a simulation from 1492 to 1999 driven by natural forcings alone.
- (3) ALL250 – a simulation from 1750 to 1999 driven by anthropogenic and natural forcings.

The forcings used within these simulations are described in full in Tett *et al.* (2006). The natural forcings are volcanic aerosol loading, solar irradiance variations and orbital changes (the latter are quite small over the last 500 years). The anthropogenic forcings are well-mixed greenhouse gas concentrations, emissions of tropospheric sulphate aerosols, land surface changes associated with changes in land use, and tropospheric and stratospheric ozone concentration changes.

The ECHO-G coupled climate model used to carry out the simulations used within the SO&P project is described in Legutke and Voss (1999). We use results from the following set of simulations:

- (1) ERIK – a simulation with both natural and anthropogenic forcings covering the period 1000 to 1990. This simulation had already been completed by GKSS before the start of the SO&P project (Gonzalez-Rouco *et al.*, 2003).
- (2) ENAT – a simulation with only natural forcings covering the period 1756 to 1999 was completed by Free University Berlin (FUB) with SO&P funding.
- (3) ECHO-G ensemble – a further seven experiments (extended so that each is a three-member ensemble) were carried out by FUB and GKSS for the period since 1756 with solar, volcanic and greenhouse gases specified individually or in all possible combinations. FUB have used these to isolate the contributions from specific forcings or combinations of forcings.

The forcings used within these simulations are volcanic forcing, solar irradiance variations and concentrations of carbon dioxide, methane and nitrous oxide.

A common set of climate variables was extracted from the HadCM3 and ECHO-G simulations, converted to a common netCDF format, and built into a web-based structured data base.

These simulations were then compared with one another, and with already available millennial-length control simulations (with constant external forcings), to enable the identification of robust climate responses to external forcing on global and regional scales; and the quantification of the relative importance of forced and internally-generated climate variability.

6.3.2.2. Diagnosing the anthropogenic impacts on climate in the HadCM3 simulations

The zonal-mean difference in radiative forcing between ALL250 and NAT500 (Figure 2a) shows a steady increase over all regions except the northern mid-latitudes. Here there is a strong negative forcing difference which reaches its most negative value in the 1960s and 1970s, but is substantially negative from the late 19th century onwards. The negative forcing is mainly from aerosols (mainly the indirect effect) with a smaller cooling contribution from land-surface changes (Betts, 2001). Forcing differences in the southern extra-tropics are +2 W m⁻² by the 1990s.

Also apparent from the 1980s onwards is strong negative forcing over Antarctica. This net negative forcing arises from the stratospheric adjustment which associated with the intense stratospheric cooling caused by ozone depletion.

Resulting from these forcing differences are tropical warming and northern mid-latitude cooling (Figure 2b). Differences in trends associated with the inclusion of anthropogenic forcing are significant from 1830 onwards in the tropics. This suggests that anthropogenic forcings could have had a significant impact on climate even by the early part of the 19th century.

The relative warming and cooling are more apparent in trends in zonal-mean temperature for the period 1750 to 1999 (Figure 2c). The tropics are warming at a rate of 2 K/millennium while at 45°N there is no significant positive or negative trend.

6.3.2.3. Effect of natural forcing on climate variability in the HadCM3 simulations

To examine the role of natural forcing on small-scale variability over the globe, we computed the ratio between the temporal standard deviations of decadal-mean near-surface temperatures from the NAT500 and CONTROL simulations, for all grid boxes. We find significant enhancements in grid-box temperature variability across most of the tropics and subtropics (Figure 3a) when natural external forcings are included. Largest increases occur over the Indian Ocean and tropical Africa. Significant reductions in variance are apparent in eastern Europe and the eastern USA. These are regions which have less snow cover in NAT500 than in CONTROL; it is expected that reduced mean snow cover would reduce the inter-annual and inter-decadal variability of temperature because one source of such variability (the variability in surface albedo) is reduced. There is little evidence of significantly enhanced variability on decadal time scales in extra-tropical regions at the grid-box scale.

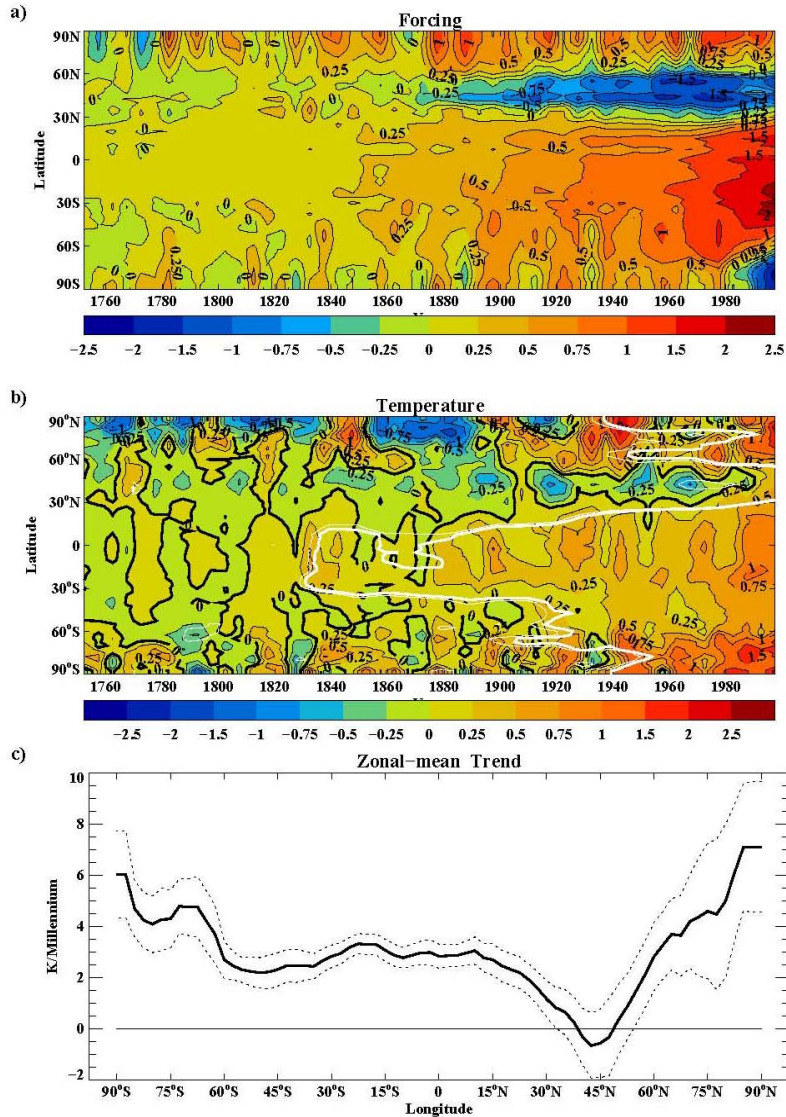


Figure 2. (a) Zonal-mean plot of 5-year-mean adjusted forcing difference between ALL250 and NAT500 simulations. Positive forcings are an increase in forcing due to anthropogenic effects. A contour interval of 0.5 W/m^2 is used with additional contours at ± 0.25 and $\pm 0.75 \text{ W/m}^2$. (b) Temperature differences between 5-year-mean ALL250 and NAT500 simulations. Contours as in (a). Thin (thick) white contours show where trend from 1750 onwards is significantly different from control run variability with 90% confidence. (c) Zonal-mean trend in temperature difference. Dotted lines show 5 – 95% uncertainty range estimated from CON.

We also find a significant enhancement in zonal-mean temperature standard deviation throughout the tropics and sub-tropics (Figure 3b). Zonal-mean temperature variability at mid-latitudes is marginally enhanced (though marginal, the increased variance *is* statistically significant). These results have implications for the collection of new proxy records. The importance of tropical data for identifying the influence of natural external forcing is clearly emphasised, though there are other issues to consider (see Tett *et al.*, 2006, for further discussion).

6.3.2.4. Radiative Forcing, Top of the Atmosphere (TOA) flux imbalance and Climate Sensitivity

Since, in the simulations, both the radiative forcing (F) and the net downward TOA radiative flux (N) are known, it is possible to estimate the climate sensitivity from the heat budget of the climate system, which can be written (Gregory *et al.*, 2004):

$$F(t) = N(t) + \alpha T(t) \quad (1)$$

where $T(t)$ is global-average surface air temperature anomaly at time t . The anomaly is from the equilibrium temperature when $F = 0$, and α is the climate feedback parameter. Equation (1) states that the radiative forcing is partitioned between storage in the system (N) and the radiative response due to climate change (αT). In equilibrium, when by definition $N = 0$, $T = F/\alpha$. Hence α is related to the equilibrium climate sensitivity. While the system is not in equilibrium, a time-dependent α can be diagnosed as $\alpha = (F - N)/T$ (Senior and Mitchell, 2000). Another way to examine the behaviour of the feedbacks is to plot $(F - N)$ versus T . If climate sensitivity is constant, this will be a straight line of slope α (Gregory *et al.*, 2004).

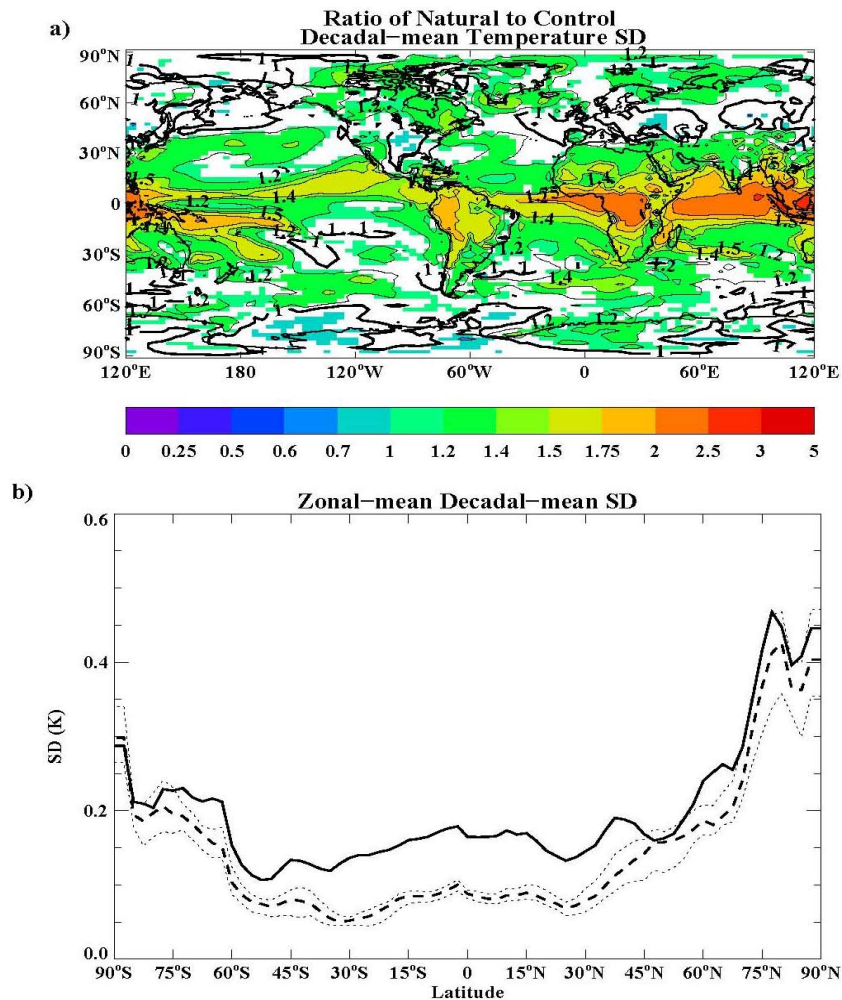


Figure 3. (a) Ratio between NAT500 and CONTROL standard deviations for decadal-mean temperature. Coloured values are where NAT500 has significantly different standard deviation from CONTROL. The 1.0 contour is drawn bold. (b) Standard deviation of zonal-mean decadal-mean temperature for NAT500 (solid) and CONTROL (dashed). 5% and 95% values from empirical CONTROL are shown as thin dotted lines. When values from NAT500 are outside this range the simulation has significantly different decadal variability than CONTROL.

When diagnosed from the ALL250 simulation, α is not constant (Figure 4), with very different values of α prior to and post 1900. A change in α could arise because the nature of the forcing is changing, if the sensitivity differs for different kinds of forcing (Hansen *et al.*, 1997, Joshi *et al.*, 2003, Roberts and Jones, 2004), or if local feedbacks vary and the pattern of temperature changes differs between forcings. Gregory *et al.* (2004) found that HadCM3 has values of α that depend on the forcing, and this is confirmed by HadCM3 simulations with time-dependent amplified solar forcing (Stott *et al.*, 2003) and amplified volcanic forcing; with $\alpha = 1.95 \pm 0.55$ and $1.59 \pm 0.55 \text{ W m}^{-2} \text{ K}^{-1}$, respectively. The value of α diagnosed from the pre-1900 part of the ALL250 simulation is similar to these values.

In NAT500 we find that $\alpha = 1.26 \pm 0.21 \text{ W m}^{-2} \text{ K}^{-1}$ (Figure 4). However in this experiment there is less spring snow cover (and more ice cover) than in the simulations discussed above which all use CONTROL land-surface values. It is possible that this change in base state could increase the sensitivity of the model to external forcings compensating for a change in sensitivity due to the use of volcanic or solar forcing. We difference NAT500 and ALL250 to give estimated anthropogenic values (Figure 4) and calculate α for this of $0.57 \pm 0.58 \text{ W m}^{-2} \text{ K}^{-1}$. This is similar to ALL250 post 1900. The decrease in α in ALL250 is therefore consistent with the dominance of anthropogenic over natural forcing in the 20th century. A possible explanation is that climate sensitivity to land surface changes is very large (relative to other forcings).

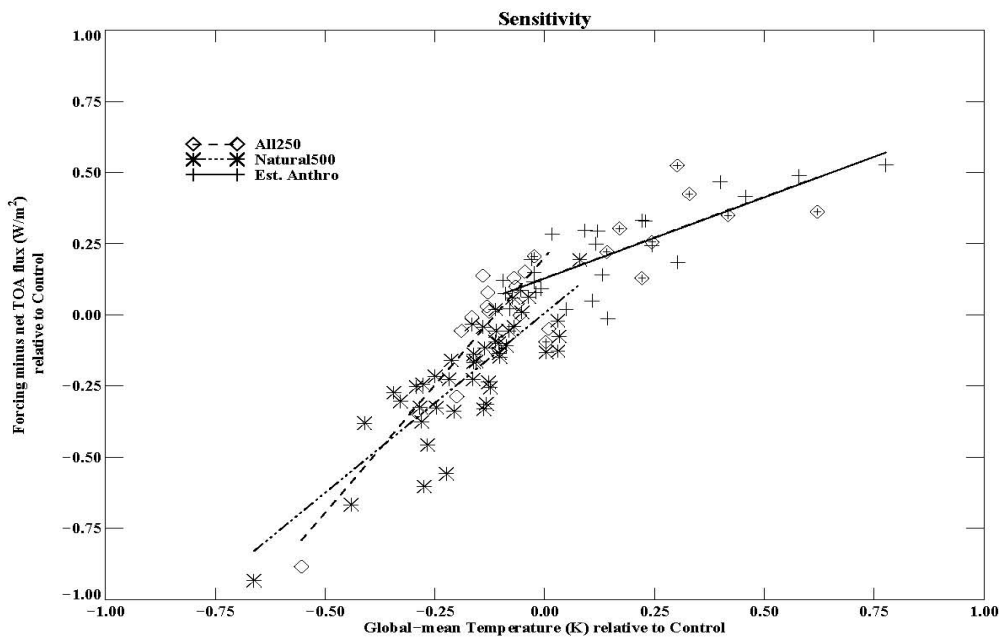


Figure 4. Scatter plot of decadal-mean net TOA flux minus forcing against decadal-mean global-mean temperature for NAT500 (stars), ALL250 (diamonds) and ALL250 minus NAT500 (Estimated Anthropogenic – pluses). ALL250 values post 1900 are shown as diamonds overplotted with small +s. All values are relative to average CONTROL. Lines show best-fit linear regressions for NAT500 (dot-dot-dot-dashed), ALL250 from 1750–1900 (dashed), ALL250 from 1900–2000 (dashed top right) and the difference between ALL250 and NAT500 (Estimated Anthropogenic – solid) which overlaps with that of ALL250 post 1900. Slopes are proportional to inverse climate sensitivity.

If realistic, the dependence of climate sensitivity on the nature of the forcing, and possibly the base state, means that the assumption commonly made in simple climate models (e.g., Crowley, 2000) of constant α is inadequate for simulating the climate system over periods during which the mix of forcing agents changes. It may also call into question attempts to constrain the climate response to future forcing on the basis of historical changes (e.g., Gregory *et al.*, 2002).

6.3.2.5. *Annular Modes in the HadCM3 and ECHO-G simulations*

An analysis of atmospheric circulation in the HadCM3 and ECHO-G all-forcings simulations, and the HadCM3 natural forcings and ECHO-G natural forcings simulations was undertaken, focussing on the Annular Modes (Thompson and Wallace, 2000). These are the major modes of extra-tropical atmospheric circulation in both hemispheres: the Arctic Oscillation (AO) in the Northern Hemisphere, and the Antarctic Oscillation (AAO) in the Southern Hemisphere.

It was found that, in all the simulations analysed, the AO pattern is too strongly related to variability over the North Pacific compared to ERA40 reanalysis data. The mid-latitude Atlantic centre-of-action was weaker than observed for ECHO-G under natural forcings and for HadCM3 under all forcings, but similar to that observed in the other simulations.

Analysis of the Southern Hemisphere summer (December–January) demonstrated that the mean sea-level pressure (SLP) is too low over the poles in the HadCM3 simulations and too high in the ECHO-G simulations. The AAO (first empirical orthogonal function [EOF] of extra-tropical sea-level pressure) in both the ERIK and the ENAT simulations have a stronger negative centre-of-action than in the ERA40 data, and the mid-latitude high pressure centre is slightly weaker in the ENAT than in the ERIK simulation. The lower mean SLP in the Hadley Centre simulations results in stronger circumpolar westerly flow in the positive and negative AAO phases compared with the ERA40 reanalysis.

6.3.2.6. *Modes of temperature variability under anthropogenic and naturally forcings*

An EOF analysis of the simulated 2 m air temperature field in the pre-industrial period of the ECHO-G ERIK simulation revealed that the dominant mode of variability, which is related to the natural external forcing, is also able to describe the spatial pattern of warming due to anthropogenic forcing simulated for the 20th and 21st centuries (the simulation was continued up to year 2100 under SRES scenario A2 without tropospheric sulphate aerosol forcing). This pattern can be roughly described by a land-sea contrast and by greater amplitudes of temperature change at high latitudes. During the final stages of the 21st-century simulation, however, the anthropogenic forcing seems to project more strongly on other natural modes (ENSO, AO), than does the response to natural forcings during the pre-industrial period (Zorita *et al.*, 2005).

6.3.2.7. *Role of natural forcings in the Dalton Minimum*

Ensemble simulations were initialised from the ERIK simulations in year 1750 and driven by different combinations of natural forcings showed that the cooling simulated during the early 1800s cannot be simulated without considering volcanic forcing. Therefore, although this period coincides with the Dalton Minimum – a period of lower solar activity – even the relatively strong solar variations used in the ERIK simulation were not able to produce a distinct temperature minimum without the additional cooling effect of enhanced volcanic activity during this period (Wagner and Zorita, 2005).

6.3.2.8. Role of individual and combined forcings during the last 250 years

A number of ensemble simulations covering the period from 1756 to 2000 and forced with different combinations of three time-evolving forcing factors (solar irradiance (S), volcanic activity (V), and atmospheric concentrations of greenhouse gases (G)) were performed by FUB using the coupled climate model ECHO-G. The 3-member ensembles were generated by taking the initial conditions from years with global-mean temperature similar to the 1755 conditions in the millennial simulation ERIK (Gonzalez-Rouco *et al.*, 2003, von Storch *et al.*, 2004). The last 235 years of ERIK itself constitute the first realisation in the SVG ensemble. Table 2 summarised the experiments performed.

Table 2. List of transient experiments S: solar, V: volcanic, G: greenhouse gases and their possible combinations. CTL: control experiment with all forcing agents set constant. T: time-varying forcing as in ERIK. Experiments marked with a star were carried out by SO&P partner GKSS.

Forcing	CTL	S	V	G	SV	SG*	VG*	SVG*
CO ₂ (ppm)	280	280	280	T	280	T	T	T
CH ₄ (ppb)	700	700	700	T	700	T	T	T
N ₂ O (ppb)	265	265	265	T	265	T	T	T
Solar Constant (W/m ²)	1365.0	T	1365.0	1365.0	T	T	1364.6	T
Volcanism	—	—	T	—	T	—	T	T

Figure 5 shows the globally and annually averaged ensemble-mean temperatures simulated in response to all possible combinations of the forcings S, V and G. Significant cooling events coincide with outbreaks of volcanoes. Only very weak pure solar cooling is apparent around 1820 (Dalton Minimum, simulation S). During the late 20th century the negative volcanic forcing and increased solar irradiance act against each other, so that global temperature changes in SV are mainly in the range of the internal variability given by control run. The temperature trend in the most recent decades can only be captured, if greenhouse gas forcing is included. The temperature increase in the “all forcings” simulation SVG (equivalent to ERIK) is, however, stronger than in the instrumental measurements (Figure 5, bottom). This discrepancy is more pronounced during the summer (not shown) and is likely caused by the omission of the cooling effect of anthropogenic sulphate aerosols in the ECHO-G simulations.

The multiple ensemble experiments provide a framework within which to test the linearity of the large-scale temperature response to the imposed external forcings and to consider whether the response to a combination of different forcing agents is additive (i.e., equal to the sum of responses to the individual forcings). The most straightforward approach is linear regression between climate system response and imposed radiative forcing: $T_{\text{LIN}} = \beta_0 + \beta_i F_i$. The regression slope β_i can be understood as a measure of the instantaneous non-equilibrium sensitivity of the system to the given forcing F_i . We found that, at the global scale, the externally-forced temperature variability can be well reproduced by a linear transformation of the prescribed forcing time series (Figure 6a–c: compare blue and black lines). One of the main limitations of the approach is that it does not account for inertia of the climate system (e.g., the recovery phase after strong volcanic eruptions is not well captured by the linear model). Figure 6d shows the simulated global annual mean temperature in experiment SVG and two linear response models. The first one is constructed via multiple linear regression between temperature and all of the forcing factors; in the second, the linear model regression

slopes from the individual forcing experiments are used. The regression coefficients for the responses to solar and greenhouse gas forcing obtained by the two methods are significantly different. This reflects the problem (among others) of estimating regression coefficients when the predictors (in this case, the forcing agents) are correlated, which occurs here because of the concurrent increases of solar insolation and greenhouse-gas forcing during the 20th century.

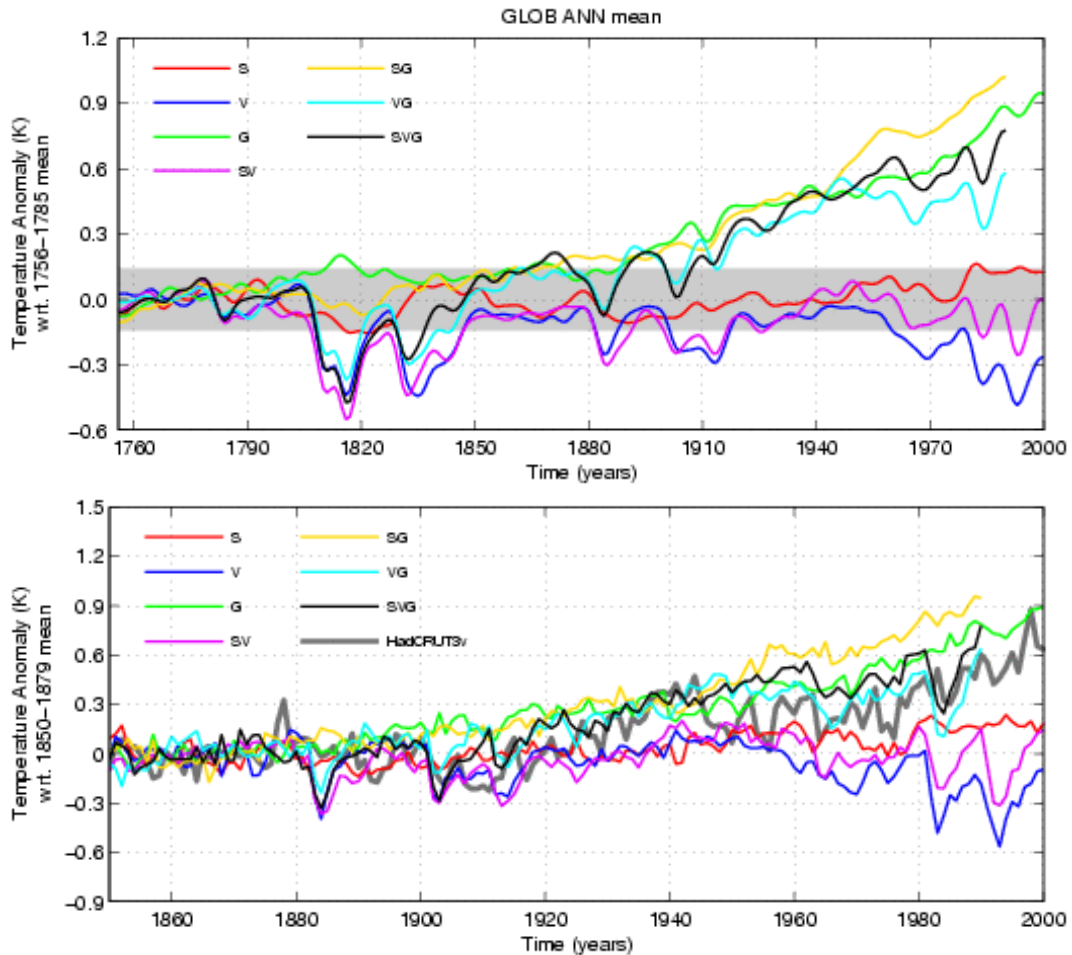


Figure 5. (top) Decadally-smoothed simulated global annual ensemble-mean surface air temperature anomalies for 7 experiments relative to the 1756–1789 mean. The grey band indicates the ± 2 standard deviation range of internal variability estimated from the control experiment CTL. (bottom) Annual temperature anomalies relative to the 1850–1879 mean with instrumental measurements (HadCRUT3v, grey line) included.

In the following we concentrate on comparison of the experiments with natural (SV) and anthropogenic (G) forcing. Figure 7 shows the time evolution of global-mean temperature changes at different heights in the model atmosphere. The simulated vertical temperature structure strongly depends on the nature of the forcing. The greenhouse gas forcing produces warming in the troposphere and cooling in the stratosphere. The solar and volcanic forced temperature changes are more uniform through the whole atmosphere. The weak solar signal in the stratosphere is unrealistic and is likely due to the poor representation of the stratosphere in ECHO-G. Volcanic events are apparent as short-lived coolings. As volcanic forcing is implemented simply via a reduction of the solar constant, warming in the lower stratosphere due to volcanic aerosol absorption is absent. Independent of the forcing, the largest temperature changes occur in the middle and upper troposphere.

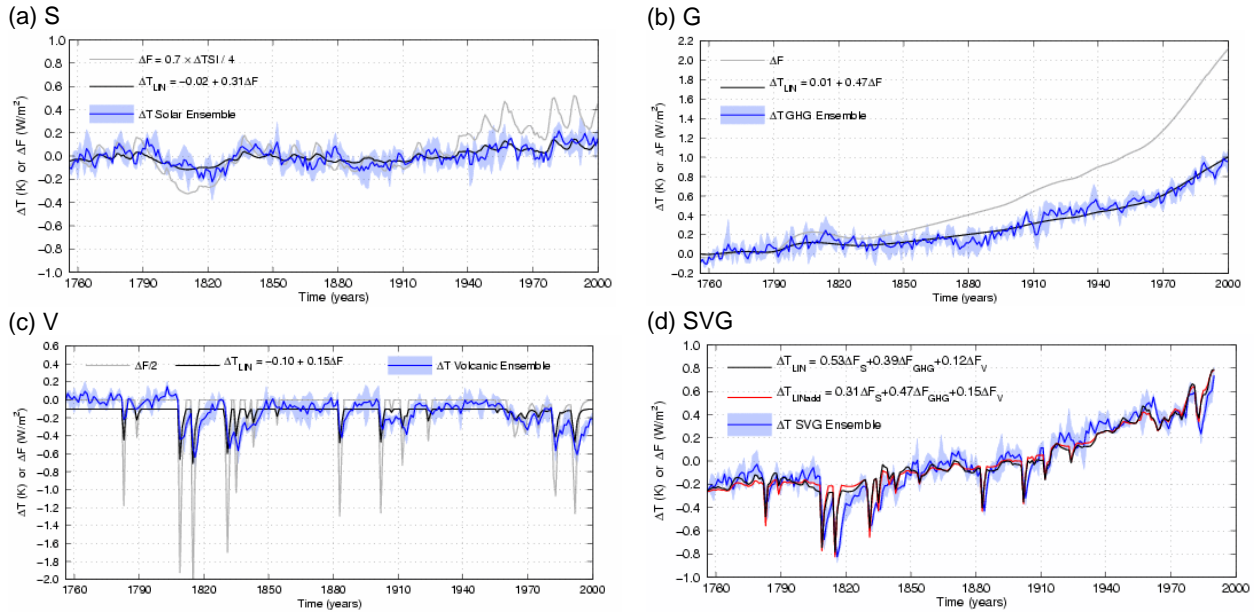


Figure 6. (a–c) Anomalies (with respect to the mean over the first 30 years) of the radiative forcing (grey), simulated global-mean temperature (blue, ensemble-mean and spread) and linear temperature response (black) for “single forcing” simulations S, G and V, respectively. (d) Simulated global-mean temperature (blue, ensemble mean and spread) and two linear response models for the “all forcing” SVG simulations, expressed as anomalies from the overall mean.

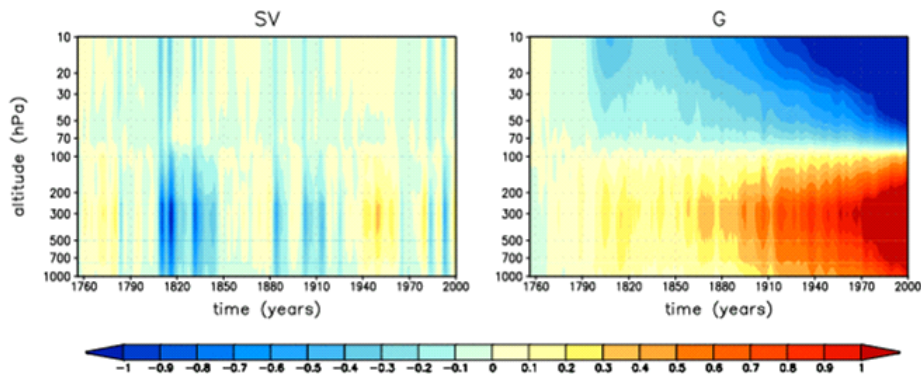


Figure 7. Global annual-mean temperature anomalies (relative to the mean of the first 30 years) as function of time and height for natural (SV) and greenhouse gas (G) experiments.

In Figure 8 near-surface air temperature, sea-level pressure and precipitation fields from the final decades (1971–2000 means) of the G and SV simulations are compared to the corresponding long-term mean fields from the pre-industrial control experiment. Simulation G shows a hemispheric-wide warming (Figure 8a), except for a significant cooling south of Greenland which is connected to a decline of the meridional overturning circulation in North Atlantic. The mean sea-level pressure anomalies project on the AO/NAO pattern (Figure 8b) and the NAO index tends to become more positive in the last decades of simulation G. Winter precipitation increases in the high latitudes of the NH while the subtropics become drier. The simulation forced only by natural forcings shows very few significant changes in 1971–2000 with respect to the control run (Figure 8d–f).

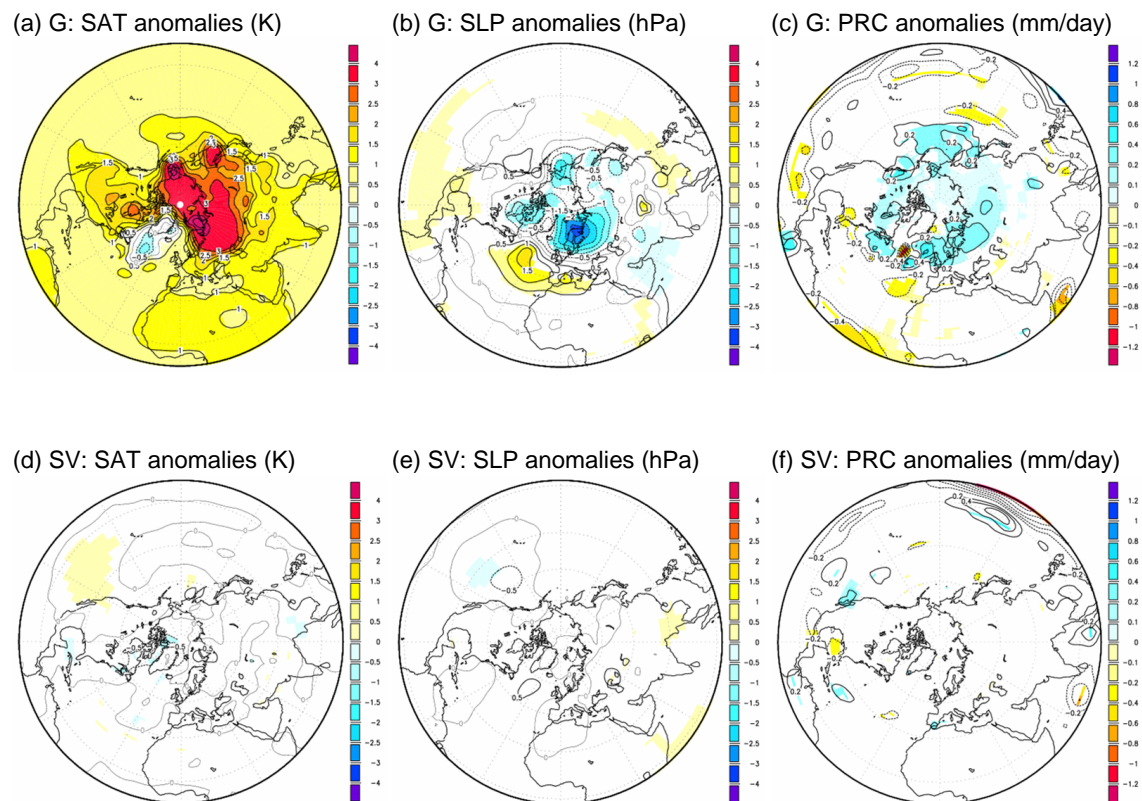


Figure 8. Simulated 1971–2000 winter temperature (a, d), sea-level pressure (b, e) and precipitation (c, f) anomalies with respect to the pre-industrial control run for greenhouse gas (G, a–c) and natural (SV, d–f) simulations.

We also analysed the NAO variability and its possible connection to external forcing during the Dalton Minimum (1790-1830) as well as after strong volcanic eruptions. We found an increased incidence of the negative phase of the NAO in the first two years following a volcanic eruption, which is at odds with observations. Note that in these ECHO-G simulations the volcanic forcing was approximated by a reduction in solar irradiance, thus omitting some important aspects of the volcanic influence on the Earth's radiation budget – particularly the absorption that causes stratospheric warming and which might be important in affecting the polar vortex and the NAO in the aftermath of a large eruption. Details are discussed in the SO&P deliverable 14 and in Cubasch *et al.* (2005).

6.3.3. Workpackage 3: Amalgamation and calibration of 500 years of high-resolution climate data

The main objectives of this workpackage were (i) to assemble, assess and, where possible, develop improved reconstructions of past climate variations; (ii) to identify and interpret the major climate variations depicted by these reconstructions; and (iii) to provide the explicit measures of uncertainty that are necessary to allow quantitative comparison between these reconstructions and climate model simulations (see workpackage 4). To achieve these objectives it was also necessary to assemble many existing raw climate proxy records and to assess their interpretation and processing.

A number of new reconstructions were developed with either full or partial funding from the SO&P project. These are listed in Table 3 including a reference where they are fully described. Short descriptions of some of these reconstructions are also provided in the

following subsections of this report.

Table 3. New reconstructions developed with full or partial support from the SO&P project.

Climate variable	Season(s)	Region	Resolution	Period	Reference
Temperature	Summer	Western Europe	Spatially resolved (5° resolution)	1068–1987	Guiot <i>et al.</i> (2005)
Temperature	Winter, Spring, Summer, Autumn	Europe	Spatially resolved (0.5° resolution)	1500–1900	Luterbacher <i>et al.</i> (2004); Xoplaki <i>et al.</i> (2005)
Precipitation	Winter, Spring, Summer, Autumn	Europe	Spatially resolved (0.5° resolution)	1500–1900	Pauling <i>et al.</i> (2006)
Drought severity	Summer	Mediterranean	Spatially resolved (2.5° resolution)	1350–2000	Nicault <i>et al.</i> (2006a)
Temperature	Summer	NW Eurasia	Area-average	1–2000	Briffa <i>et al.</i> (in preparation)
Sea-surface temperature	Annual	Tropics	Area-average	1750–1989	Wilson <i>et al.</i> (2006)
Antarctic Oscillation	Summer	Southern Hemisphere	Index time series	1905–2000	Jones & Widmann (2004)
Temperature	Winter, Summer, Annual	Northern Hemisphere	Spatially resolved (5° resolution)	1400–18550	Rutherford <i>et al.</i> (2005)
Temperature	Mixed	Northern Hemisphere	Index of the spatial extent of warmth	800–1995	Osborn & Briffa (2006)

6.3.3.1. Data bases of proxy record measurements

A number of sets of raw climate proxy records have been assembled to support the development of improved climate reconstructions. One particular achievement that will be of use to the scientific community after the completion of the SO&P project is the development and population of the DENDRODB tree-ring data base by CNRS/UDESAM. The DENDRODB data base now contains almost 800 sites from 28 countries (Figure 9), covering all of Europe (with a notable density of sites in Mediterranean countries). This data base includes 136 sites with data series longer than 300 years (i.e., starting before 1700). Besides ring-width measurements, the collections at many of these sites include density data – e.g., minimum and maximum density. This data base was constructed using PostgreSQL on a Linux server and is available at the following web site: <http://servpal.cerege.fr/webdbdendro/>. The web interface has a new design and users can extract either raw or indexed (standardised) series. A new tool has also been added to allow users to use a new standardisation tool (ARGC, see section 6.3.3.2).

6.3.3.2. Standardisation of tree-ring records

Many regional or hemisphere-scale temperature reconstructions include (or, in some cases, rely entirely on) tree-ring data, especially reconstructions that span the entire last millennium or longer. A particular difficulty that arises in the use of tree-ring records is the need to account for fluctuations in tree growth over time that are the result of factors other than

climate. The relationship between tree geometry and age is a major issue because tree rings tend to be narrower the older the tree becomes. Many methods (low-pass filter, fitting exponential functions, fitting polynomial functions, autoregressive modelling, etc.) have been used to account for this effect, but a majority of these methods remove or suppress the low and medium frequencies of the chronologies, including real fluctuations of climatic origin. Few methods have been developed to remove the age trend and yet keep the low-frequency climate signal in the chronologies (e.g., Briffa *et al.*, 2001). They are based on the theoretical (or, more usually, empirical) growth curve based on cambial age and have been applied by Briffa *et al.* (1992), Esper *et al.* (2002) and others to climate reconstruction.

There are still some problems that arise in applying these methods. First, they need a very large sample of tree-ring data covering a given region, and second, the inclusion of populations which exhibit an age trend that differs greatly from the theoretical/empirical growth curve for that region could induce large errors.

CNRS/UDESAM have developed and tested a new method intended to address the latter issue: the *adaptive* regional growth curve (ARGC), using the Artificial Neural Network method. The tree growth is expressed as a function of its cambial age *and* two other parameters related to the shape of the growth curve during the first decades of the tree's lifetime (Nicault *et al.*, 2006b).

Separately, UEA have also developed new standardisation methods (size-adjusted regional curve standardisation – Melvin, 2004) that, in a similar way, adapt the assumed “expected” growth curve according to the size and/or growth rate of individual trees. For the SO&P project, UEA have applied this method to tree-ring width data from Scandinavia and northern Russia, developing a 2000-year reconstruction of summer temperature for the region (Briffa *et al.*, in preparation).

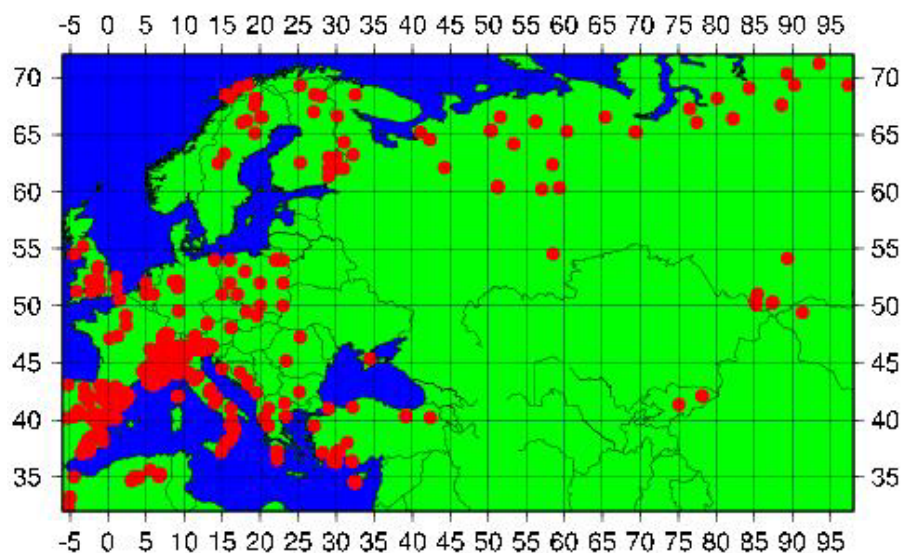


Figure 9. Map of sites with tree-ring data currently available within DENDRODB.

6.3.3.3. *New reconstructions of European temperatures*

Two major new reconstructions of European temperatures have been developed during the SO&P project.

The UBERN group have developed gridded, seasonal temperature reconstructions based on natural proxy records, documentary evidence and early instrumental temperature measurements that span all of Europe for the last 500 years (Luterbacher *et al.*, 2004; Xoplaki *et al.*, 2005). These reconstructions (Figure 10) indicate that the late 20th and early 21st century European climate is very likely (>95% confidence level) warmer than that of any time during the past 500 years. European winter average temperatures during the period 1500 to 1900 were ~0.5°C lower (0.25°C for annual mean temperatures) than the average temperature of the 20th century. The reconstructed summer temperatures, however, were not systematically cooler before 1900 than after 1900, though 2003 was by far the hottest summer.

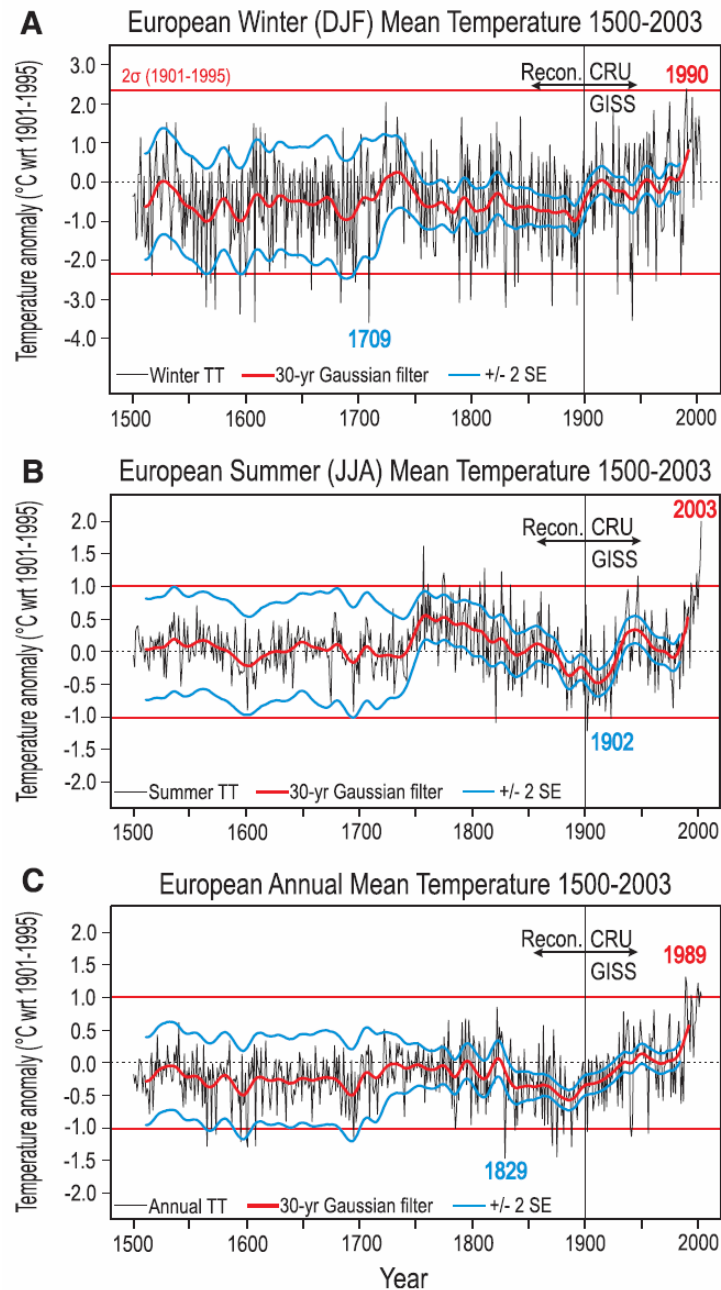


Figure 10. (a) Winter, (b) summer, and (c) annual European-average temperature anomalies (relative to the mean of the 1901–1995 calibration period) from Luterbacher *et al.* (2004). The 30-year smoothed reconstruction and its ± 2 standard errors are indicated by the red and blue curves, respectively.

CNRS/UESAM have developed a new method of multi-proxy reconstruction of climate and have applied it to reconstruct summer temperatures over western Europe since 1068 (Guiot *et al.*, 2005). The method is a combination of an analogue technique, which is able to deal with missing data, and an artificial neural network technique for an optimal non-linear calibration of the proxy series against climate variables, and then a bootstrap technique for estimating appropriate error bars for the reconstruction. The reconstruction of western European summer temperatures used this method together with long tree-ring width series, grape harvest dates, Greenland isotope series, and temperature indices based on historical documents. The time series obtained by averaging the gridded April-to-September mean temperature estimates across the reconstruction domain (10°W–20°E, 35°N–55°N) is shown in Figure 11. Comparison with the instrumental temperature record indicated that about 70% of the temperature variance was reconstructed, and the amplitude of the observed variations appears to be particularly well reconstructed. It appears that individual yearly estimates of past western European temperature may (i.e., considering the estimated uncertainty range) have reached levels equivalent to recent observations on 14 occasions during the last millennium, but earlier multi-decadal trends do not approach the degree of general warmth observed in the most recent decade. The reconstruction is in good agreement with temperature changes over the last 500 years that have been independently estimated from temperature profiles measured in ground boreholes. The Little Ice Age (1500–1800) reconstructed summer temperatures were 0.1 to 0.4°C colder than the 1961–1990 period.

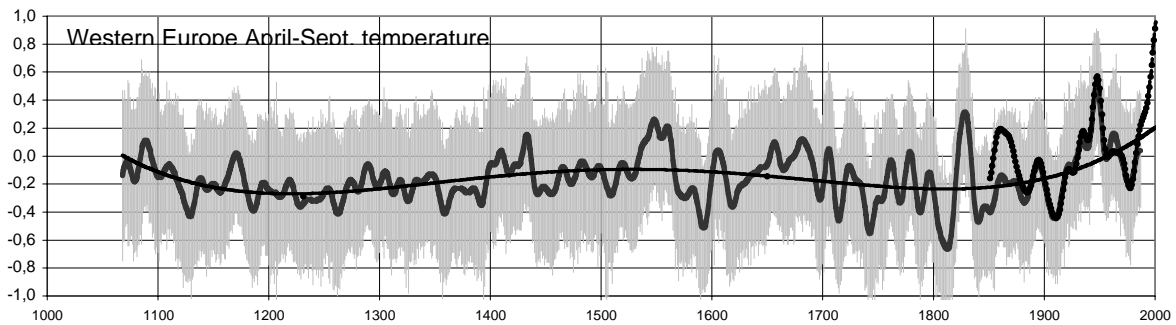


Figure 11. Reconstruction of the April–September temperature for western Europe [10°W–20°E, 35°N–55°N] from Guiot *et al.* (2005). The values are expressed as anomalies from the 1961–1990 mean and are smoothed with a 10-year low-pass filter. Grey shading is used to indicate the ± 2 standard error confidence limits. The instrumental temperature record from 1850–2001 is also shown.

6.3.3.4. New reconstruction of European precipitation

UBERN produced a new, gridded, seasonal-mean precipitation dataset covering Europe back to 1500, using many early instrumental observations, documentary records and natural climate proxies as predictors in a multi-variate statistical reconstruction. Extensive details and discussion are provided in Pauling *et al.* (2006). An overview of the seasonal precipitation evolution over the last 500 years is given by time series of European-mean precipitation (Figure 12).

The winter (DJF) reconstruction (Figure 12a) displays little variability from 1500 to 1700. Thereafter, interdecadal variability increases with a sharp rise evident at approximately 1705–1720. This is followed by a pronounced decline to the driest reconstructed values in the following two decades. A second positive peak is reached around 1770. During the 19th

century a slow decrease can be observed and the 20th century is characterized by a positive trend. The wettest winter on record is 1720 when precipitation reached around 200 mm. The dry counterpart occurred in 1744 with only 124 mm of precipitation. During the period 1500–1700, the 2 standard error uncertainty of the inter-annual variability is on the order of 35 mm. Afterwards, this gradually reduces to values of 25–30 mm in the 20th century.

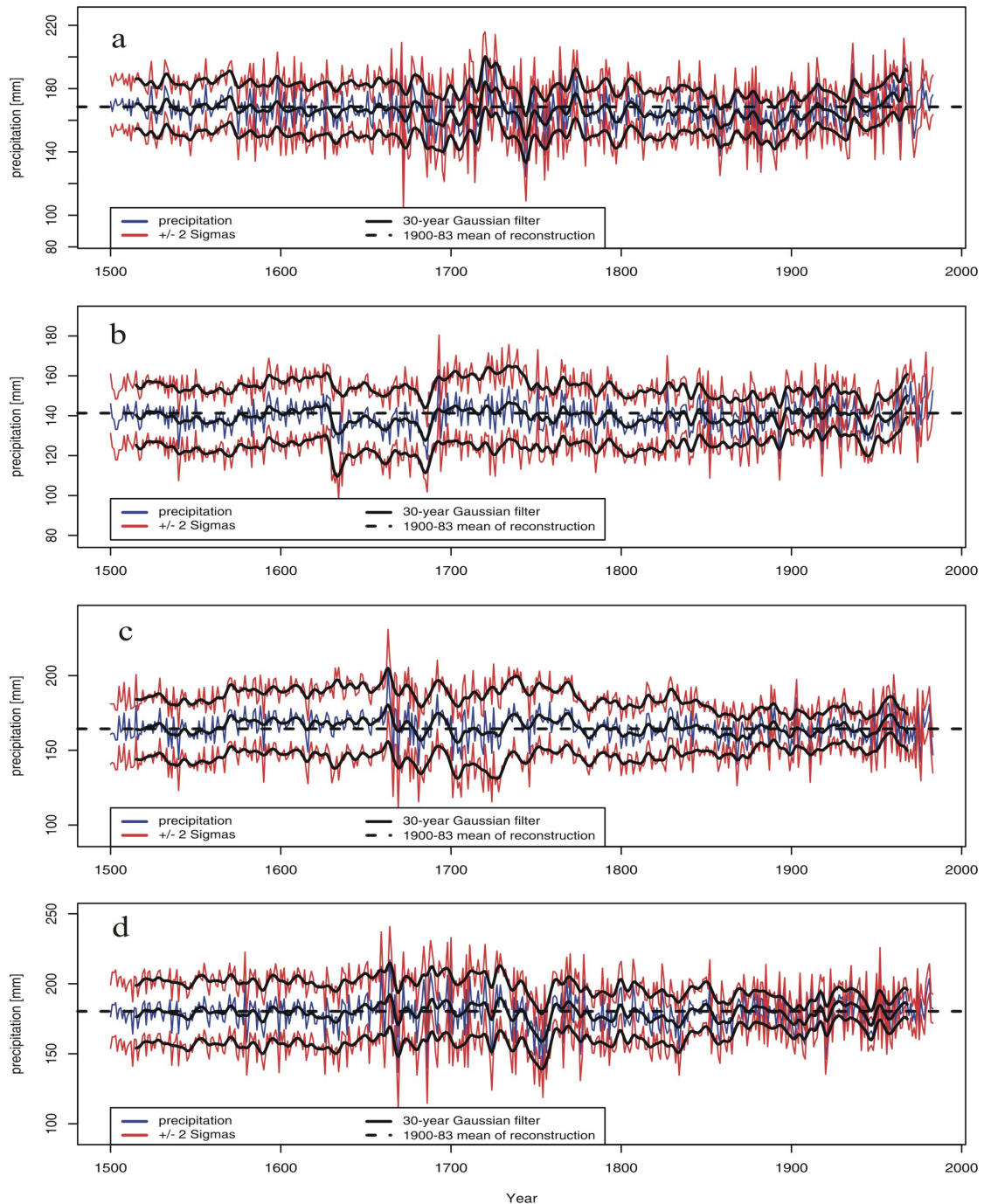


Figure 12. Spatially-averaged time series and uncertainty estimates of the European precipitation reconstructions, averaged over the land grid points with the domain 30°W–40°E, 30°N–71°N, for (a) winter, (b) spring, (c) summer, and (d) autumn, from Pauling *et al.* (2006). Individual yearly values and their uncertainties are in blue and red, respectively, with 30-year smoothed series shown in black. The smoothed interannual uncertainties do not provide real uncertainty estimates on decadal timescales.

Spring (MAM) precipitation (Figure 12b) shows a steady increase from 1540 to around 1620. Thereafter, multidecadal variability increases until 1700. The first half of the 18th century is characterized by rather stable but above average precipitation levels. This is followed by a decline until 1800. The following 180 years show a gradual increase with a short period of rather low precipitation around 1950. Spring precipitation extremes occur during the second half of the 17th century: The year 1686 is the driest (118 mm) and 1693 the wettest (163 mm) spring on record. During 1500–1750 the uncertainty amounts to approximately 35 mm. After 1750 it is considerably less at about 25 mm. In the course of the 19th century, the uncertainty reaches reduces and reaches a level that is continued into the 20th century (20 mm) with similar variability.

Summer (JJA) precipitation (Figure 12c) from 1500 to 1660 is characterized by a gradual increase. During the following 100 years, high decadal variability can be observed. From 1800 to 1983 variability decreases with no overall trends. Extremely dry summers occur in 1666 (142 mm) and 1669 (137 mm) while 1663 (204 mm) is the wettest summer on record. The uncertainties remain the same from 16th to 18th century (40 mm) but decrease slightly after 1800 (35 mm) and reach values around 25 mm in 1900.

Autumn (SON) precipitation reveals no decadal variability and no trend from 1500 to around 1650 (Figure 12d). Thereafter, strong decadal fluctuations can be observed. Around 1800, however, variability is dominated by high inter-annual variability with no obvious trend. The wettest autumn on record is estimated to be 1664 (217 mm), soon followed by the driest in 1669 (137 mm). The uncertainty of this reconstruction remains rather stable until 1750 (40 mm) when it gradually decreases until 1860 when it reaches the level of the 20th century (20 mm).

These new reconstructions have been used together with independent pressure reconstructions (i.e., they share no common predictors) by Luterbacher *et al.* (2002) to investigate the stability of the connection between European precipitation and large-scale atmospheric modes using running correlation analysis (Pauling *et al.*, 2006). Figure 13 depicts 30-year running correlations of winter (DJF) precipitation averaged over two regions with the first three Principal Components (PCs) of the North Atlantic/European SLP reconstructions. The pressure pattern of the first PC resembles the NAO pattern with pressure centres over Iceland and the Azores. The second PC is associated with a pressure centre west of Ireland. The pattern of the third PC features a blocking situation with a pressure centre over north-eastern Europe. Figure 13 shows that the correlations between the atmospheric circulation patterns and precipitation over southern Spain/Morocco or central Europe vary during the last 500 years on multi-decadal time scales. The first PC is the most important pattern for precipitation over southern Spain/Morocco (Figure 13a), while PC 2 is only relevant during some periods. Interestingly, PC 3 was important during the first part of the 18th century. Over central Europe (Figure 13b), PC 3 dominates precipitation throughout the last 500 years. Even though the two other patterns are less important, PC 2 does show highly significant correlations with central European precipitation during several periods.

This new precipitation dataset has also been used to model historic glacier fluctuations (Steiner *et al.*, 2006). Together with seasonal temperature reconstructions from Luterbacher *et al.* (2004) they were used to train an Artificial Neural Network model of glacier-length fluctuations. This model was then used to investigate the relative importance of different climate configurations for the Lower Grindelwald Glacier, Switzerland, during four well-documented historical periods of advance (1590–1610, 1690–1720, 1760–1780, 1810–1820) and retreat (1640–1665, 1780–1810, 1860–1880, 1945–1970). The results indicate that different combinations of seasonal temperature and precipitation were responsible for the variations in glacier length. As an example, Figure 14 shows the relative importance of the various climate parameters for the 1690–1720 advance. Variations in spring temperature and precipitation appear to be the most important in explaining this period of glacier advance. See Steiner *et al.* (2006) for results from the other periods of advance or retreat.

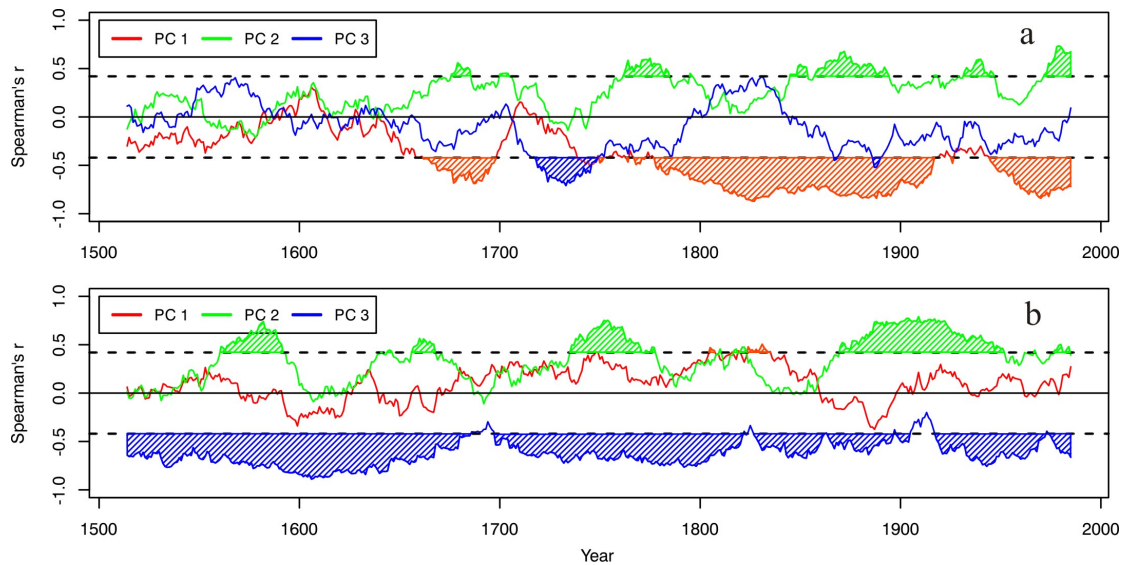


Figure 13: Thirty-year running correlations of the first three principal components of winter SLP reconstructions by Luterbacher *et al.* (2002; re-calculated using no precipitation predictors) with winter precipitation (a) averaged over southern Spain and Morocco (10°W–0°W, 33°N–40°N) and (b) averaged over parts of central Europe (3°E–5°E, 48°N–50°N). The dashed lines denote the 5% significance threshold based on 1,000 Monte-Carlo simulations.

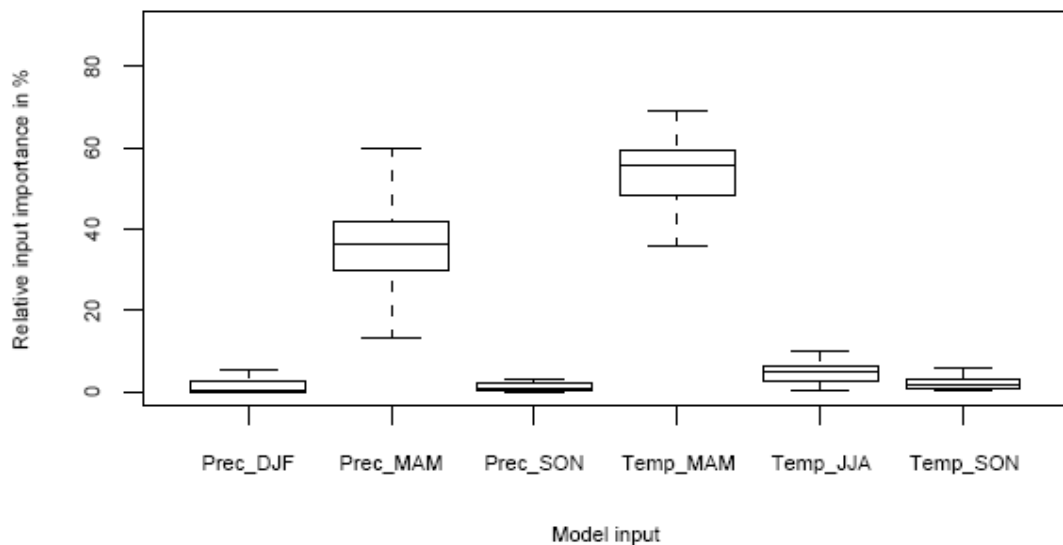


Figure 14: Relative importance of climate input variables to length fluctuations of the Lower Grindelwald Glacier (Switzerland) for the 1690–1720 advance. For each input variable the median, the first and third quartile (lower/upper box) and the 95% confidence interval for the median (lower/upper whisker) of 30 model runs are given (from Steiner *et al.*, 2006).

6.3.3.5. *New reconstruction of Mediterranean drought*

The Palmer Drought Severity Index (PDSI) represents an integrated measure of available soil moisture, standardised and expressed in relation to ‘average’ regional conditions, so as to allow direct comparison of the relative magnitude of drought or excessive moisture in different regions. Reconstructions of summer PDSI have been produced by CNRS/UDESAM

on a 2.5° grid covering the whole Mediterranean region (32.5°–47.5°N, 10°W–50°E) for the period from 1350 to 2000, with a 1901–2000 calibration period. The PDSI was reconstructed using a combination of an analogue technique, which is able to deal with missing data, coupled to an artificial neural network technique for an optimal non-linear calibration (Guiot *et al.*, 2005). A bootstrap technique was used to calculate the error bars associated with the reconstructed PDSI values. The predictors were proxy data at 136 sites covering the countries surrounding the Mediterranean basin, accessed from the DENDRODB tree-ring data base (see section 6.3.3.1). Only series longer than 300 years (i.e., starting before 1700) were used. The predictor data included total ring width, late-wood width and maximum late-wood density chronologies: a total of 165 records.

For the western and central Mediterranean regions, the most important results can be summarized as follows: (i) the 16th century and the first half of the 17th century are characterized by a strong PDSI variation between alternating dry and wet periods; (ii) then after a very dry period (1650–1660), wet conditions clearly prevailed until 1760; and (iii) the 1765–1785 period is characterised by a succession of very dry years, after which, to the beginning of 20th century, the climate was generally wet except for a drier period between 1850 and 1870. In the eastern Mediterranean region, the PDSI reconstruction shows weaker low-frequency variations and no obvious extended periods of dry or wet conditions. High variability in moisture availability characterises the reconstruction for this region, with numerous short-lived extremes.

6.3.3.6. New reconstruction of tropical sea surface temperatures

The first coral-based reconstruction (Figure 15) of tropic-wide average sea-surface temperatures (SSTs) was developed from 14 disparate coral records located in the Indian and Pacific Oceans (Wilson *et al.*, 2006). Over the most replicated period, the reconstruction explains 57% of the tropical SST variance. However, the strength of this signal weakens markedly as the number of coral records decreases. The reconstruction is highly robust between 1850 and 1993, with some fidelity indicated back as far as the mid 18th century, but we have little confidence in the reconstruction prior to that. These results suggest that ambiguities in the low-frequency domain of $\delta^{18}\text{O}$ measurements can be overcome by pooling multiple time series from different locations around the tropics.

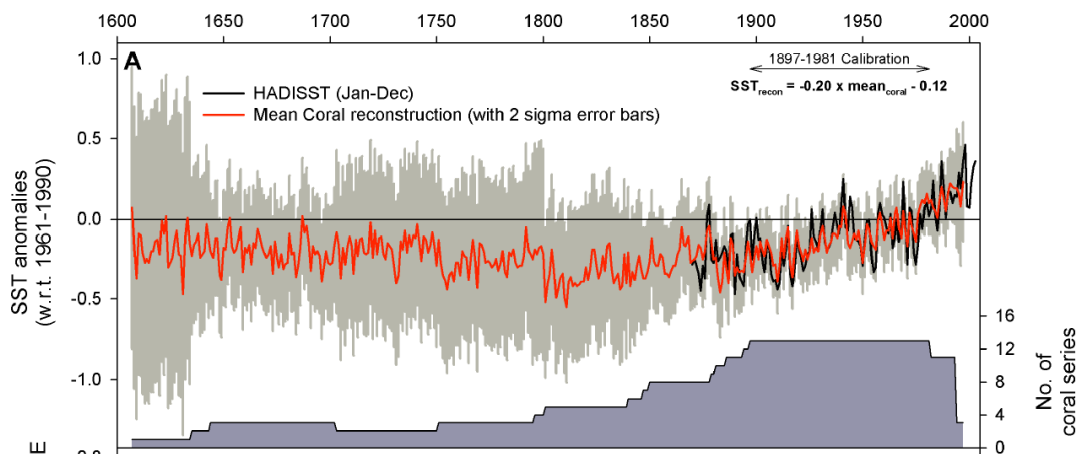


Figure 15. Coral-based reconstruction of annual-mean tropical-mean sea surface temperatures (red) with ± 2 standard error ranges (grey), compared with observed temperatures (black). The number of coral records available for the reconstruction is shown below; confidence in the reconstructed values before ~1750 is low.

6.3.3.7. *New reconstruction of the Antarctic Oscillation*

The GKSS contribution to this workpackage mostly concentrated on reconstructions of the Antarctic Oscillation (AAO). The AAO, or Southern Hemisphere Annular Mode (SAM) is the major mode of extra-tropical atmospheric circulation in the Southern Hemisphere (Thompson and Wallace, 2000), and characterises fluctuations in the strength of the circumpolar vortex. A trend during the past three decades in austral summer towards a positive AAO (stronger circumpolar westerly flow) has recently attracted much interest, with studies concentrating on anthropogenic causes (e.g., Thompson and Solomon, 2002; Shindell and Schmidt, 2004). To assess how unusual these recent trends are requires some knowledge of the magnitude of AAO variability during previous decades, yet until recently estimates of the AAO index have only been available for the re-analysis period (1948 or 1958 to present). As part of the SO&P project, reconstructions of the strength of this index have been developed using long station records of sea-level pressure (SLP). Reconstructions have been produced for austral summer and the other three seasons for three periods (1905–2001, 1951–2001 and 1958–2001), and for austral summer and autumn back to 1866 (the latter results are not discussed here). Although the shorter reconstructions do not extend back further than the reanalysis period, they nevertheless allow an assessment of how well the reconstruction method performs when a greater number of Antarctic station records are available. In addition, these shorter reconstructions provide a consistent estimate of the AAO index for the whole re-analysis period (the re-analysis data may be affected by a number of potential inhomogeneities).

The predictand data were ERA40 reanalysis data, obtained from the ECMWF. These data cover the period 1958–2003. Southern Hemisphere station SLP records with data to 2001 were obtained from Phil Jones (Climatic Research Unit; see also Jones *et al.*, 1999) and from Rob Allen and Tara Ansell (Hadley Centre). We used multiple linear regression to estimate the AAO index from the leading principal components (PCs) of normalised station SLP (so-called principal component regression). For model fitting we define the AAO index as the first PC of detrended ERA40 seasonal mean SLP for the domain 20°S–80°S. Further information on the method and data can be found in Jones and Widmann (2003, 2004).

The quality of the statistical model that can be achieved differs between seasons (Figure 16). The best fit is obtained in December–January (DJ), followed by March–May (MAM) (reflected in the size of the 95% confidence intervals). Only a poor fit is achieved for statistical models of the AAO index in September–November (SON) and, particularly, June–August (JJA). These variations in the quality of the statistical model result from the differing spatial structure of the AAO in these seasons, and hence where the centres of high AAO variability are located in relation to the land areas where the measurement stations are located, and to the differing proportion of SLP variance explained by the AAO. The AAO structure in DJ and MAM has a greater proportion of high loadings located over the continents and New Zealand than occurs in JJA and SON.

In DJ, as described in Jones and Widmann (2004), large positive values and positive trends of a similar magnitude to those over the past decades are evident around 1960, and strong negative trends occur afterwards. The strongly positive Antarctic Oscillation index and large positive trend during a period before ozone depleting chemicals were emitted into the atmosphere and before strong anthropogenic warming occurred, together with the negative trend, suggest that natural forcing factors or internal mechanisms in the climate system must also strongly influence the state of the Antarctic Oscillation. The largest trends in recent decades are in southern summer (DJ) followed by autumn (MAM), in agreement with Thompson and Solomon (2002) and Renwick (2004).

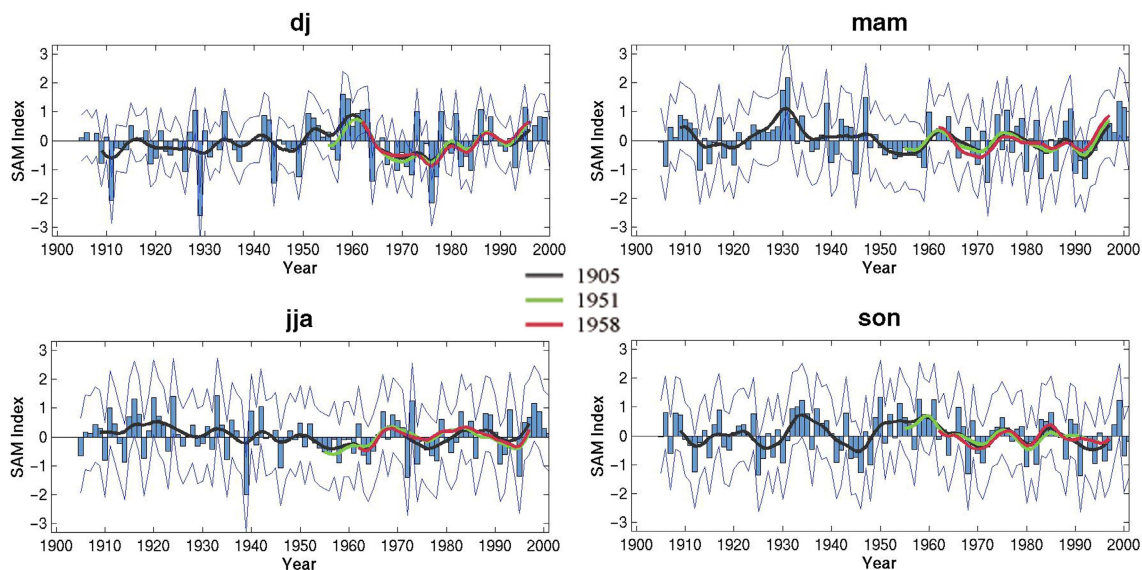


Figure 16. The 1905 reconstructed annual AAO index values (bars) and 95% confidence intervals (thin lines), and the 1905, 1951 and 1958 reconstructions subjected to a 9-year hamming filter (thick lines), for each of the seasons considered.

6.3.3.8. *New reconstructions of Northern Hemisphere temperatures*

Work described under workpackage 4 (see section 6.3.4.2) is particularly relevant to the reconstruction of NH temperatures from noisy proxy data (indeed it is also relevant to the other reconstructions that have been described in workpackage 3), because it raises the likelihood that many existing temperature reconstructions might underestimate the magnitude of departures from the climate of the calibration period. For most published NH temperature reconstructions, this might imply that the amplitude of multi-century temperature variations is underestimated. Given that few reconstructions indicate periods that are warmer than their calibration periods, any such bias is unlikely to imply that periods of greater warmth are underestimated. Unfortunately, the model-based evaluations of potential reconstruction bias can only indicate under which conditions such reconstruction bias might exist – they cannot be used to determine the magnitude of any bias.

Work has been undertaken within this workpackage towards the production of NH temperature reconstructions that are less likely to be biased. Three complementary approaches have been followed.

The first approach seeks to avoid the potential biases and uncertainties associated with regression-based calibration of NH temperature reconstructions by instead focussing on the spatial extent of warm or cold conditions rather than the average magnitude of warmth. A set of long (> 500 year) temperature-sensitive proxy records, all of which had previously been used to estimate mean NH temperatures in other published studies, was analyzed to estimate the numbers of records indicating warm conditions at any one time (or, alternatively, cool conditions), and from this to infer the spatial extent of warming (or cooling). This approach appears promising because it avoids some of the concerns that have been raised about certain regression methods that combine and calibrate the records into estimates of mean NH temperatures. Also, inferring the spatial extent of warming by counting records that indicate warmth should be more robust to individual outlier series, because a record is only counted once no matter how extreme its indication of warmth is. Our analysis (Osborn and Briffa, 2006) identified statistically significant periods of extensive warm and cold conditions, relative to the average from 800 to 1995 (Figure 17). The most significant and longest-

duration feature during the last 1200 years is the geographical extent of warmth in the mid-to-late twentieth century. Positive anomalies during 890-1170 and negative anomalies during 1580-1850 are consistent with the concepts of a ‘Medieval Warm Period’ and a ‘Little Ice Age’, but comparison with instrumental temperatures clearly shows the spatial extent of recent warmth to be of greater significance than during the Medieval period.

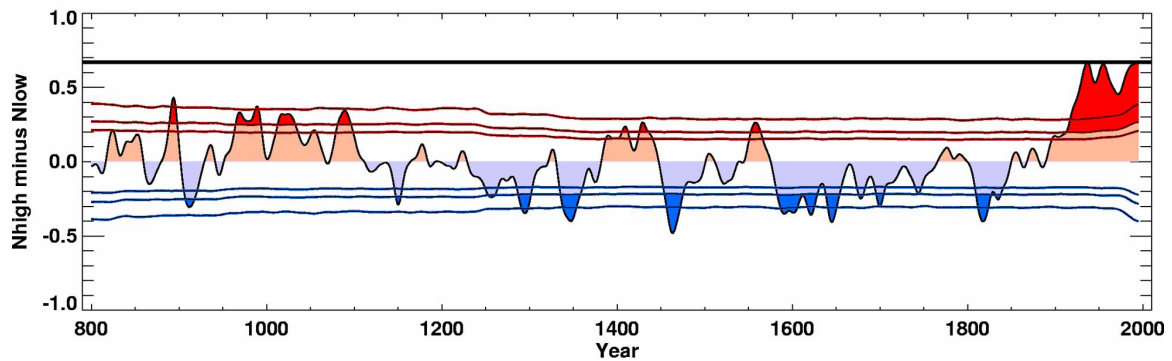


Figure 17. Difference between the fraction of the records available in each year that have normalized values > 1 and those with values < -1 for the period 800 to 1995, after smoothing to remove variations on time scales less than 20 years. Zero indicates that the number of series exceeding the upper threshold equals those with values below the lower threshold. The highest value in the series is indicated by the horizontal black line; the red and blue lines show the 99th, 95th, 90th, 10th, 5th, and 1st percentiles of distributions obtained by repeating the analysis 10,000 times with each proxy time series shifted randomly in time; and dark red and blue shading indicate times when the difference series exceeds the 95th or 5th percentiles.

Our second approach was to develop new reconstructions using the Regularized Expectation Maximisation (RegEM) algorithm which some studies indicate may be less susceptible to reconstruction bias (e.g., Mann *et al.*, 2005). These new reconstructions of NH temperature have been fully described by Rutherford *et al.* (2005). Mean temperature reconstructions are compared for the full NH (tropics and extra-tropics, land and ocean) and extra-tropical continents only, with varying target seasons (cold-season half year, warm-season half year, and annual mean). The comparisons demonstrate dependence of reconstructions on seasonal, spatial, and methodological considerations, emphasizing the primary importance of the target region and seasonal window of the reconstruction. The comparisons support the generally robust nature of several previously published estimates of NH mean temperature changes in past centuries and suggest that further improvements in reconstructive skill are most likely to arise from an emphasis on the quality, rather than quantity, of available proxy data.

Our third approach has been to consider more fully the source of potential reconstruction bias. Detailed exploration of the regression problem by METO and other SO&P partners has highlighted that unbiased regression models can be derived provided that *a priori* estimates of the uncertainty in all regression variables are available. Error models for the instrumental temperature predictands are already available (e.g., Brohan *et al.*, 2006) and we have made progress in developing quantitative error models for a network of tree-ring chronologies. This work, started with the SO&P project, is likely to come to fruition after the project has finished and may underpin future improved reconstructions of past regional and NH temperature.

6.3.4. Workpackage 4: Synthesis and interpretation of observed/reconstructed and simulated climates

All work undertaken during the SO&P project that employed a *combination* of model-simulated data and observational or proxy-based climate data was part of workpackage 4 (except that dealing with sea-level change, which was undertaken instead within workpackage 5). Applications that made combined use of models and data include (i) comparisons of simulated and reconstructed climate to assess the ability of the models to simulate past climate variations, (ii) use of simulated climates to interpret and assess the ability of proxy-based reconstructions to provide reliable quantitative information about past climate variations; and (iii) combined use of models and observational data to detect the response of climate to natural and anthropogenic forcings.

6.3.4.1. Comparing reconstructed and simulated climates

A wide range of data–model comparisons have been undertaken within this workpackage. Those that involve the assessment of the magnitude of variability or of its spatial structure implicitly incorporate both internally-generated and externally-forced variability. Analyses that specifically compare the temporal evolution of climate in the simulations and the reconstructions require special consideration of the ratio of the forced changes (the ‘signal’, in this context) to the internal variability (the ‘noise’, in this context). This is because the internal variability observed in the real climate system will not, in general, be correlated with the internal variability simulated by any model run. It is only the response to external forcings that might be expected to follow the same temporal evolution in both observations and simulations (and only, of course, if the external forcings – shown in Figure 18a-c – applied to the models are good estimates of the forcings that drove the real climate system). For this reason, it is only for cases (regions, climate variables, seasons) with a strong signal-to-noise ratio that a comparison of the temporal evolution of simulated and reconstructed climate will represent a strong test of model performance.

Given that the signal-to-noise ratio of forced change to internal variability is strongest at the largest spatial scales, and stronger for temperature than most other climate variables, most effort was directed towards comparing simulated and reconstructed temperatures at the hemispheric scale. Figure 18d shows a visual intercomparison of the ECHO-G ERIK and the HadCM3 combined NAT (for 1500–1749) and ALL (for 1750 onwards) simulations of NH temperature. As discussed extensively by Osborn *et al.* (2006), the greater 20th century warming in ECHO-G compared with HadCM3 is very likely associated with the omission of anthropogenic tropospheric sulphate aerosols in ECHO-G (Figure 18c). The ECHO-G ERIK simulation also began from relatively warm conditions in 1000 (again see discussion in Osborn *et al.*, 2006) which probably resulted in unrealistic warmth persisting through the first few centuries of that simulation. Shown in Figure 18d is an adjustment of the ECHO-G ERIK simulation achieved using results from the MAGICC simple climate model to estimate the possible magnitudes of these effects.

The three model simulations (HadCM3, ECHO-G ERIK and the adjusted version of ECHO-G ERIK) were compared with a synthesis of ten published reconstructions of NH temperature. The latter are represented in Figure 18d by grey shading to indicate the degree to which the uncertainty ranges of those reconstructed temperatures overlap. The reconstruction uncertainties were taken from the individual publications, using values appropriate for multi-decadal time scales wherever these were available. Although somewhat *ad hoc*, this semi-quantitative synthesis of published NH temperature reconstructions facilitates data–model comparisons which are not reliant on individual reconstructions, and that focus attention on the uncertainty ranges of the reconstructed values rather than the central values of these ranges. Although the overlap of reconstructed temperatures is relatively wide, it is nevertheless promising that the HadCM3 simulation lies close to the regions of greatest

overlap throughout most of the last 500 years. The ECHO-G ERIK simulation is also close to the regions of greatest overlap from 1250 to 1850, but deviates significantly from the reconstructed ranges outside of these times. At least part of these deviations can be explained by the warm initial conditions and the omission of tropospheric sulphate aerosol forcing, because when adjustments to the ERIK simulation are made using estimates of these factors, there is better agreement with the reconstructions of NH temperature. It should be noted, however, that both the climate conditions in 1000 and the magnitude of tropospheric sulphate aerosol forcings during the 20th century are very poorly known, and the adjustments applied are themselves quite uncertain.

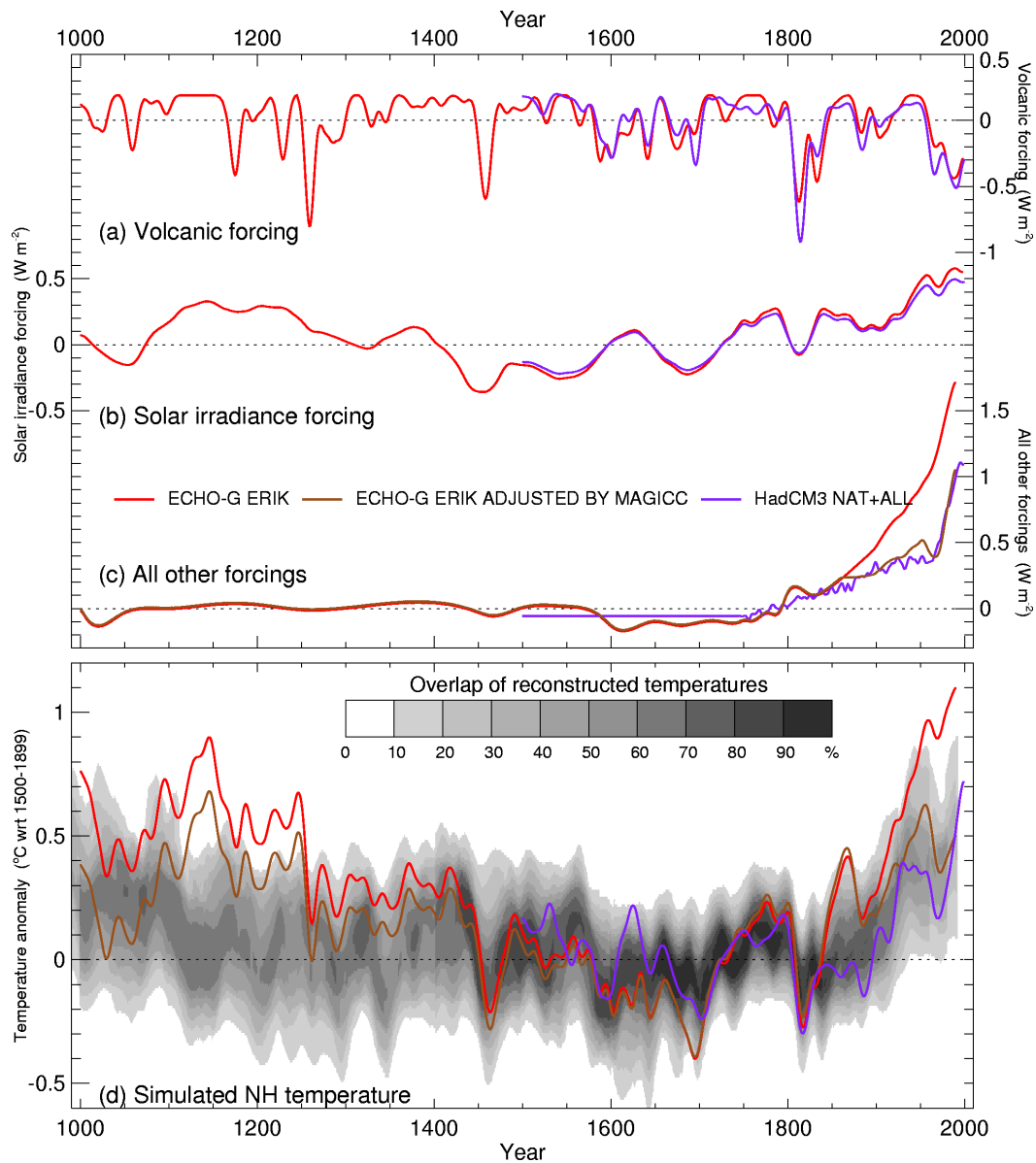


Figure 18. Comparison of the (a) volcanic, (b) solar, and (c) other forcings used in the HadCM3 and ECHO-G simulations, and (d) their simulated NH temperatures overlaid on a multi-study composite of published NH temperature reconstructions. All series have been expressed as anomalies from their 1500–1899 means and then smoothed with a 30-year low-pass filter. Also shown in brown are the ECHO-G results after modification using simulations with the MAGICC simple climate model to estimate the effects of too warm initial conditions and the neglect of anthropogenic tropospheric sulphate aerosol forcing. In (d), the grey shading expresses the degree to which the 95% confidence ranges of 10 published temperature reconstructions overlap.

Quantitative comparisons of the simulated and reconstructed climate variability have been undertaken for a number of other regions and variables. For example, Casty *et al.* (2005) showed that the basic modes of wintertime 500 hPa geopotential height variation are comparable in simulations and reconstructions. Zorita *et al.* (2004) evaluated a simulation with ECHO-G that is similar to ERIK (but only spans the period since 1500) and compared it to reconstructions in terms of global temperature, NAO, and the Late Maunder Minimum. Raible *et al.* (2005) investigated long-term trends in simulated, observed, and reconstructed atmospheric circulation patterns. They showed that trends in certain atmospheric indices observed over the most recent 50 years are very unlikely to be of natural origin and can be attributed, at least partly, to external causes.

Comparisons were also undertaken for the tropics, making use of the new reconstruction of tropical-mean SST described in section 6.3.3.6 (Wilson *et al.*, 2006). Low frequency agreement between the reconstruction and the tropical SST from the two climate model simulations indicates that the 1990s were the warmest period in the last 250 years in the tropics and that there has been a 0.5–1.0 °C increase in annual tropical SSTs from the coolest period in the early 19th century to the present time (Figure 19). Comparative analysis suggests that prior to the 20th century, natural forcing (the combined influence of solar and volcanic forcing) explains much of the reconstructed variability in tropical climate. However, the natural forcing used in these simulations cannot explain 20th century warming, which is only reproduced by simulations that include anthropogenic forcing (essentially increases in greenhouse gas concentrations).

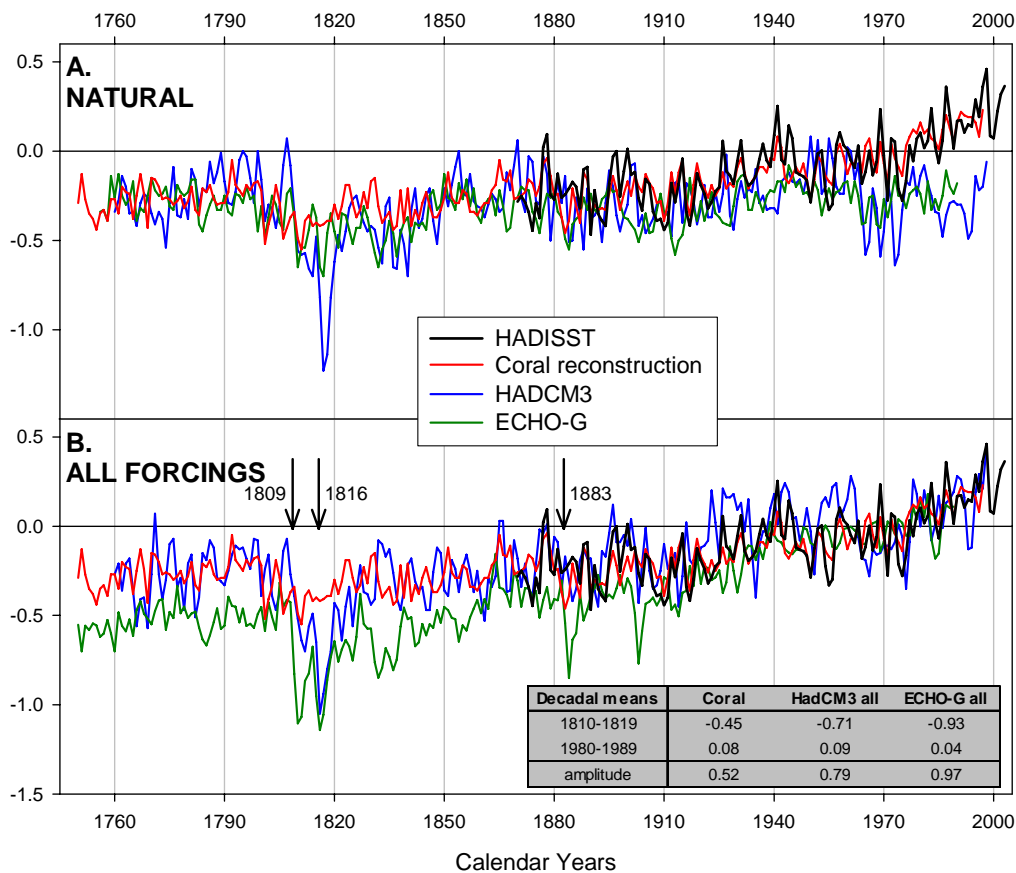


Figure 19. Comparison of the mean coral reconstruction (Wilson *et al.*, 2006) with the HadCM3 and ECHO-G model simulations: (a) with runs using only natural forcings (the mean of the simulated data was adjusted to the mean of the scaled reconstruction over the pre-anthropogenic period, 1760–1849); (b) with runs using anthropogenic and natural forcings (all series are expressed as anomalies relative to their 1961–1990 means).

In Jones *et al.* (2003), we presented evidence for changes in the seasonal range of temperatures during the last millennium, and noted that it would be a useful additional assessment of climate model performance to consider simulated changes in seasonal temperature range. Figure 20 shows simulated time series of seasonal temperature range from HadCM3 and ECHO-G for six small regions in Europe and east Asia. These models do, in general, simulate changes in the summer–winter temperature differences that are in agreement with many of the (limited) instrumental and documentary-based records. A reduction in seasonal temperature range over the past one to two centuries is apparent in both models and observational records. The simulations of the summer and winter temperatures themselves are, however, quite different between the two models. In the ECHO-G simulation, 20th century warming occurs in both summer and winter, but is much greater in winter than in summer. In the HadCM3 simulation, on the contrary, the reduced seasonal temperature range arises because of a combination of moderate winter warming and virtually no summer temperature trends during the last 150 years.

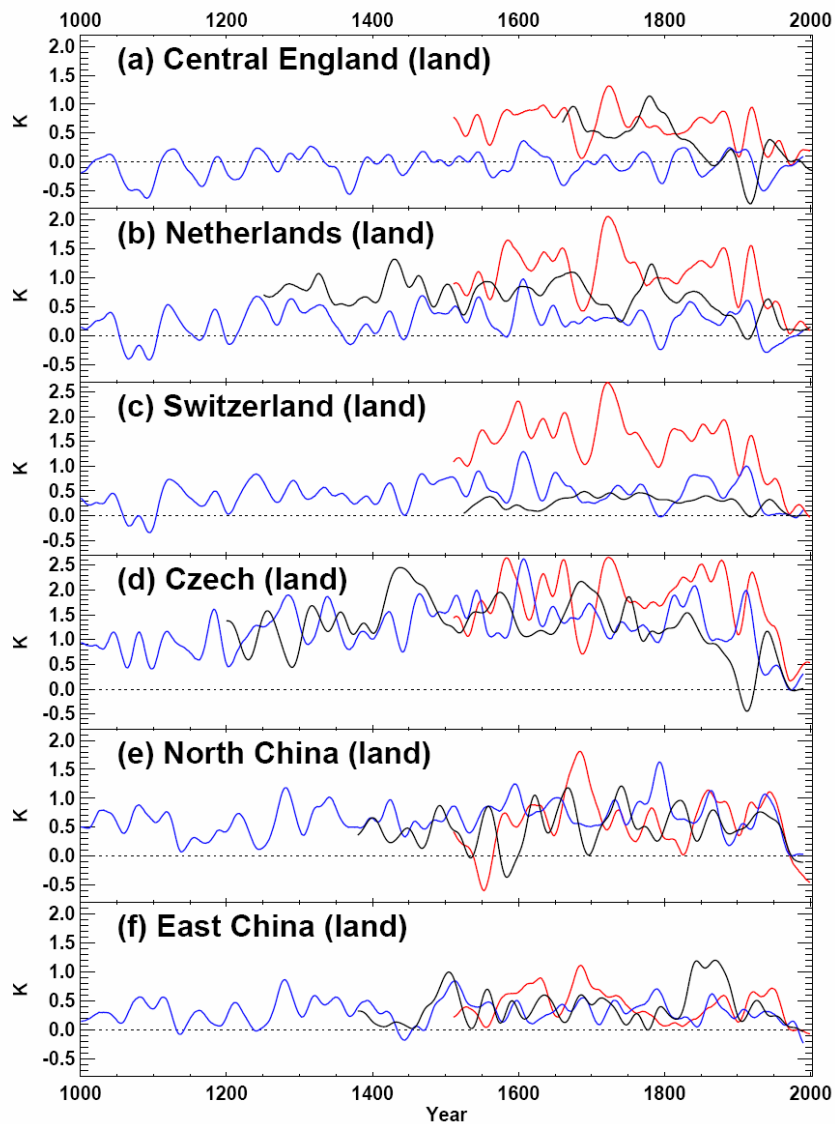


Figure 20. Summer minus winter temperature time series (K) for six land regions in the NH, as simulated by HadCM3 (red) and ECHO-G (blue) and as estimated using long instrumental and documentary records (black), for (a) central England, (b) Netherlands, (c) Switzerland, (d) Czech Republic, (e) North China, and (f) East China. Each series is expressed as anomalies from its 1961–1990 mean and then smoothed with a 50-year Gaussian filter.

Figure 21 presents the first EOF of the annual surface air temperature of three externally-forced simulations (HadCM3, ECHO-G “Columbus” and ECHO-G ERIK, respectively) and of the gridded reconstruction of Luterbacher *et al.* (2004). The comparison of the simulated EOF loading patterns and the EOF patterns of the empirical reconstruction shows strong spatial resemblances with higher values towards the northeast of the European continent. The magnitude is largest in the ECHO runs. This resemblance between simulations and reconstructed variability is not, however, as strong between the principal component time series associated with these EOFs. The ECHO-G simulations show higher temporal variability compared to HadCM3 and the reconstruction. Trend calculations indicate an important disagreement between the model runs and the reconstruction, though this is not shown here because only the component of temporal variability that is driven by external forcings could be expected to coincide in the simulations and reconstructions. Nevertheless, the ECHO-G simulations are characterized by stronger warming trends in this region, over the period 1750–1990, than occur in the HadCM3 ALL simulation or in the reconstructions of Luterbacher *et al.* (2004).

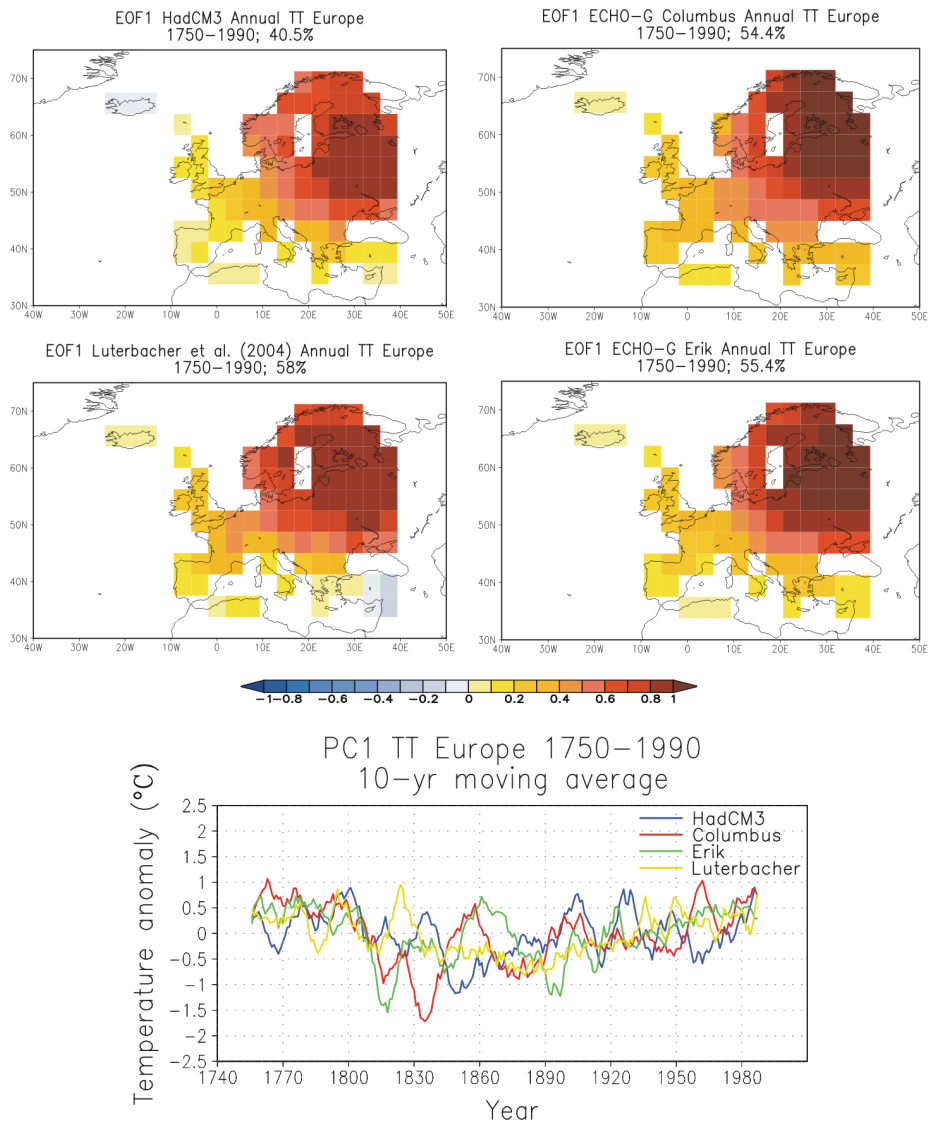


Figure 21. EOF1 pattern of annual surface air temperature of HadCM3, ECHO-G simulations and empirical reconstruction by Luterbacher *et al.* (2004) and corresponding PCs (10 year moving averages) from 1750 to 1990.

6.3.4.2. *Assessment of reconstruction methods using pseudo-proxies generated from model simulations*

Some of the main statistical methods that have been commonly used for the calibration of climate reconstructions have been extensively and critically investigated with the SO&P project, using the so-called pseudo-proxy approach. This approach uses non-proxy data, either instrumental or model-simulated, to mimic palaeoclimate proxy data (Mann and Rutherford, 2002; Zorita *et al.*, 2003). The pseudo-proxy approach is particularly powerful in cases where the target of a reconstruction is perfectly known (i.e., when a climate model simulation is used as a surrogate for the real climate system) because then the potential performance of a reconstruction can be easily evaluated, albeit under a number of idealised assumptions. The approach is useful for investigating the interaction between the behaviour of particular statistical methods and the extent and characteristics of proxy data networks.

Within SO&P, a number of such GCM-based pseudo-proxy studies have been undertaken, and these have resulted in a series of highly discussed papers (von Storch *et al.*, 2004; von Storch and Zorita, 2005; Bürger and Cubasch, 2005; Bürger *et al.*, 2006; von Storch *et al.*, 2006). Key findings of this work are centred on the inherent reduction of simulated amplitudes by any regression model (and the level of model uncertainty) and how this might combine with the limitations of using relatively short calibration and validation periods to result in a reconstruction that is biased either on time scales longer than those that are well-sampled in the calibration period or for periods during which the climate moved outside the range of climates sampled in the calibration period (see also Osborn and Briffa, 2004). This work has clearly demonstrated that many regression-based methods, whether univariate or multi-variate, can suffer from potential bias, but the magnitude, and therefore the significance, of such bias is unclear and probably depends on the characteristics of both climate variability and the proxy records. Any bias is likely to decrease with increasing coverage and quality of climate proxy data.

von Storch *et al.* (2004) used the pseudo-proxy approach, applied to both the ECHO-G ERIK simulation and the HadCM3 ALL simulation, to investigate the influence of noise on statistical reconstruction methods, including that of Mann *et al.* (1998, henceforth MBH) – though see the discussion below, where it is noted that there was a critical difference between their implementation of the MBH method and that actually used by MBH. von Storch *et al.* (2004) found that their implementation of the MBH reconstruction method very likely underestimates the amplitude of past temperature variations (Figure 22). The level of underestimation depends on the amount of noise contained in the pseudo-proxies (which mimics the non-climate signal in the real proxies). However, the underestimation of past variations in the MBH method appeared as a very robust feature in both simulations. Moreover, the presence of red (autocorrelated) noise in the pseudo-proxies further deteriorates the skill of the pseudo-reconstructions. As real proxies likely contain auto-correlated noise, and also the proxy network shrinks backwards in time, the magnitude of the bias of the MBH reconstruction method estimated under the assumptions of only white-noise pseudo-proxies and a complete proxy network is probably a lower bound for the real bias.

It was then noted by Bürger *et al.* (2006) that von Storch *et al.* (2004) had calibrated their model using detrended data, unlike MBH (see also Wahl *et al.*, 2006; von Storch *et al.*, 2006). It is clear that removing trends in proxy data and temperature data during the calibration process might lead to a greatly overestimated bias in the resulting reconstruction (Wahl *et al.*, 2006), but it is also apparent that (i) the potential for bias still remains even if detrending is not done (Bürger *et al.*, 2006); (ii) the bias might still be very large in some situations – e.g., with noisier proxy data (Bürger *et al.*, 2006) or strongly autocorrelated noise in the proxy data (von Storch *et al.*, 2006); and (iii) there are clear statistical arguments for avoiding the use of trend-dominated data when calibrating regression models (von Storch *et al.*, 2006). Bürger *et al.* (2006) show, in another pseudo-proxy study with ECHO-G ERIK, that, along with the

trend, there are a number of other data processing details and statistical calibration choices that can considerably influence the final outcome (Figure 23).

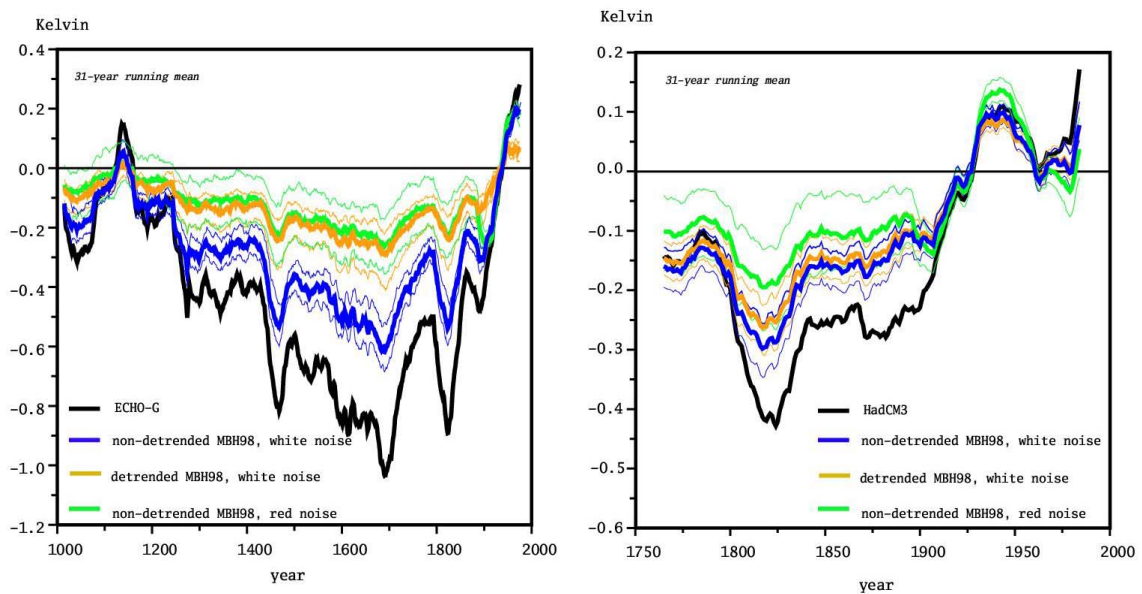


Figure 22. Northern Hemisphere temperature deviations from the 1900–1980 mean simulated and pseudo-reconstructed from a network of pseudo-proxies and two implementations of a multi-variate reconstruction method: with detrended (a variant of the MBH method) and non-detrended (the MBH method) data used in the calibration period.

Bürger and Cubasch (2005) show that the uncertainty persists if one uses real proxy data (the AD-1400 network of MBH). Moreover, by relating the range of millennial variations to the range sampled with the calibration period, they demonstrate that a large part of the uncertainty stems from an extrapolative usage of the regression models, by which the calibration error grows with increased extrapolation outside the calibration range. This enhanced uncertainty can only be approximated with an appropriate error model.

The trend discussion revealed another problem regarding the verification of climate reconstructions. If the calibration and validation sets contain a strong trend many derived statistics, including the regression model itself and the verification statistic *RE* (Reduction of Error), are estimated from very few degrees of freedom. As a result, their uncertainty can be very large. For example, the so-called artificial hockey sticks (which are derived from synthetic red noise proxy series, cf. McIntyre and McKittrick, 2005) cannot be rejected if the verification is based on a statistic such as *RE*. Artificial hockey sticks result from the de-centred principal component analysis that had been applied by MBH. Using the pseudo-proxy method, von Storch and Zorita (2005) examined the practical impact of this on their pseudo-reconstruction and concluded that it was very minor (subject to the assumptions that they made in the generation of their pseudo-proxy data, of course).

Given these concerns regarding the evaluation of reconstruction performance when using trend-dominated data, either the significance level of *RE* has to be re-evaluated, or performance metrics that are not dominated by the influence of trends should be used – such as the Coefficient of Efficiency. A re-assessment of the skill of climate reconstructions has been attempted by Bürger and Cubasch (2006). They apply a resampling technique (bootstrapping) to the full instrumental period and assess the sampling variability of likely *RE* values. The *RE* skill of millennial reconstructions of about 0.5 (implying that 50% of the variance has been reconstructed) as reported by MBH appears as a statistical outlier, caused

by the specific partitioning into calibration and validation periods of the trended series. Burger and Cubasch (2006) estimate that the “true” *RE* skill of such reconstructions is likely to be around 0.25.

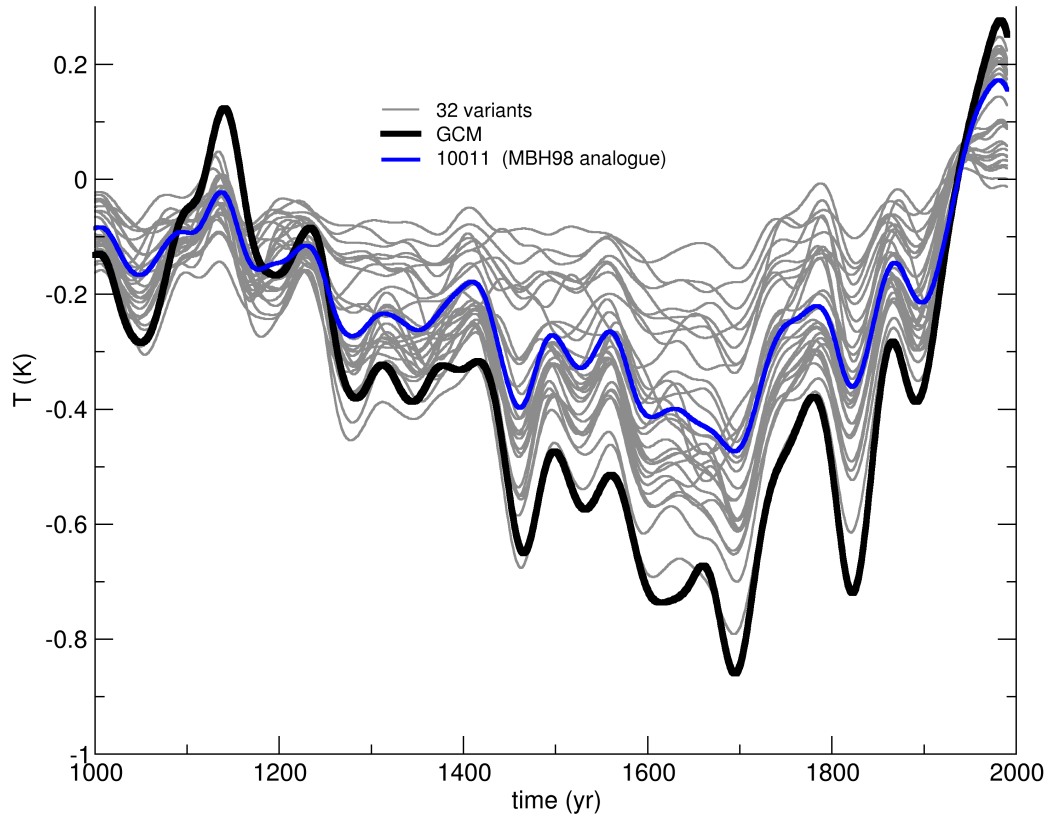


Figure 23. 32 variants of pseudo-reconstructions of simulated NH temperature using regression from pseudo-proxies (grey), relative to the actual ECHO-G ERIK simulated NH history (black). The 32 variants span almost the entire spectrum between no long-term variations and full variability. The MBH analogue (blue) shows significantly reduced variations. The overall variations are well beyond those of the calibration period. A 30-year smoothing has been applied to all curves.

Küttel *et al.* (2006) tested the reconstruction of European surface air temperature of the last 500 years produced by Luterbacher *et al.* (2004) in the surrogate climate of the ECHO-G and HadCM3 simulations. The approach followed the pseudo-proxy methodology used by von Storch *et al.* (2004). For this much more regional application (compared with that of von Storch *et al.*, 2004) no systematic underestimation of low-frequency temperature variability was found when a dense network of predictor variables was available. The availability of sufficient predictors and their individual reliability appear to be the key factors that determine reconstruction bias and skill, with bias only apparent with reduced spatial availability of predictors or poor quality predictors. Additionally, the results seem to be strongly dependent on the climate model used, with the pseudo-reconstructions based on ECHO-G generally showing worse skill than those based on HadCM3.

UDESAM/CNRS have also applied the pseudo-proxy approach, this time to test their combined analogue-infilling and artificial neural network method, and specifically the application of this method to the reconstruction of Mediterranean summer Palmer Drought Severity Index (see section 6.3.3.5; Nicault *et al.*, 2006a). They calculated the PDSI for the

Mediterranean region from the ECHO-G ERIK simulation of temperature and precipitation, and then generated pseudo-proxies from the simulated PDSI time series, with temporal variations in the numbers of pseudo-proxies chosen to match the changing availability of real proxy data. Figure 24 shows the spatial variations in the calibration correlations obtained for four different networks of pseudo-proxy data, assuming that they are perfect proxies with no non-climatic noise. The correlations exceed 0.9 at locations where pseudo-proxies are available, but fall below 0.5 in regions/periods where no pseudo-proxies are used (the denser networks available from 1600 onwards have very few unsampled locations and consequently have fewer regions with poor calibration correlations). The Mediterranean-wide average PDSI reconstructed using the perfect pseudo-proxies are highly correlated during the calibration period with the actual simulated Mediterranean time series, falling from $r = 0.92$ for 165 proxies to $r = 0.78$ for 7 proxies, with associated increases in the magnitude of the estimated uncertainty ranges.

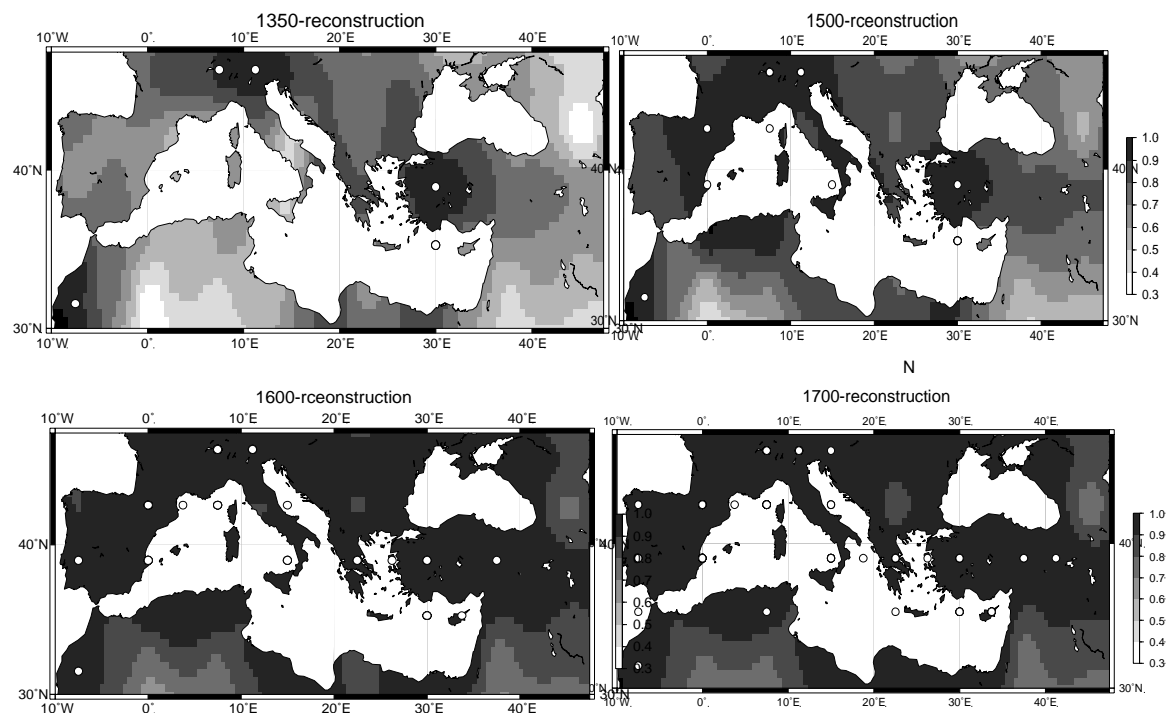


Figure 24. Calibration correlations for the pseudo-proxy reconstruction of the summer PDSI obtained for four different networks of pseudo-proxies (taken from model grid boxes indicated by the white points circles) corresponding to the numbers of real proxy records available in 1350, 1500, 1600 and 1700.

The CNRS/UESAM pseudo-proxy assessment was then extended to cases where the proxy data are not perfect, but instead contain varying levels of white (uncorrelated) non-climatic noise. For each set of pseudo-proxies, noise with variance equal to the pseudo-proxy PDSI variance multiplied by a factor of 0.5, 1, 2 or 3 is added. These reconstructions are compared to the actual ECHO-G ERIK PDSI (Figure 25). As expected, the correlations between the pseudo-reconstructions and actual simulated PDSI decrease with increasing proxy noise variance (from $r = 0.86$ to $r = 0.73$ for the full proxy network), but they remain highly significant. The variance of the reconstructions is also reduced with increasing levels of (predictor) noise. Although intermediate time scale variability is relatively well preserved (i.e., the same type of fluctuations are apparent in all the curves of Figure 25), the low-frequency variations are clearly suppressed to some extent, though mainly during the 1800–1900 when the pseudo-reconstructions diverge from the actual simulated PDSI.

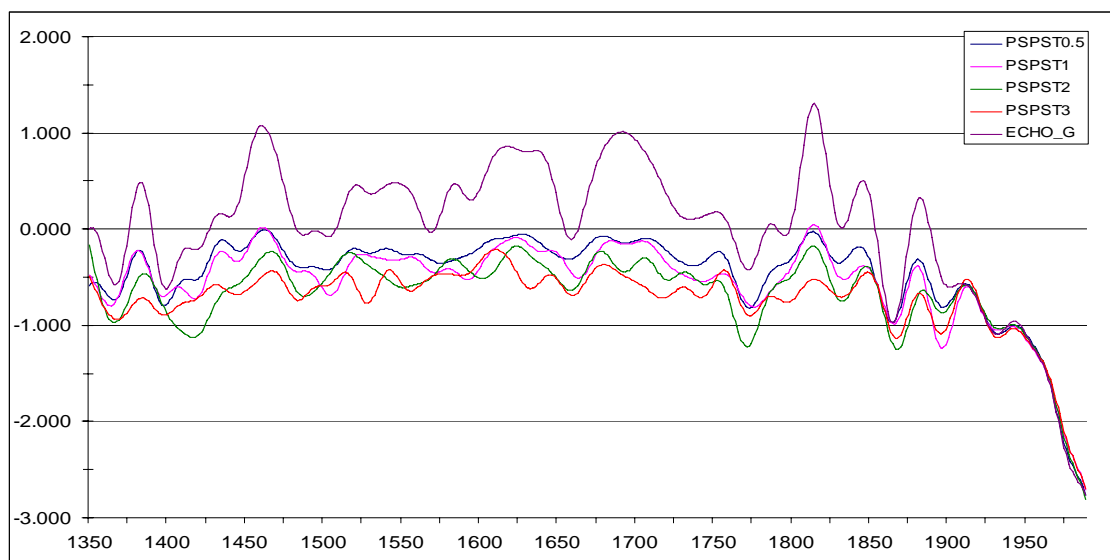


Figure 25. Reconstruction of mean Mediterranean summer PDSI using noisy pseudo-proxies with a ratio of white-noise variance to climate-signal variance of 0.5, 1, 2 or 3, compared with the mean Mediterranean summer PDSI from the ECHO-G ERIK simulation.

The GKSS, together with Fidel González-Rouco of the Universidad Computense de Madrid, have also used the pseudo-proxy approach to assess the potential reliability of temperature reconstructions derived from the inversion of vertical ground temperature profiles measured in boreholes. The first stage of this work was an analysis within the ERIK simulation of the relationship between the terrestrial deep soil temperature and surface air temperature (González-Rouco *et al.*, 2003), a key relationship in borehole-based reconstructions of surface air temperature. In the model, the deep soil temperature appears to be strongly coupled to the surface air temperature on decadal time scales and longer. In Gonzalez-Rouco *et al.* (2006), forward models of vertical heat diffusion were applied to simulate the development of vertical temperature profiles in response to the surface temperature variations simulated during the ERIK simulation and a control simulation with the ECHO-G model. The purpose of this exercise was to test some aspects of the methods used to reconstruct NH temperature variations from borehole data – specifically, the sensitivity to spatial sampling and the inversion of vertical profiles to yield temperature histories. The borehole sampling and the methodology appear to be sufficiently robust to reconstruct the simulated NH annual temperature. The temperature evolution simulated by ECHO-G is compatible with the borehole temperature reconstructions.

6.3.4.3. Detection and attribution of the climate response to external forcings

The detection and attribution (D&A) studies undertaken within the SO&P project have followed two distinct approaches. The first approach is to characterise the signals by the time-evolving shape of the estimated forcing histories. Attempts can then be made to detect these temporal fingerprints in the available long climate reconstructions, and to utilise the differences between the time series of the various forcing factors to distinguish the contribution of each factor. The second approach makes use of differences in the spatial patterns of climate response to different forcings to characterise and distinguish the various forcing factors. These spatial fingerprints can be defined by appropriately-forced model simulations and then used in an attempt to detect those signals in spatially-resolved climate information. The temporal fingerprints are more suitable for the detection of longer-term

climate fluctuations of the past millennium, while the spatial fingerprints can be applied to the assessment of the recent warming that is evident within the instrumental record.

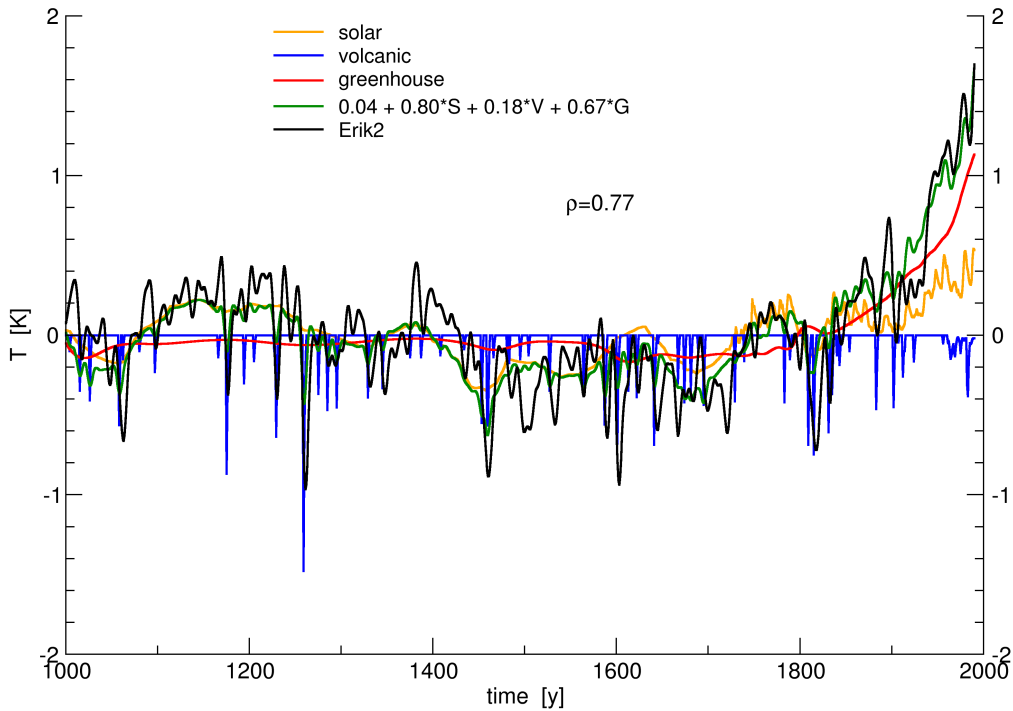


Figure 26. Solar (yellow), volcanic (blue) and greenhouse (red) temporal fingerprint (i.e. the respective forcing) and their contribution to ERIK2 (a simulation with ECHO-G that is similar to ERIK but started from cooler initial conditions) simulated Northern hemisphere (>20°N) land temperature (black), as anomalies from the overall mean. Their combined effect (green) has a correlation of $r = 0.77$. The black and green curves are smoothed to remove variations on time scales below 5 years.

To detect and attribute a signal within a noisy background, the utilization of fingerprints is a useful vehicle. If one is able to define *a priori* a likely response to a given external forcing, such as solar or volcanic, one can analyze the fields in question solely in terms of this response and thus enhance the expected signal-to-noise ratio (SNR). This is conveniently done in the framework of generalized least squares (GLS, cf. Allen and Tett, 1999; IPCC, 2001). Having defined fingerprints for solar (S), volcanic (V), and greenhouse gas (G) forcing, f_S , f_V , and f_G , respectively, the GLS approximation for temperature T is

$$T = \beta_0 + \beta_S f_S + \beta_V f_V + \beta_G f_G + \varepsilon \quad (2)$$

All variations that are unexplained by the external forcings, that is, all internally-generated fluctuations, are represented by ε and considered to be noise. For a millennial temperature record, for example, the most basic temporal fingerprint of a given external forcing is the forcing record itself, $f_S = S$, etc., or some estimated model response thereof, such as in Hegerl *et al.* (2003). For SO&P, the first variant was applied; but note that this approach does not deal properly with the response time of the climate to these forcings due, for example, to the thermal inertia of the oceans. Figure 26 shows the results obtained when equation (2) is applied to the ECHO-G ERIK2 simulation (this is the same as the ERIK simulation but started from cooler initial conditions). The results demonstrate that it is possible to approximate the global model response to a large extent by a simple linear model with three

parameters (β_S , β_V and β_G), each representing the magnitude of response to a specific forcing. This being the case, it is further possible to decompose the temperature time series into the contributions from the three single forcing mechanisms and the residual internal variability. This can be used to provide attribution measures for individual years or specific periods. Major climatic fluctuations during the millennium can then be attributed to a mix of specific forcings. For example, the simulated Dalton minimum in the early 19th century appears as a combined effect of reduced solar and enhanced volcanic activity, as does the pronounced temperature minimum around 1450. Note, however, that this is an anomaly model whose quality, along with the long-term behaviour of its coefficients, is sensitive to the basic state (this also affects the forcing amplitudes). For example, if the model is calibrated using only data from the pre-industrial period then the recent warming is not reproduced so well, and corresponding attribution amplitudes differ markedly. The results have, therefore, to be interpreted with caution. The above approach is also sensitive to errors in the forcing histories. If they contain errors, using them as temporal fingerprints for reconstructions will therefore yield a lower SNR.

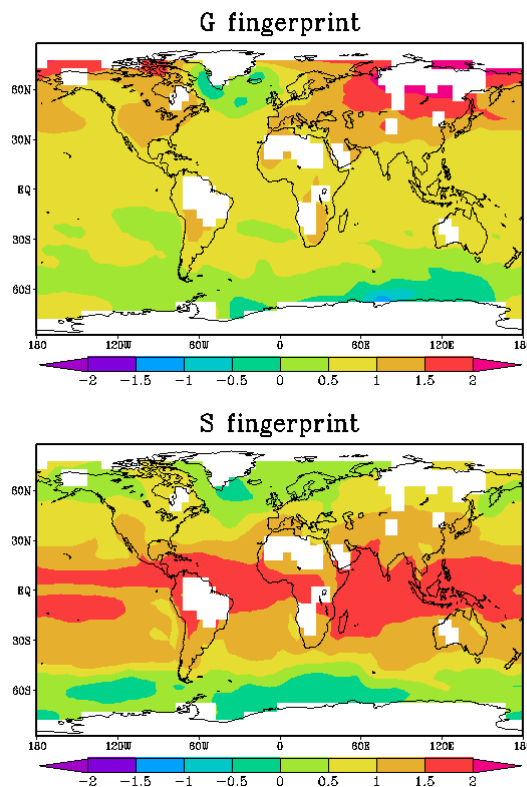


Figure 27. The S and G fingerprints. A continental NH signature dominates the G fingerprint, while the S fingerprint is characterized by a widespread tropical signature. The fingerprints are almost orthogonal with a spatial correlation of just 0.18.

When equation (2) is applied to a range of existing NH temperature reconstructions, together with the forcing histories used in the ECHO-G ERIK simulation, then the attribution results are much weaker because the linear response model fits the reconstructions rather poorly. Of the reconstructions considered so far, the linear model fits the Crowley and Lowery (2000) reconstruction best, though it is still much poorer than the results shown for the ECHO-G ERIK2 simulations. The performance for the other reconstructions (Jones *et al.*, 1998; Mann *et al.*, 1999; Briffa *et al.*, 2001; Briffa, 2000; Overpeck *et al.*, 1997; Esper *et al.*, 2002; Moberg *et al.*, 2005) is even worse. Besides possible errors in the radiative forcing, the

reconstructions themselves contain a certain amount of error. Both errors accumulate and hinder an accurate attribution by way of temporal fingerprints.

Mathematically, spatial and temporal fingerprints are applied in an equivalent manner (i.e., equation (2) still applies, but with the forcing time series replaced by spatial fields of response to forcings. In the spatial case, a signal can be better extracted by considering variations that are aligned with predefined spatial patterns. This has the consequence that the noise has now a multi-dimensional structure that has to be prescribed *a priori*, as discussed below. Due to their sporadic temporal nature, volcanic spatial fingerprints are not useful; for SO&P, we used spatial fingerprints only for solar and greenhouse forcing, f_S and f_G , respectively. While f_G is defined in the conventional way as the simulated trend in a warming G scenario, the definition of f_S is more intricate because a “solar scenario” is not available at present. A new simulation with ECHO-G was undertaken from which a solar spatial fingerprint could be estimated. This new simulation was forced with solar forcing following a sinusoid with a 760-year period and an amplitude of 2.5 W m^{-2} . The dominant EOF of this simulation, based on the temperature correlation matrix, was used to define the solar spatial fingerprint.

The spatial fingerprints f_S and f_G are shown in Figure 27. While f_S is dominated by coherent tropical temperature variations, f_G is dominated by a continental NH signature. The pattern correlation between these fingerprints is less than 0.2, supporting the possibility that solar and greenhouse signals can be detected separately. The detection variables are the fingerprint amplitudes β_S and β_G (not shown). Estimates of these amplitudes, plus their uncertainties, determine the main D&A results. Overall, these were strongly affected by the improved solar fingerprint. The D&A analysis moreover depends on an *a priori* estimate of the climate noise (estimated from internal fluctuations), particularly the level of spatial truncation that has to be used for its estimation. We tested the sensitivity of the final D&A outcome to that level and found indications that if the truncation is too strong – as in many previous studies – the results are poorer. These analyses will be described in a forthcoming paper.

6.3.5. Workpackage 5: Sea level changes over the last 500 years

The major components of the SO&P project deal with variations in climate over recent centuries, but the coupled ocean-atmosphere models used for climate simulations of the past 500 years also produce spatial estimates of sea-level variation associated with thermal expansion of sea water and ocean-circulation changes. Hence, by adding a model-generated melt-water component and then comparing these sea-level simulations with available, critically evaluated sea-level reconstructions and long (>70 years) tide-gauge records from the North Atlantic region, we aim to assess also the capability of the current generation of coupled GCM climate models and ice-melt models to realistically hindcast North Atlantic sea-level variability over the past 500 years. Furthermore, these estimates of sea-level change and variability, under natural and all forcings, and from the control integrations with unchanging external forcing, will allow several pertinent questions to be addressed: for example, what proportion of sea-level variations over past centuries might be attributed to naturally- and anthropogenically-forced climate changes? Also, therefore, we may explore what fraction of the rise observed during the 20th century is a commitment (delayed response) to earlier, naturally-forced climate variations (such as the ending of the Little Ice Age)? How large is the variability in global and regional sea level driven by natural external forcings?

6.3.5.1. Sea-level simulations of the past 500 years

Spatially-resolved sea-level variations associated with oceanic temperature (thermal expansion), regional variations in salinity and circulation changes were diagnosed from HadCM3 simulations. Thermal expansion is expected to provide the largest contribution to global sea-level change on multi-annual timescales. A global land ice mass balance model

was run after the climate simulations had been completed, taking seasonal temperature change patterns simulated by the model as input, to estimate the change in mass of glaciers and ice caps and hence their contribution to sea-level variations. The contribution to sea level from this change in ice mass was assumed to be geographically uniform – i.e., the added/subtracted water is spread evenly over the world ocean. The Greenland and Antarctic ice sheets are not taken into account, because their contribution is estimated to be smaller and is more uncertain, especially since there are no observations of historical changes in the ice sheets. Other contributions to sea level, such as change in snow and soil moisture, are indicated by the model to be negligible on multi-annual timescales. These procedures have been applied to calculate sea-level change from the HadCM3 CONTROL, NAT500, and ALL250 integrations (Gregory *et al.*, 2006).

Global mean sea-level changes simulated by HadCM3 are shown in Figure 28 (top panel).

- The model suggests that the apparent onset of sea-level rise and glacier retreat during the first part of the 19th century was due to natural forcing. Global mean sea-level changes as produced by the NAT500 run and the ALL250 run differ by less than 10 mm before 1900 AD, and vary within a vertical range of 20 mm over the previous centuries.
- Simulated global mean sea level is characterized by a very slight negative trend from 1550 to 1700, followed by a stronger rise until about 1820, when it fell by about 20 mm due to the cooling associated with the eruption of Tambora. This and subsequent volcanic eruptions, notably Krakatoa and Pinatubo, cause rapid falls in sea level, followed by recovery over many decades.
- Simulated contributions to global-mean sea-level rise during recent decades due to thermal expansion (the largest term) and to mass loss from glaciers and ice caps agree within uncertainties with observational estimates of these terms (the latter partly on account of the calibration of the model), but their sum falls short of the observed rate of sea-level rise. During the 20th century, global-mean sea level rose by about 50 mm in the ALL250 run, whereas the tide-gauge estimate is 100–200 mm. This discrepancy has been discussed by previous authors; a completely satisfactory explanation of 20th-century sea-level rise is lacking.
- The rate of sea-level rise was larger during the 20th century than during the previous centuries because of warming associated with anthropogenic forcing. Sea level rose by only 10 mm during the 20th century in the NAT500 run.
- Decreasing natural forcing during the second half of the 20th century tended to offset the anthropogenic acceleration in the rate of global-mean sea-level rise, tending to produce a relatively constant simulated rate of sea-level rise during the century, apparently consistent with the evidence from tide gauges.
- The model shows substantially less decadal variability in sea level and its thermal expansion component than 20th-century observations indicate, either because it does not generate sufficient ocean internal variability, or because the observational analyses overestimate the variability.

Changes in the zonally-averaged sea level simulated by HadCM3 are shown in Figure 29. Within the NAT500 run, there is some coherence between low-latitude sea level and the forcings (e.g., sea level falls after large volcanic eruptions in the late 1600s and the early 1800s, and rises during the mid twentieth century increase in solar irradiance). In the high northern latitudes there appears to be relatively strong (± 100 mm or more) variability on multi-decadal time scales, which is not obviously linked to the forcings applied to the model. In the high southern latitudes, sea level is below the reference level (1500–1549 mean) for most of the simulations, perhaps reflecting some early adjustment to the lower NAT500 forcing that took place in this region within the first century of the simulation.

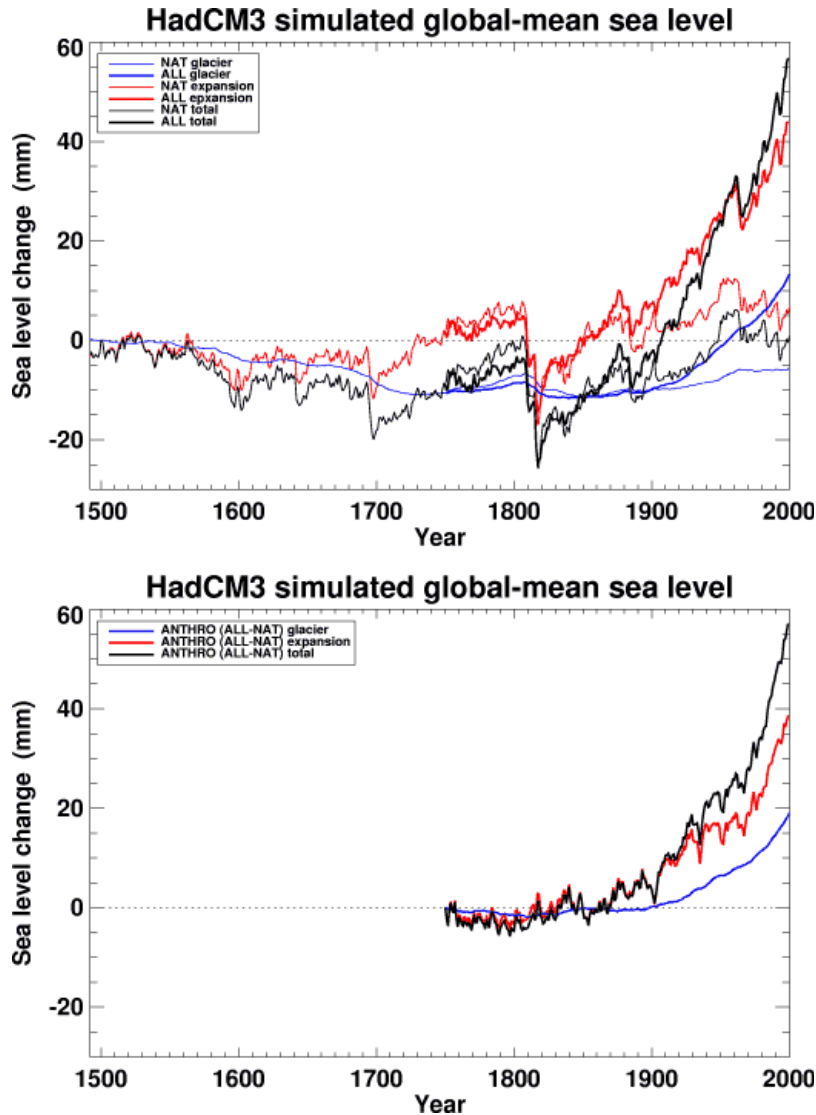


Figure 28. Global-mean sea level simulated by HadCM3 over the last 500 years. The contributions from ocean expansion/contraction and from changes in the mass of glaciers/ice-caps are indicated by red and blue, respectively, and their sum indicates total sea-level variations, shown in black. Top panel: the thin curves include only natural forcings (from NAT500) while the thick curves also include the response to anthropogenic forcings (from ALL250). Bottom panel: the curves show the difference between the ALL250 and NAT500 simulations, as an estimate of the response to anthropogenic forcings alone.

The response to the stronger forcing of the ALL250 run is clearest between 60°S and 40°N, where coherent sea-level rises during the twentieth century of about 64 mm are simulated (Figure 29b). In the mid to high latitudes of the Northern Hemisphere, although there is a rise of similar magnitude during the late twentieth century, this was preceded by a strong and very sudden lowering of sea level shortly after 1900 and sea level did not exceed the levels simulated during the late nineteenth century. These changes are of great importance because they occur in the region from which most of the long palaeo-sea-level records that we have used for comparison with the simulated changes are taken. Further analysis of the model simulations indicates that the fall in sea level shortly after 1900 was particularly strong in the western North Atlantic Ocean, and the simulated sea level in that region is highly anti-correlated ($r = -0.69$ at decadal time scales) with the simulated strength of the Atlantic Meridional Overturning Circulation (MOC). The Atlantic MOC strengthens considerably (by

~10%) around 1900 in the ALL250 simulation, but not in the NAT500 simulation. It is unclear whether this is a response to the external anthropogenic forcing (and, therefore, whether it should be expected to occur in the observational data) or is due to random internal variability of the ocean–atmosphere system. If the latter is the case, then there is no reason to expect such a change to occur at the same time in the observational record, and it is such a strong regional signal that it would hamper efforts to compare simulated and reconstructed sea level along the east coast of North America.

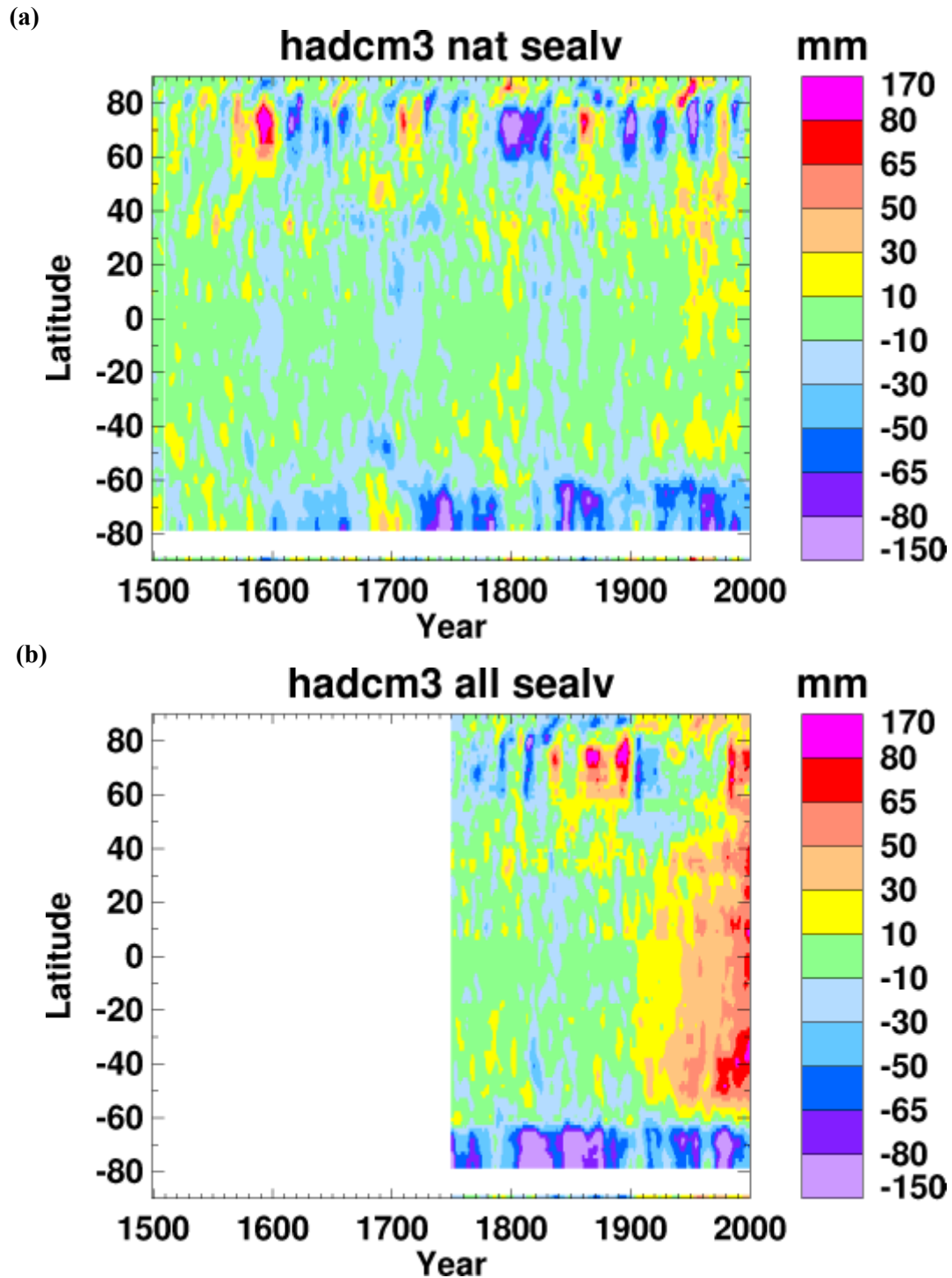


Figure 29. Zonal-mean sea level simulated by HadCM3 (a) over the last 500 years due only to natural forcings (from NAT500) and (b) over the last 250 years due to natural and anthropogenic forcings (from ALL250).

The anthropogenic component of simulated sea-level rise can be estimated as the difference between the ALL250 and NAT500 simulations (Figure 28, bottom panel), which shows an accelerating increase during the 20th century, as might be expected from the accelerating anthropogenic forcing. It is clear, therefore, that the quasi-linear increase during the ALL250 run is due to an anthropogenic forcing that accelerates throughout the 20th century, combined with natural forcing that acts to enhance sea-level rise during the first half of the century (due to quiescent volcanism and stronger solar forcing) and retards it during the second half of the century (due to more active volcanism). It appears that the response to anthropogenic forcing appears first in the thermal expansion of the oceans, and somewhat later in the melting of land ice.

6.3.5.2. Sea-level reconstructions of the past 500–1000 years: methodology

Comparison of the different simulated sea-level estimates against observational evidence – tide-gauge records with a length of >70 yrs and high-resolution (50-150 yrs) sea-level reconstructions for the past 1000 yrs – is necessary to assess our confidence in the simulations. Our approach has been to assemble all (un)published sea-level reconstructions based on salt-marsh foraminifera as sea-level proxies, evaluate these critically and (further) test the reconstruction method by comparing the youngest 70–120 years of those reconstructions that meet the selection criteria with the instrumental sea-level record nearest to each study site.

In our evaluation of the relevant (un)published literature we have considered, with one exception, only those studies of (sub-)centennial sea-level variations which used salt-marsh foraminifera as a proxy for past sea levels, by far the most widely used sea-level indicator in recent palaeo-sea-level research. The reconstruction of sea-level variations using salt-marsh foraminifera can be summarised in four main steps: (i) determine the height at which palaeomorph surfaces (PMSs) formed above local palaeo-mean high water (PMHW); (ii) reconstruct the rate at which PMSs accreted vertically; (iii) correct for any sediment compaction and changes in palaeotidal range; and (iv) remove the millennial-scale trend of relative sea-level (RSL) change. Steps (i) and (ii) combine to produce a record of relative PMHW. The corrections applied in step (iii) renders it a relative palaeo-mean tide level record, and removal of the millennial-scale RSL trend, attributed to processes of glacio- (and hydro-)isostatic adjustment (GIA), in step (iv) results in a reconstruction of mean tide level change which can be compared to the sea-level simulations. For a full discussion of each of the four steps, reference is made to SO&P Deliverable 16/17.

Both published and unpublished RSL reconstructions were evaluated to determine their suitability for comparison with the results of sea-level simulations on the basis of six criteria: (1) all data used for the reconstruction are available for interrogation; (2) the record is at least 500 years long; (3) the age model includes a high-resolution/precision chronology during the past 100–200 years; (4) the age model for the past 500–1000 years is based on a sufficient number of ¹⁴C dates; (5) the sea-level proxy used is of high-resolution and achieves useful precision; and (6) the record includes, or can be compared to, compaction-free (basal) data.

6.3.5.3. Sea-level reconstructions of the past 500–1000 years: results

Out of 23 sea-level reconstructions that were assessed (see SO&P Deliverable 16/17), only six meet the criteria listed above. These six reconstructions have a geographical spread from North Carolina to Iceland (Figure 30). These six RSL reconstructions for the past 1000 years are shown in Figure 31a, compared to nearest instrumental records of mean sea-level change in Figure 31b, and presented in detrended format in Figure 31c. Further discussion of the records is presented in Deliverable 16/17, but it is relevant to note here that (i) the low-

resolution (pre-1880) part of the Barn Island record, Connecticut (CT), which is based on a large number of compaction-free basal organic index data (using marsh flora as sea-level proxy), provides a valuable reference for the high-resolution RSL record from Pattagansett (CT) nearby, which has no basal data; (ii) the amplitude of (some of) the larger sea-level fluctuations in the Machiasport, Maine (ME) reconstruction may be exaggerated owing to the fact that the transfer function is defined in terms of flooding frequency rather than of marsh-surface elevation relative to MHW, (iii) the Machiasport RSL curve presented here differs from those previously published (Gehrels, 1999, 2000; Gehrels et al., 2002) in that it (a) has not been smoothed by application of a 5 point running average, and (b) is a composite of the well dated SN-10.1 core, taken from AD 1770 to recent, attached to the less well dated core SN-VC-1, which covers the period 1000-1770 (Gehrels, pers. comm.) and (iv) the reconstruction of RSL change for Oak Island, North Carolina (NC) results in, as yet unexplained and seemingly unlikely, large amplitude sea-level oscillations, most noticeably before ~1850. This oscillatory record should therefore be considered with reservation. The average rate of RSL rise pre-1850 is 0.04 cm/yr, as documented reliably by both the rate of vertical marsh-fringe displacement (basal peat data) and the rate of in-core PMS accumulation.

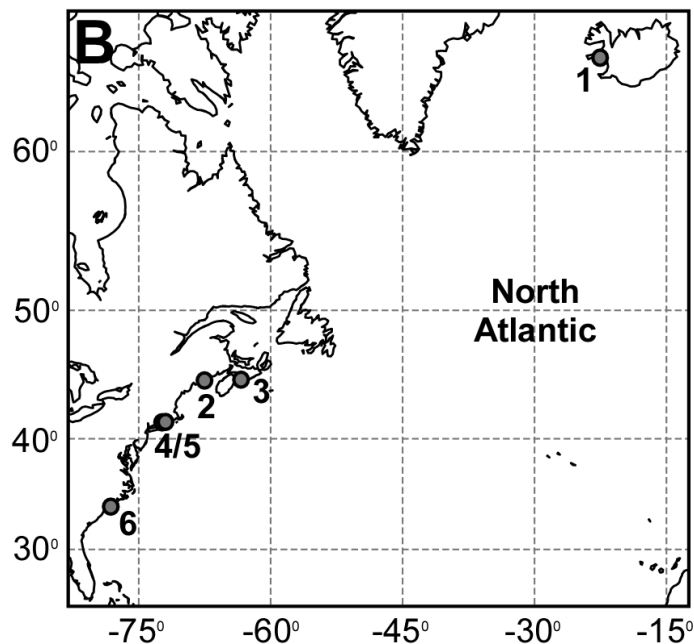


Figure 30. Site locations for 1000-year reconstructed sea levels: (1) Vidarhólmi, Snæfellsnes, Iceland (Gehrels *et al.*, 2006), (2) Machiasport, Maine, USA (Gehrels 1999, 2000; Gehrels *et al.*, 2002; Gehrels, pers. com.), (3) Chezzetcook, Nova Scotia, Canada (Gehrels *et al.*, 2005), (4) Pattagansett, Connecticut, USA (Wright *et al.*, unpubl.), (5) Barn Island, Connecticut, USA (Donnelly *et al.*, 2004) and (6) Oak Island, North Carolina, USA (Wright *et al.*, unpubl.).

The modern part of the sea-level reconstructions have been compared with tide-gauge data in Figure 31b, with mean trends during the overlap listed in the caption to that Figure. Assuming a constant tidal range, the comparison shows that whilst the methodology is unable to resolve annual sea-level variability, it is capable of reproducing multi-decadal to centennial sea-level changes.

All six sea-level reconstructions show, compared to the trend for the past 1000 years, a more or less recent increase in the rate of sea-level rise. The two records that resemble each other most are those from Chezzetcook and Pattagansett, each showing a slight and temporary

acceleration beginning close to 1700, and another rate increase around 1900. The Machiasport curve shows a pronounced, temporary increase in sea-level rise at ~1750 and suggests a slight increase around 1900. The Vidarhólmi record shows a single increase in the rate of sea-level rise beginning at ~1830. The composite Barn Island curve, which relies on the New York tide-gauge record, suggests a slight sea-level rise acceleration beginning in the 1880's and shows a clear rate increase after about 1920. Finally, the PMS accumulation record and youngest part of the in-core sea-level reconstruction from the Oak Island record can be interpreted as indicating an increase in sea-level rise beginning around 1880. The lack of significant sea-level anomalies pre-1700 may be largely a consequence of the limited resolution achievable with standard AMS ^{14}C dating, which hinders the identification of periods of increased rates of PMS accumulation.

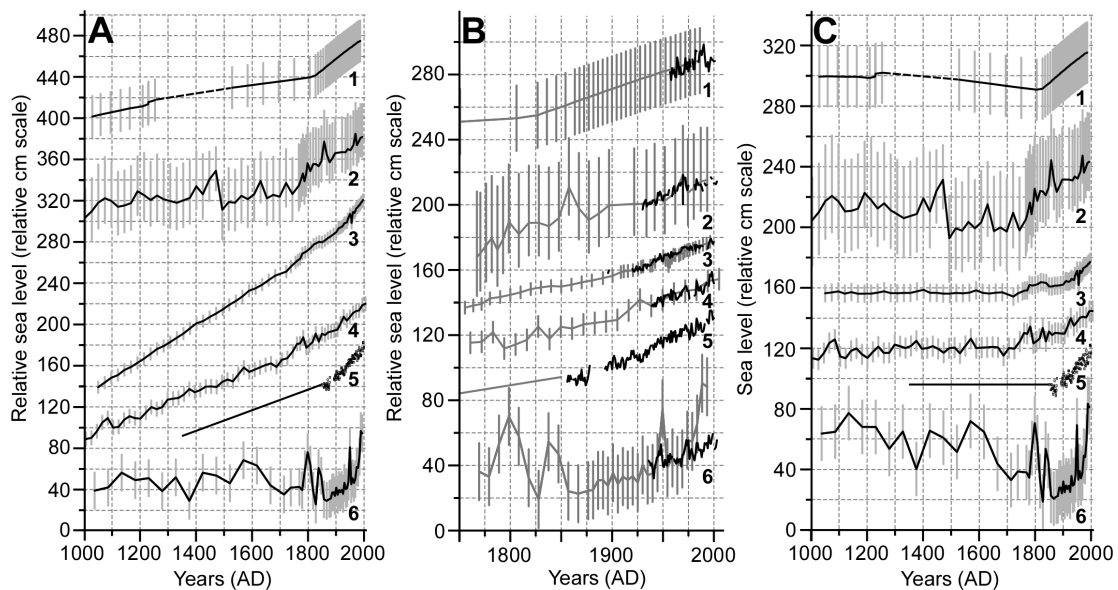


Figure 31. (a) 1000-year reconstructed relative sea levels, (b) comparison with nearest instrumental mean sea-level records, and (c) 1000-year reconstructed sea levels after removing relative sea-level trends of (1) 0.065 cm/yr, (2) 0.04 cm/yr, (3) 0.173 cm/yr, (4) 0.1 cm/yr, (5) 0.1 cm/yr and (6) 0.04 cm/yr. In (b), reconstructed and tide-gauge trends are: (1) Vidarhólmi (0.20 cm/yr) vs. Reykjavik (0.23 cm/yr), (2) Machiasport (0.23 cm/yr) vs. Eastport (0.21 cm/yr), (3) Chezzetcook (0.32 cm/yr) vs. Halifax (0.32 cm/yr), (4) Pattagansett (0.24 cm/yr) vs. New London (0.22 cm/yr), (5) New York (0.28 cm/yr), and (6) Oak Island (RSL 0.75 cm/yr, PMS 0.21 cm/yr) vs. Wilmington (0.21 cm/yr).

6.3.5.4. Comparison of simulated and reconstructed sea-level changes

Regional sea-level simulations have been compared with local palaeo-sea-level records (the last 70 years of which are known to have trends that are similar to the trends indicated by the nearest instrumental records), and are shown together in Figure 32.

- The pre-1880 part of the reconstructions from Oak Island and Barn Island is not included in this comparison, because the one from Oak Island is realistic only between about 1880 and 1970 and the one from Barn Island is insufficiently resolved between 1500 and 1880.
- Notwithstanding the seemingly good correspondence between the simulation and reconstruction for the study site on Iceland, the overall negative sea-level trend during the period 1500–1830 in the simulations cannot (yet) be confirmed conclusively by

the detrended sea-level reconstructions. The simulated lowering of sea level during this period would likely have ceased after 1700 if it were not for the low sea level during the early 19th century that is simulated in response to the cooling associated with the eruption of Tambora.

- The sea-level reconstructions do not resolve the simulated decadal variability, including the most pronounced fluctuations.

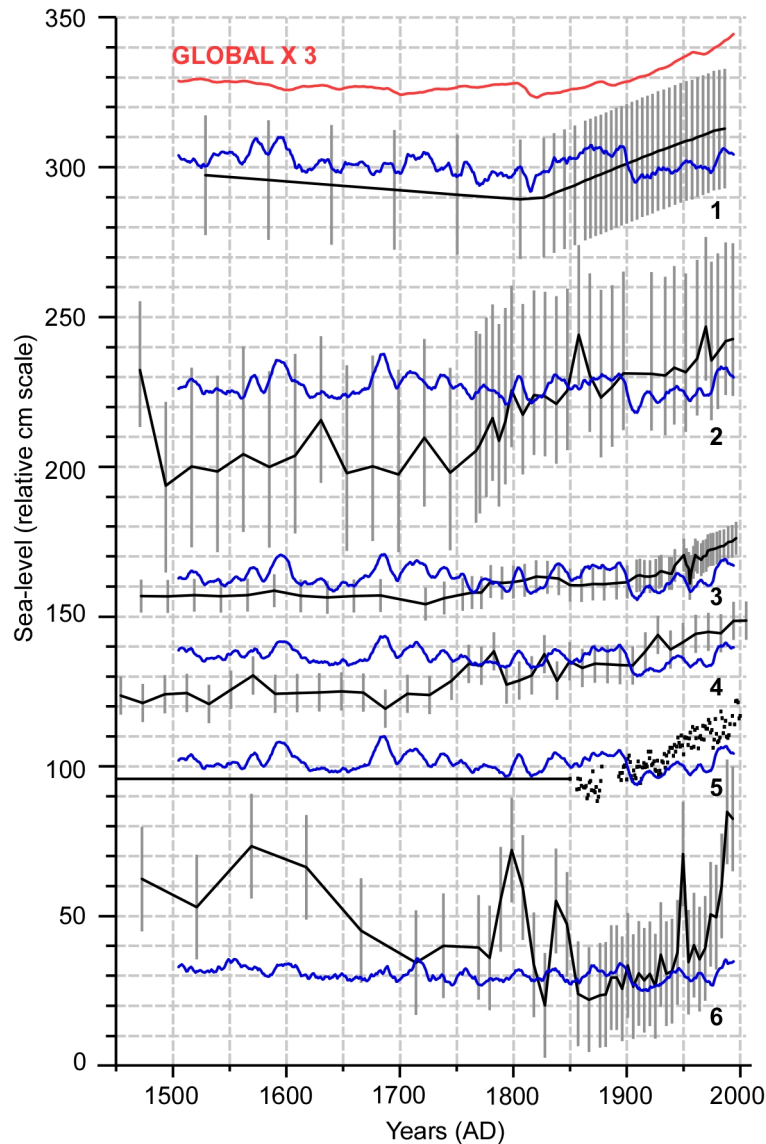


Figure 32. Comparison of simulated (concatenated NAT500 and ALL250 runs of HadCM3) and reconstructed sea-level changes. Regional simulated sea-level variations are shown in blue, together with reconstructed sea levels after removal of relative sea-level trends in black (with error bars). The simulated global-mean sea level is also shown in red (multiplied by 3). Locations and references are given in Figure 30.

- Comparison of the pre-1900 part of the two reconstructions that resemble each other most (Chezzetcook and Pattagansett) with their very similar regional simulations shows (i) opposite trends between 1700 and 1800 (positive for the reconstructions, negative for the simulations) and (ii) different trends between 1800 and 1900 (stable for the reconstructions and rising for the simulations).

- The significant drop in simulated sea level around 1900 is not apparent in any of the local sea-level reconstructions, nor the long tide-gauge records from Florida. This simulated fall in regional sea level appears to be associated with a strengthening of the Atlantic Meridional Overturning Circulation; if this ocean circulation change is generated purely by internal variability of the climate, rather than in response to some external forcing or combination of forcings, then there is no reason to expect the timing of it, or the associated sea level falls along the east coast of North America, to be matched by similar falls in the observed sea level.
- For the 20th century, all local sea-level reconstructions and all regional sea-level simulations show a positive trend, but the mean rate of rise in the reconstructions exceeds that in the simulations by a factor of 2–3. This higher rate of rise is documented also by the nearest instrumental records to each of the study sites.

Given that the regional sea-level simulations may be impacted by internally-generated variability, it is also appropriate to compare the local reconstructions against the simulated global-mean sea level.

- The maximum vertical range of sea-level change in the simulation is a factor of 3 to 4 smaller than that of the local reconstructions.
- For the period 1700–1800, the reconstructions that resemble each other most (Chezzetcook and Pattagansett), both show sea-level rise, in agreement with the computed global mean (and in contrast to the regional simulations, which show sea level falling during the 18th century). The palaeorecord from Machiasport shows sea level rising between 1750 and 1800. The 16th century rise is conspicuously absent in the reconstruction from Iceland, which otherwise corresponds well with the trends in the global-mean record.

6.3.6. Deliverables from the SO&P project

A total of 18 deliverables were generated by the SO&P (Simulations, Observations & Palaeoclimatic data: climate variability over the last 500 years) project (numbered D1 – D19, with the exclusion of D5 which was removed during contract negotiation). These are listed in Table 4. Some of the deliverables are in a form (e.g., an entire website or data base) that prevents their inclusion within this annex. For simplicity, therefore, all of these deliverables have been made available from the SO&P project website (<http://www.cru.uea.ac.uk/projects/soap/>) at the specific URL addresses shown in Table 4, and they must be accessed from there instead of including them in this annex.

Note that some of the deliverables are password-protected because they are not appropriate for completely open dissemination. The password can be requested from the project coordinator (Tim Osborn, t.osborn@uea.ac.uk). Data will be provided in most cases for agreed collaborative projects.

Table 4. Deliverables from the SO&P project.

No.	Deliverable title and URL for obtaining the deliverable
D1	Dedicated project website (with private & public sections) http://www.cru.uea.ac.uk/cru/projects/soap/
D2	Assembly of climate proxy, documentary & long instrumental data, & existing palaeoclimate reconstructions completed, & distributed via the project website http://www.cru.uea.ac.uk/cru/projects/soap/data/
D3	Simulated data in the project data base http://www.cru.uea.ac.uk/cru/projects/soap/data/model/
D4	Methods for comparison of palaeo & model data developed & documented, & algorithms made available http://www.cru.uea.ac.uk/projects/soap/pw/pubs/reports/soap_deliverable_4.pdf
D6	Improvement of European gridded temperature & precipitation/drought reconstructions http://www.cru.uea.ac.uk/projects/soap/data/recon/deliv6.htm
D7	Comparison, improvement & combination of Northern Hemisphere gridded temperature reconstructions http://www.cru.uea.ac.uk/projects/soap/data/recon/deliv7.htm
D8	Report on simulated response to external forcings http://www.cru.uea.ac.uk/projects/soap/pw/pubs/reports/soap_deliverable_8.pdf
D9	Reconstruction of atmospheric circulation patterns & circulation indices & ENSO http://www.cru.uea.ac.uk/projects/soap/pw/pubs/reports/soap_deliverable_9.pdf
D10	Spatio-temporal analysis of reconstructed climate variability over 1500-2000 http://www.cru.uea.ac.uk/projects/soap/pw/pubs/reports/soap_deliverable_10.pdf
D11	Report on difference between control & forced simulations http://www.cru.uea.ac.uk/projects/soap/pw/pubs/reports/soap_deliverable_11.pdf
D12	Simulated sea-level from all GCM simulations in the project data base http://www.cru.uea.ac.uk/projects/soap/data/model/deliv12.htm
D13	Regional estimates of observed sea level rise (from North Atlantic tide gauge & proxy records) in the project data base http://www.cru.uea.ac.uk/projects/soap/pw/data/sealevel/deliv13.htm
D14	Report on the evaluation of simulated climate variability & climate response to forcing using the palaeo reconstructions http://www.cru.uea.ac.uk/projects/soap/pw/pubs/reports/soap_deliverable_14.pdf
D15	Report on the interpretation of palaeodata using climate simulations http://www.cru.uea.ac.uk/projects/soap/pw/pubs/reports/soap_deliverable_15.pdf
D16	Report estimating the natural & anthropogenic contributions to sea level variations over the past 500 years, & evaluating the simple climate/sea-level models http://www.cru.uea.ac.uk/projects/soap/pw/pubs/reports/soap_deliverable_1617.pdf
D17	Report on the comparison of simulated & observed sea levels & on relationships with climate forcing http://www.cru.uea.ac.uk/projects/soap/pw/pubs/reports/soap_deliverable_1617.pdf
D18	Report on climate signal detection using the palaeo-based, model-based, & synthesis estimates of natural climate variability http://www.cru.uea.ac.uk/projects/soap/pw/pubs/reports/soap_deliverable_18.pdf
D19	Final project report, draft TIP plan & dissemination of project results & data sets http://www.cru.uea.ac.uk/projects/soap/pubs/reports/final/

6.3.7. References cited within the progress report

- Allen MR and Tett SFB (1999) Checking for model consistency in optimal fingerprinting. *Climate Dynamics* **15**, 419-34.
- Betts RA (2001) Biogeophysical impacts of land use on present-day climate: near-surface temperature and radiative forcing. *Atmospheric Science Letters*, doi:10.1006/asle.2000.0023.
- Briffa KR (2000) Annual climate variability in the Holocene: interpreting the message of ancient trees. *Quaternary Science Reviews* **19**, 87-105.
- Briffa KR, Jones PD, Bartholin TS, Eckstein D, Schweingruber FH, Karlen W, Zetterberg P and Eronen M (1992) Fennoscandian summers from A.D. 500: temperature changes on short and long timescales. *Climate Dynamics* **7**, 111-119.
- Briffa KR, Osborn TJ, Schweingruber FH, Harris IC, Jones PD, Shiyatov SG and Vaganov EA (2001) Low-frequency temperature variations from a northern tree ring density network. *J. Geophys. Res.* **106**, 2929-2941.
- Brohan P, Kennedy JJ, Harris I, Tett SFB and Jones PD (2006) Uncertainty estimates in regional and global observed temperature changes: a new dataset from 1850. *J. Geophys. Res.* **111**, D12106, doi: 10.1029/2005JD006548.
- Bürger G and Cubasch U (2005) Are multiproxy climate reconstructions robust? *Geoph. Res. Lett.* **32**, L23711, doi: 10.1029/2005GL0241550.
- Bürger G and Cubasch U (2006) On the verification of climate reconstructions. *Climate of the Past* (submitted).
- Bürger G, Fast I and Cubasch U (2006) Climate reconstruction by regression – 32 variations on a theme. *Tellus* **58A**, 227-235.
- Casty C, Handorf D, Raible CC, Gonzalez-Rouco JF, Weisheimer A, Xoplaki E, Luterbacher J, Dethloff K and Wanner H (2005) Recurrent climate winter regimes in reconstructed and modelled 500 hPa geopotential height fields over the North Atlantic/European sector 1659-1990. *Climate Dynamics* **24**, 809–822.
- Collins M, Tett SFB and Cooper C (2001) The internal climate variability of HadCM3, a version of the Hadley Centre coupled model without flux adjustments. *Clim. Dyn.* **17**, 61-81.
- Crowley TJ (2000) Causes of climate change over the past 1000 years. *Science* **289**, 270-277.
- Crowley TJ and Lowery TS (2000) How warm was the medieval warm period? *Ambio* **29**, 51-54.
- Crowley TJ, Baum SK, Kim K-Y, Hegerl GC and Hyde WT (2003) Modeling ocean heat content changes during the last millennium. *Geophys. Res. Lett.* **30**, 1932, doi: 10.1029/2003GL017801.
- Cubasch U, Bürger G, Fast I, Spanghel T and Wagner S (2005) The direct solar influence on climate: modelling the lower atmosphere. *Mem. S.A.It.* **76**, 810-818.
- Donnelly JP, Cleary P, Newby P and Ettinger R (2004) Coupling instrumental and geological records of sea-level change: evidence from southern New England of an increase in the rate of sea-level rise in the late 19th century. *Geophys. Res. Lett.* **31**, L05203.
- Esper J, Cook ER and Schweingruber FH (2002) Low frequency signals in long tree-ring chronologies for reconstructing past temperature variability. *Science* **295**, 2250-2253.
- Gehrels WR (1999) Middle and late Holocene sea-level changes in eastern Maine reconstructed from foraminiferal stratigraphy and AMS 14 C dates on basal peat. *Quaternary Research* **52**, 350-359.
- Gehrels WR (2000) Using foraminiferal transfer functions to produce high-resolution sea-level records from salt-marsh deposits, Maine, USA. *Holocene* **10**, 367-376.
- Gehrels WR, Belknap DF, Black S and Newnham RM (2002) Rapid sea-level rise in the Gulf of Maine, USA, since AD 1800. *Holocene* **12**, 383-389.

- Gehrels WR, Kirby JR, Prokoph A, Newnham RM, Achterberg EP, Evans H, Black S and Scott DB (2005) Onset of recent rapid sea-level rise in the western Atlantic Ocean. *Quaternary Science Reviews* **24**, 2083-2100.
- Gonzalez-Rouco F, von Storch H and Zorita E (2003) Deep soil temperature as proxy for surface air temperature in a coupled model simulation of the last thousand years. *Geophys. Res. Lett.* **30**, L03205.
- Gonzalez-Rouco F, Beltrami H, Zorita E and von Storch H (2006) Simulation and inversion of borehole temperature profiles in simulated climates: spatial distribution and surface coupling. *Geoph. Res. Lett.* **33**, L01703.
- Gordon C, Cooper C, Senior CA, Banks H, Gregory JM, Johns TC, Mitchell JFB and Wood RA (2000) The simulation of SST, sea ice extents and ocean heat transports in a version of the Hadley Centre coupled model without flux adjustments. *Clim. Dyn.* **16**, 147-168.
- Gregory JM, Stouffer RJ, Raper SCB, Stott PA and Rayner NA (2002) An observationally based estimate of the climate sensitivity. *J. Climate* **15**, 3117-3121.
- Gregory JM, Ingram WJ, Palmer MA, Jones GS, Stott PA, Thorpe RB, Lowe JA, Johns TC and Williams KD (2004) A new method for diagnosing radiative forcing and climate sensitivity. *Geophys. Res. Lett.* **31**, L03205, doi:10.1029/2003gl018747.
- Gregory JM, Lowe JA and Tett SFB (2006) Simulated global-mean sea-level changes over the last half-millennium. *Journal of Climate* **19**, 4576-4591.
- Guiot J, Nicault A, Rathgeber C, Edouard JL, Guibal F, Pichard G and Till C (2005) Last-millennium summer-temperature variations in western Europe based on proxy data. *The Holocene* **15**, 1-12.
- Hansen J, Sato M and Reudy R (1997) Radiative forcing and climate response. *J. Geophys. Res.* **102**, 6831-6864.
- Hegerl GC, Crowley TJ, Baum SK, Kim KY and Hyde WT (2003) Detection of volcanic, solar and greenhouse gas signals in paleoreconstructions of northern hemispheric temperature. *Geophys. Res. Lett.* **30**, 1242 (doi: 10.1029/2002GL016635).
- IPCC (2001) *Climate Change 2001: The Scientific Basis. Contribution of Working Group I to the Third Assessment Report of the Intergovernmental Panel on Climate Change*. Cambridge University Press, Cambridge, pp. 944.
- Jones JM and Widmann M (2003) Instrument- and tree-ring-based estimates of the Antarctic Oscillation. *J. Climate* **16**, 3511-3524.
- Jones JM and Widmann M (2004) Early peak in Antarctic oscillation index. *Nature* **432**, 290-291.
- Jones PD, Briffa KR, Barnett TP and Tett SFB (1998) High-resolution palaeoclimatic records for the last millennium: interpretation, integration and comparison with General Circulation Model control-run temperatures. *The Holocene* **4**, 455-471.
- Jones PD, New M, Parker DE, Martin S and Rigor IG (1999) Surface air temperature and its variations over the last 150 years. *Reviews Geophys.* **37**, 173-99.
- Jones PD, Osborn TJ and Briffa KR (2003) Changes in the Northern Hemisphere annual cycle: implications for paleoclimatology? *J. Geophys. Res.* **108**, 4588 doi: 10.1029/2003JD003695.
- Joshi M, Shine K, Ponater M, Stuber N, Sausen R and Li L (2003) A comparison of climate response to different radiative forcings in three general circulation models: towards an improved metric of climate change. *Clim. Dyn.* **20**, 843-854 (doi: 10.1007/s00382-003-0305-9).
- Kuettel M, Luterbacher J, Zorita E, Xoplaki E, Reidwyl N and Wanner H (2006) Testing a European winter surface temperature reconstruction in a surrogate climate. *Geophys. Res. Lett.* (submitted).
- Legutke S and Voss R (1999) ECHO-G, the Hamburg atmosphere-ocean coupled circulation model. *DKRZ technical report* **18**, DKRZ, Hamburg.
- Luterbacher J, Xoplaki E, Dietrich D, Rickli R, Jacobeit J, Beck Z, Gyalistras D, Schmutz C, and Wanner H (2002) Reconstruction of sea-level pressure fields over the eastern North Atlantic and Europe back to 1500. *Clim. Dyn.* **18**, 545-561

- Luterbacher J, Dietrich D, Xoplaki E, Grosjean M and Wanner H (2004) European seasonal and annual temperature variability, trends and extremes since 1500. *Science* **303**, 1499-1503.
- Mann ME and Rutherford S (2002) Climate reconstruction using 'pseudoproxies'. *Geophys. Res. Lett.* **29**, 139 (doi: 10.1029/2001GL014554).
- Mann ME, Bradley RS and Hughes MK (1998) Global-scale temperature patterns and climate forcing over the past six centuries. *Nature* **392**, 779-787.
- Mann ME, Bradley RS and Hughes MK (1999) Northern Hemisphere temperatures during the past millennium: inferences, uncertainties and limitations. *Geophysical Research Letters* **26**, 759-762.
- Mann ME, Rutherford S, Wahl E and Ammann (2005) Testing the fidelity of methods used in proxy-based reconstructions of past climate. *J. Climate* **18**, 4097-4107.
- McIntyre S and McKittrick R (2005) Hockey sticks, principal components, and spurious significance. *Geophys. Res. Lett.* **32**, L03710.
- Melvin T (2004) *Historical growth rates and changing climatic sensitivity of boreal conifers*. PhD thesis, University of East Anglia, Norwich, UK.
- Moberg A, Sonechkin DM, Holmgren K, Datsenko NM and Karlen W (2005) Highly variable Northern Hemisphere temperatures reconstructed from low- and high-resolution proxy data. *Nature* **433**, 613-617.
- Nicault A, Alleaume S, Brewer S and Guiot J (2006a) Mediterranean drought fluctuation during the last 650 years based on tree-ring data. *Climate Dynamics*, submitted.
- Nicault A, Guiot J, Edouard JL and Brewer S (2006b) Preserving long-term climatic changes in standardisation of tree-ring series by the Adaptive Regional Growth Curve (ARGC) and its validation with Southern Alps PDSI reconstruction. *Dendrochronologia*, submitted.
- Osborn TJ and Briffa KR (2004) The real color of climate change? *Science* **306**, 621-622.
- Osborn TJ and Briffa KR (2006) The spatial extent of 20th-century warmth in the context of the past 1200 years. *Science* **311**, 841-844.
- Osborn TJ, Raper SCB and Briffa KR (2006) Simulated climate change during the last 1,000 years: comparing the ECHO-G general circulation model with the MAGICC simple climate model. *Climate Dynamics* **27**, 185-197.
- Overpeck J, Hughen K, Hardy D, Bradley R, Case R, Douglas M, Finney B, Gajewski K, Jacoby G, Jennings A, Lamoureux S, Lasca A, MacDonald G, Moore J, Retelle M, Smith S, Wolfe A and Zielinski G (1997) Arctic environmental change of the last four centuries. *Science* **278**, 1251-1256.
- Pauling A, Luterbacher J, Casty C and Wanner H (2006) Five hundred years of gridded high-resolution precipitation reconstructions over Europe and the connection to large-scale circulation. *Clim. Dyn.* **26**, 387-405.
- Pope VD, Gallani ML, Rowntree PR and Stratton RA (2000) The impact of new physical parameterizations in the Hadley Centre climate model – HadAM3. *Clim. Dyn.* **16**, 123-146.
- Raible CC, Stocker TF, Yoshimori M, Renold M, Beyerle U, Casty C and Luterbacher J (2005) Northern hemispheric trends of pressure indices and atmospheric circulation patterns in observations, reconstructions, and coupled GCM simulations. *J. Climate* **19**, 3968-3982.
- Renwick JA (2004) Trends in the Southern Hemisphere polar vortex in NCEP and ECMWF reanalyses. *Geophys. Res. Lett.*, **31**, L07209, doi:10.1029/2003GL019302.
- Roberts DL and Jones A (2004) Climate sensitivity to black carbon aerosol from fossil fuel combustion. *J. Geophys. Res.* **109**, :doi:10.1029/2004jd004676.
- Rutherford SD, Mann ME, Osborn TJ, Bradley RS, Briffa KR, Hughes MK and Jones PD (2005) Proxy-based Northern Hemisphere surface temperature reconstructions: sensitivity to method, predictor network, target season and target domain. *Journal of Climate* **18**, 2308-2329.
- Senior CA and Mitchell JFB (2000) The time dependence of climate sensitivity. *Geophys. Res. Lett.*, **27**, 2685-2688.

- Shindell DT and Schmidt GA (2004) Southern Hemisphere climate response to ozone changes and greenhouse gas increases. *Geophys. Res. Lett.* **31**, L18209, doi:10.1029/2004GL020724.
- Steiner D, Pauling A, Nesje A, Luterbacher J, Wanner H and Zumbühl HJ (2006) Sensitivity of European glaciers to precipitation and temperature – two case studies. *Clim. Dyn.*, submitted.
- Stott PA, Jones GS and Mitchell JFB (2003) Do models underestimate the solar contribution to recent climate change? *J. Climate* **16**, 4079-4093.
- Tett SFB, Betts R, Crowley TJ, Gregory J, Johns TC, Jones A, Osborn TJ, Ostrom E, Roberts DL and Woodage MJ (2006) The impact of natural and anthropogenic forcings on climate and hydrology since 1550. *Clim. Dyn.*, in press.
- Thompson DWJ and Solomon S (2002) Interpretation of recent Southern Hemisphere climate change. *Science* **296**, 895-899.
- Thompson DWJ and Wallace JM (2000) Annular modes in the extratropical circulation, part 1: month-to-month variability. *J. Climate* **13**, 1000-1016.
- von Storch H, Zorita E, Jones JM, Dimitriev Y, Gonzales-Rouco F and Tett SFB (2004) Reconstructing past climate from noisy data. *Science* **306**, 769-682.
- Wagner S and Zorita E (2005) The influence of volcanic, solar and CO₂ forcing on the temperatures in the Dalton Minimum (1790–1830): a model study. *Clim. Dyn.* **25**, 205-218.
- von Storch H and Zorita E (2005) Comment on “Hockey sticks, principal components, and spurious significance” by S. McIntyre and R. McKittrick. *Geophys. Res. Lett.* L20701, doi: 10.1029/2005GL022753.
- von Storch H, Zorita E, Jones JM, Gonzalez-Rouco F and Tett SFB (2006) Response to Comment on "Reconstructing Past Climate from Noisy Data". *Science* **312**, 529.
- Wahl ER, Ritson DM and Ammann CM (2006) Comment on “Reconstructing past climate from noisy data”. *Science* **312**, 529, doi: 10.1126/science.1120866.
- Wilson R, Tudhope A, Brohan P, Briffa K, Osborn T and Tett S (2006) 250 years of reconstructed and modeled tropical temperatures. *J. Geophys. Res.*, in press.
- Xoplaki E, Luterbacher J, Paeth H, Dietrich D, Steiner N, Grosjean M and Wanner H (2005) European spring and autumn temperature variability and change of extremes over the last half millennium. *Geophys. Res. Lett.* **32** L15713, doi: 10.1029/2005GL023424.
- Zorita E, González-Rouco F and Legutke S (2003) Testing the Mann et al. (1998) approach to paleoclimate reconstructions in the context of a 1000-year control simulation with the ECHO-G coupled climate model. *J. Climate* **16**, 1368-1390.
- Zorita E, von Storch H, Gonzalez-Rouco FJ, Cubasch U, Luterbacher J, Legutke S, Fischer-Bruns I and Schlese U (2004) Climate evolution in the last five centuries simulated by an atmosphere-ocean model: global temperatures, the North Atlantic Oscillation and the Late Maunder Minimum. *Meteorologische Zeitschrift* **4**, 271-289.
- Zorita E, Gonzalez-Rouco FJ, von Storch H, Montavez J and Valero F (2005) Natural and anthropogenic modes of surface temperature variations in the last thousand years. *Geophys. Res. Lett.* **32**, doi: 10.1029/2004/GL021563.

6.4. Conclusions including socio-economic relevance, strategic aspects and policy implications

6.4.1.1. *Scientific achievements*

- We have developed new approaches to, and demonstrated the value of, integrated data-model analyses for the purpose of understanding climate variability.
- We have simulated the climate of the last 500 or 1000 years using two complementary state-of-the-art ocean-atmosphere general circulation climate models and comprehensive sets of natural and anthropogenic forcing factors.
- We have analyzed and compared the climate model simulations to identify the influence of forcings on aspects of global and regional climate, cryosphere, hydrology and sea level.
- We have developed new reconstructions of European, tropical, Antarctic and Northern Hemisphere climate (temperature, precipitation, drought and atmospheric circulation) and North Atlantic sea level.
- We have developed and applied methods by which so-called ‘pseudo-proxy’ records, based on simulated climate data, may be used to test the potential accuracy of climate reconstructions and their dependence on the specific statistical methods employed to produce them, as well as the particular coverage and characteristics of the climate proxy data.
- We have compared climate model output and climate reconstructions to assess the consistency of data and models, and have attempted to detect the effect of natural and anthropogenic forcings on climate. Comparisons have been made for many aspects and regions, including tropical sea surface temperature changes, European temperatures and droughts, Northern Hemisphere temperature changes, and changes in temperature seasonality in Europe and China.

6.4.1.2. *Main deliverables*

- This project has developed new reconstructions of:
 - summer temperatures across western Europe for the last 900 years;
 - temperatures across a large European region for all seasons for the last 500 years;
 - precipitation across a large European region for all seasons for the last 500 years;
 - summer drought severity across the Mediterranean region for the last 650 years;
 - north-western Eurasian regional summer temperatures for the last 2000 years;
 - average tropical annual-mean sea surface temperatures for the last 250 years;
 - summer Antarctic Oscillation index for the last 100 years;
 - Northern Hemisphere temperatures (winter, summer and annual) for the last 600 years;
 - the spatial extent of warming and cooling in the Northern Hemisphere for the last 1200 years; and
 - estimates of relative sea level from the east coast of the North America for the last 500 years or more.
- Climate simulations with two climate models with only natural forcings and with combined natural and anthropogenic forcings:
 - HadCM3 for the last 500 years; and

- ECHO-G for the last 1000 years.
- A comprehensive website to provide a focus for current and future work of this nature and to provide continuing access to and extensive visualisation of the climate model data and the climate reconstructions.

6.4.1.3. Conclusions

- The pseudo-proxy evaluations of the potential reliability of Northern Hemisphere temperature reconstructions indicate that many published reconstructions are likely to be affected by bias, in addition to the random error that was already considered in many cases. The bias most likely results in reconstructions having reduced amplitude multi-century temperature variations, but it is not yet possible to determine the magnitude of this bias because it depends upon the reconstruction method, on the characteristics of climate variability, and on the characteristics of the proxy data. In particular, we have demonstrated that explicit statistical descriptions of the errors in the proxy data are needed if reconstruction bias is to be completely avoided. These aspects of SO&P project work have stimulated further research by other groups and by international research bodies such as CLIVAR/PAGES.
- Despite these potential biases, climate reconstructions developed with SO&P support have shown that:
 - it is likely that the Northern Hemisphere is warmer now than at any time for at least 600 years;
 - it is likely that the spatial extent of warmth over Northern Hemisphere land is greater now than at any time for at least 1200 years; and
 - it is very likely that European temperatures have been higher in recent decades than at any other period in at least the last 500 years and that 2003 was by far the hottest summer during that period.
- The climate model simulations indicate that, in the absence of anthropogenic forcings, global-mean temperature would have warmed by only around 0.1°C due to natural forcings, though this result is dependent upon the sensitivity of the climate model. The simulations suggest that anthropogenic forcings may have had a significant impact on climate since the early 19th century (particularly in the tropics). Both the hydrological cycle and cryosphere are also affected by anthropogenic forcings in the model and changes in land-use influence hydrology and spring snow cover.
- This project has established that future work should focus immediately on further understanding the sources of bias and uncertainty in the different reconstructions of past temperature, and the degree to which these can be reduced by the development of improved methods. Improved reconstructions should then be used to continue the testing of climate models that was begun during the SO&P project, and to extend the application of data and models to such issues as constraining the range of climate sensitivity that is compatible with our evidence of past climate change.

6.4.1.4. Socio-economic relevance and policy implications of the SO&P project

This work has clear policy relevance in two areas; first, in assessing the reliability of the climate models that have been used to make projections of our future climate, and second, in determining how unusual twentieth century climate change was in the context of the last 1,000 years.

6.5. Dissemination and exploitation of the results

A number of different means of dissemination have been used to ensure widespread awareness and use of SO&P results and outputs.

The major focus for dissemination of information about the project, the climate reconstructions, the model simulations and the scientific achievements of SO&P has been the project website. All of the data are available on this website, many in common formats and with a range of visualisations and regional-average time series already available to facilitate a “quick-look” at the data and their main characteristics. Some of these data currently require a password to access them, though it is anticipated that this will be made available in response to most requests following agreement on collaboration and co-authorship of any subsequent publications. A full listing of publications that describe results of the SO&P project is available on the website; copies of these publications are, of course, restricted in access because the copyright is held in most cases by the publisher. It is expected that the website will provide a useful focus for the scientific community involved in simulating and reconstructing the climate of the last millennium. It will be maintained (and updated with additional scientific papers when they appear) for three years after the end of the project.

The new scientific knowledge obtained through the research undertaken for the SO&P project has been disseminated principally via the peer-reviewed scientific literature and by presentations and posters at scientific conferences. It is expected that more such output will follow in the next one-to-two years. A number of outputs are also in the form of new or improved data sets, including:

- output from simulations of the last 500 or 1000 years using climate models;
- new collations of climate proxy data sets; and
- new or alternative reconstructions of past climate variations (temperature, precipitation, circulation) developed from climate proxy records.

All of these data sets will support many further analyses of the detailed evolution of past climate changes and our ability to model them as a response to external forcings and internal variability. These data will continue to be used by the project partners, but many are also available for other scientific use (though mostly requiring initial agreement of the project coordinators and/or data set owners to avoid duplicating work planned by the SOAP partners).

The scientific achievements and the conclusions drawn from these results are being communicated to policymakers and stakeholders in a number of ways. Many scientists that received support from the SO&P project are authors of the forthcoming Fourth Assessment Report of the Intergovernmental Panel on Climate Change (IPCC) and SO&P results and data sets are included in the current draft of that report, especially Chapter 6 (Paleoclimate). The coordinators of SO&P, Keith Briffa and Tim Osborn, are lead author and contributing author on this chapter, respectively.

Individual SO&P partners have also fed project results into national and regional stakeholder/policy bodies and have been involved in educational activities where SO&P project results have been used (including, among many, scientific advice to Dutch, German and UK governments, participation in the European Science Foundation HOLIVAR programme, lecturing at the European Research Course on Atmospheres, etc.).

Main literature produced

This section contains details of the scientific publications that have been produced with full or partial support from the SO&P project. So far, 48 papers have been published or are in press in the peer-reviewed scientific literature, and a further 4 have been submitted for consideration. It is expected that many more publications will arise as a direct result of the SO&P project, based on manuscripts that are currently in preparation.

The 52 published, in press or submitted papers are listed below, categorised according to project area and year of publication/submission. Copies of all these publications are available from the SO&P project website (<http://www.cru.uea.ac.uk/projects/soap/pubs/papers/>). Some of these electronic reprints are password-protected because of copyright issues. The password can be requested from the project coordinator (Tim Osborn, t.osborn@uea.ac.uk) so that the European Commission can obtain copies of these papers.

Climate simulations

- **2004**
 - Renssen H, Braconot P, Tett SFB, von Storch H and Weber SL (2004) Recent developments in Holocene climate modelling. In *Past climate variability through Europe and Africa* (eds. Battarbee RW *et al.*), Kluwer Academic Publishers, Dordrecht, Netherlands, 495-514.
 - von Storch H (2004) A discourse about quasi-realistic climate models and their applications in paleoclimatic studies. In *The KIHZ project: towards a synthesis of Holocene proxy data and climate models* (eds. Fischer *et al.*), Springer, Heidelberg, Berlin, New York, 43-56.
- **2005**
 - Cubasch U, Burger G, Fast I, Spanghel T and Wagner S (2005) The direct solar influence on climate: modeling the lower atmosphere. *Memorie della Societa Astronomica Italiana* **76**, 810-818.
 - Fischer-Bruns I, von Storch H, Gonzalez-Rouco JF and Zorita E (2005) Modelling the variability of midlatitude storm activity on decadal to century time scales. *Climate Dynamics* **25**, 461-476.
 - Wagner S and Zorita E (2005) The influence of volcanic, solar and CO₂ forcing on the temperatures in the Dalton Minimum (1790-1830): a model study. *Climate Dynamics* **25**, 205-218.
 - Zorita E, Gonzalez-Rouco JF, von Storch H, Montavez JP and Valero F (2005) Natural and anthropogenic modes of surface temperature variations in the last 1000 years. *Geophysical Research Letters* **32**, L08707 (doi: 10.1029/2004GL021563).
- **2006**
 - Osborn TJ, Raper SCB and Briffa KR (2006) Simulated climate change during the last 1,000 years: comparing the ECHO-G general circulation model with the MAGICC simple climate model. *Climate Dynamics* **27**, 185-197.

- Tett SFB, Betts R, Crowley TJ, Gregory J, Johns TC, Jones A, Osborn TJ, Ostrom E, Roberts DL and Woodage MJ (2006) The impact of natural and anthropogenic forcings on climate and hydrology since 1500. *Climate Dynamics* (in press).

Climate proxies

- **2003**

- Pauling A, Luterbacher J and Wanner H (2003) Evaluation of proxies for European and North Atlantic temperature field reconstructions. *Geophysical Research Letters* **30**, 1787 (doi: 10.1029/2003GL017589).

Climate reconstructions

- **2003**

- Bradley RS, Briffa KR, Cole J, Hughes MK and Osborn TJ (2003) The climate of the last millennium. In *Paleoclimate, global change and the future* (ed. Alverson KD, Bradley RS and Pedersen TF), Springer Verlag, Berlin, 105-141.
- Briffa KR, Osborn TJ and Schweingruber FH (2003) Large-scale temperature inferences from tree rings: a review. *Global and Planetary Change* **40**, 11-26 (doi:10.1016/S0921-8181(03)00095-X).
- Jones PD, Moberg A, Osborn TJ and Briffa KR (2003) Surface climate responses to explosive volcanic eruptions seen in long European temperature records and mid-to-high latitude tree-ring density around the Northern Hemisphere. In *Volcanism and the Earth's atmosphere* (eds. Robock A and Oppenheimer C), American Geophysical Union, Washington, DC, 239-254.
- Jones PD, Osborn TJ and Briffa KR (2003) Changes in the Northern Hemisphere annual cycle: implications for paleoclimatology? *Journal of Geophysical Research* **108**, 4588 (doi:10.1029/2003JD003695).
- Mann M, Ammann C, Bradley R, Briffa K, Jones P, Osborn T, Crowley T, Hughes M, Oppenheimer M, Overpeck J, Rutherford S, Trenberth K and Wigley T (2003) On past temperatures and anomalous late-20th century warmth. *EOS* **84**, 256-257.
- Mann M, Ammann C, Bradley R, Briffa K, Jones P, Osborn T, Crowley T, Hughes M, Oppenheimer M, Overpeck J, Rutherford S, Trenberth K and Wigley T (2003) Response to Soon et al.'s comment on "On past temperatures and anomalous late- 20th century warmth". *EOS* **84**, 473-474.

- **2004**

- Esper J, Frank DC and Wilson RJS (2004) Climate reconstructions: low-frequency ambition and high-frequency ratification. *EOS* **85**, 113-115.
- Luterbacher J, Dietrich D, Xoplaki E, Grosjean M and Wanner H (2004) European seasonal and annual temperature variability, trends and extremes since 1500. *Science* **303**, 1499-1503.

- Snowball I, Korhola A, Briffa KR and Koc N (2004) Holocene climate dynamics in Fennoscandia and the North Atlantic. In *Past climate variability through Europe and Africa* (eds. Battarbee RW, Gasse F and Stickley CE), Springer, Dordrecht, Netherlands, pp. 465-494.
- Verschuren D, Briffa KR, Hoelzmann P, Barber K, Barker P, Scott L, Snowball I Roberts N and Battarbee RW (2004) Climate variability in Europe and Africa: a PAGES - PEP III Time Stream I synthesis. In *Past climate variability through Europe and Africa* (eds. Battarbee RW, Gasse F and Stickley CE), Springer, Dordrecht, Netherlands, pp. 567-582.
- Zinke J, von Storch H, Muller B, Zorita E, Rein B, Mieding HB, Miller H, Lucke A, Schleser GH, Schwab MJ, Negendank JFW, Kienel U, Gonzalez-Ruoco JF, Dullo C and Eisenhauser A (2004) Evidence for the climate during the Late Maunder Minimum from proxy data available within KIHZ. In *The KIHZ project: towards a synthesis of Holocene proxy data and climate models* (eds. Fischer *et al.*), Springer, Heidelberg, Berlin, New York.
- **2005**
 - Burger G and Cubasch U (2005) Are multiproxy climate reconstructions robust? *Geophysical Research Letters* **32**, L23711 (doi: 10.1029/2005GL024155).
 - D'Arrigo R, Wilson R, Deser C, Wiles G, Cook E, Villalba R, Tudhope A, Cole J and Linsley B (2005) Tropical-North Pacific climate linkages over the past four centuries. *Journal of Climate* **18**, 5253-5265.
 - Esper J, Frank DC, Wilson RJS and Briffa KR (2005) Effect of scaling and regression on reconstructed temperature amplitude for the past millennium. *Geophysical Research Letters* **32**, L0711 (doi: 10.1029/2004GL021236).
 - Esper J, Wilson RJS, Frank DC, Moberg A, Wanner H and Luterbacher J (2005) Climate: past ranges and future changes. *Quaternary Science Reviews* **24**, 2164-2166.
 - Guiot J, Nicault A, Rathgeber C, Edouard JL, Guibal F, Pichard G and Till C (2005) Last-millennium summer-temperature variations in western Europe based on proxy data. *The Holocene* **15**, 489-500.
 - Matthews JA and Briffa KR (2005) The 'Little Ice Age': re-evaluation of an evolving concept. *Geografiska Annaler* **87 A**, 17-36.
 - Rutherford SD, Mann ME, Osborn TJ, Bradley RS, Briffa KR, Hughes MK and Jones PD (2005) Proxy-based Northern Hemisphere surface temperature reconstructions: sensitivity to method, predictor network, target season and target domain. *Journal of Climate* **18**, 2308-2329.
 - Touchan R, Xoplaki E, Funkhouser G, Luterbacher J, Hughes MK, Erkan N, Akkemik U and Stephan J (2005) Reconstructions of spring/summer precipitation for the eastern Mediterranean from tree-ring widths and its connection to large-scale atmospheric circulation. *Climate Dynamics* **25**, 75-98 (doi: 10.1007/s00382-005-0016-5).

- Wilson R, Tudhope A, Brohan P, Briffa K, Osborn T and Tett S (2006) 250-years of reconstructed and modeled tropical temperatures. *Journal of Geophysical Research*, in press.
- Xoplaki E, Luterbacher J, Paeth H, Dietrich D, Steiner N, Grosjean M and Wanner H (2005) European spring and autumn temperature variability and change of extremes over the last half millennium. *Geophysical Research Letters* **32** L15713 (doi: 10.1029/2005GL023424).
- **2006**
 - Bronnimann S, Xoplaki E, Casty C, Pauling A and Luterbacher J (2006) ENSO influence on Europe during the last centuries. *Climate Dynamics* (doi: 10.1007/s00382-006-0175-z).
 - D'Arrigo R, Wilson R, Palmer J, Krusic P, Curtis A, Sakulich J, Bijaksana S, Zulaikah S, Ngkoimani LO and Tudhope A (2006) The reconstructed Indonesian warm pool sea surface temperatures from tree rings and corals: linkages to Asian monsoon drought and El Nino-Southern Oscillation. *Paleoceanography* **21**, PA3005 (doi: 10.1029/2005PA001256).
 - Jones PD and Briffa KR (2006) Unusual climate in northwest Europe during the period 1730 to 1745 based on instrumental and documentary data. *Climatic Change* (doi: 10.1007/s10584-006-9078-6).
 - Luterbacher J and 48 co-authors (2006) Mediterranean climate variability over the last centuries: a review. In *The Mediterranean climate: an overview of the main characteristics and issues* (eds. Lionello P, Malanotte-Rizzoli P and Boscolo R), Elsevier, Amsterdam, Netherlands, 27-148.
 - Osborn TJ and Briffa KR (2006) The spatial extent of 20th-century warmth in the context of the past 1200 years. *Science* **311**, 841-844.
 - Pauling A and Paeth H (2006) On the variability of return periods of European winter precipitation extremes over the last five centuries. *Climate of the Past* (submitted).
 - Pauling A, Luterbacher J, Casty C and Wanner H (2006) Five hundred years of gridded high-resolution precipitation reconstructions over Europe and the connection to large-scale circulation. *Climate Dynamics* **26**, 387-405.
 - Pfister C, Weingartner R and Luterbacher J (2006) Reconstruction of extreme hydrological winter droughts over the last 450 years in the Upper Rhine basin. A methodological approach. *Hydrological Sciences Journal* (in press).
 - Trigo and 21 co-authors (2006) Relations between variability in the Mediterranean region and mid-latitude variability. In *The Mediterranean climate: an overview of the main characteristics and issues* (eds. Lionello P, Malanotte-Rizzoli P and Boscolo R), Elsevier, Amsterdam, Netherlands, 179-226.

Data-model comparisons

- **2004**
 - Jones JM and Widmann M (2004) Reconstructing large-scale variability from palaeoclimatic evidence by means of Data Assimilation Through Upscaling and Nudging (DATUN). In *The KIHZ project: towards a synthesis of Holocene proxy data and climate models* (eds. Fischer *et al.*), Springer, Heidelberg, Berlin, New York, 171-193.
 - von Storch, H, Zorita E, Jones JM, Dmitriev Y, and Tett SFB (2004) Reconstructing past climate from noisy data. *Science* **304**, 679-682.
- **2005**
 - Casty C, Handorf D, Raible CC, Gonzalez-Rouco JF, Xoplaki E, Luterbacher J, Weisheimer A, Dethloff K and Wanner H (2005) Recurrent climate winter regimes in reconstructed and modelled 500 hPa geopotential height fields over the North Atlantic/European sector 1659-1990. *Climate Dynamics* **24**, 809-822 (doi: 10.1007/s00382-004-0496-8).
 - Raible CC, Stocker TF, Yoshimori M, Renold M, Beyerle U, Casty C and Luterbacher J (2005) Northern Hemispheric trends of pressure indices and atmospheric circulation patterns in observations, reconstructions, and coupled GCM simulations. *Journal of Climate* **18**, 3968-3982.
 - von Storch H and Zorita E (2005) Comment on "Hockey sticks, principal components, and spurious significance" by S. McIntyre and R. McKittrick. *Geophysical Research Letters* **32**, L20701 (doi: 10.1029/2005GL022753).
- **2006**
 - Burger G, Fast I and Cubasch U (2006) Climate reconstruction by regression - 32 variations on a theme. *Tellus* **58A**, 227-235.
 - Gonzalez-Rouco JF, Beltrami H, Zorita E and von Storch H (2006) Simulation and inversion of borehole temperature profiles in surrogate climates: spatial distribution and surface coupling. *Geophysical Research Letters* **33**, L01703 (doi: 10.1029/2005GL024693).
 - Goosse H, Arzel O, Luterbacher J, Mann ME, Renssen H, Riedwyl N, Timmermann A, Xoplaki E and Wanner H (2006) The origin of the European 'Medieval Warm Period'. *Climate of the Past* (submitted).
 - Kuettel M, Luterbacher J, Zorita E, Xoplaki E, Riedwyl N and Wanner H (2006) Testing a European winter surface temperature reconstruction in a surrogate climate. *Geophysical Research Letters* (submitted).

Sea level

- **2006**
 - Gregory JM, Lowe JA and Tett SFB (2006) Simulated global-mean sea-level changes over the last half-millennium. *Journal of Climate* **19**, 4576-4591.

- Hunicke B, Luterbacher J, Pauling A, Wagner S and Zorita E (2006) Regional climate-drivers of decadal winter Baltic sea level variability in 1800-2100. *Geophysical Research Letters* (submitted).

Others

- **2004**

- Jones JM and Widmann M (2004) Early peak in Antarctic Oscillation Index. *Nature* **432**, 290-291.
- Osborn TJ (2004) Simulating the winter North Atlantic Oscillation: the roles of internal variability and greenhouse gas forcing. *Climate Dynamics* **22**, 605-623.
- Xoplaki E, Gonzalez-Rouco JF, Luterbacher J and Wanner H (2004) Wet season Mediterranean precipitation variability: influence of large-scale dynamics and trends. *Climate Dynamics* **23**, 63-78 (doi: 10.1007/s00382-004-0422-0).